

Archive ouverte UNIGE

https://archive-ouverte.unige.ch

Thèse 2020

Open Access

This version of the publication is provided by the author(s) and made available in accordance with the copyright holder(s).

Polydiacetylene-Peptide Interaction Mechanism in Mixed Lipid Systems

Nuck, Johann

How to cite

NUCK, Johann. Polydiacetylene-Peptide Interaction Mechanism in Mixed Lipid Systems. Doctoral Thesis, 2020. doi: 10.13097/archive-ouverte/unige:149515

This publication URL: https://archive-ouverte.unige.ch/unige:149515

Publication DOI: <u>10.13097/archive-ouverte/unige:149515</u>

© This document is protected by copyright. Please refer to copyright holder(s) for terms of use.

Section de chimie et biochimie Département de chimie physique Professeur H. R. Hagemann Professeure Kaori Sugihara

Polydiacetylene-Peptide Interaction Mechanism in Mixed Lipid Systems

THÈSE

Présentée à la Faculté des sciences de l'Université de Genève pour obtenir le grade de Docteur ès Sciences, mention Chimie

par

Johann Nuck

de

Berlin (Allemagne)

Thèse N°5538

GENÈVE

Atelier ReproMail



DOCTORAT ÈS SCIENCES, MENTION CHIMIE

Thèse de Monsieur Johann NUCK

intitulée:

«Polydiacetylene-Peptide Interaction Mechanism in Mixed Lipid Systems»

La Faculté des sciences, sur le préavis de Monsieur H.-R. HAGEMANN, professeur associé et directeur de thèse (Département de chimie physique), Madame K. SUGIHARA, professeure assistante et codirecteur de thèse (Département de chimie physique), Monsieur A. FÜRSTENBERG, docteur (Départements de chimie physique et chimie minérale et analytique) et Monsieur T. ZAMBELLI, professeur (Département de Technologie de l'information et Génie électrique, École polytechnique fédérale de Zurich (ETH Zurich), Suisse), autorise l'impression de la présente thèse, sans exprimer d'opinion sur les propositions qui y sont énoncées.

Genève, le 1 février 2021

Thèse - 5538 -

Le Doyen

Acknowledgements

We finish our PhD with this document, a small insight of the work achieved. The time spent at the University of Geneva contained so much more - professional and private. The strength to finish this step would not have been possible without all the beautiful moments and good friends around me!

Long discussion with colleagues formed my understanding towards this research, friends and family are always there to animate me and nature around Geneva provides diversion, inspiration and relaxation.

Thank you

Preamble

To expand our knowledge, the basic concept is simple: A hypothesis is proposed for a new phenomenon. When it withstands all objections, a theory can be formulated. But how can we prove or disprove the hypothesis in our experimental world? We have to verify the parameters involved with the aid of measuring instruments. Therefore, *sensors* of such an instrument are essential not only for the scientific community but mankind itself.

Summary

The fascinating characteristics of Polydiacetylene (PDA) have attracted scientists around the world since its discovery in the late 19th century. Due to the polymer's mechanochromism it has been widely employed to study the peptide-lipid interaction in biological systems. PDA possesses two different electronic structures described as "blue" and "red" state according to its optical appearance. Various stimuli are able to induce a transition between the first and the second state. Furthermore, the red state has a fluorescence pathway from the electronic excited to its ground state. Thanks to this characteristic, PDA is able to detect different types of membrane active peptides. Despite its popularity, the mechanism behind the interaction between lipid-like PDA derivatives and peptides still remains unknown.

Wegner et. al published (1969) a systematic investigation of the polymerizability for different diacetylene derivatives.

The requisite for a successful topochemical solid state 1,4-addition reaction, the correct spacing around $d \approx 5$ Å and positioning between adjacent monomers were clarified. They concluded that hydrogen bonds and Van der Waals forces play a major role in this self-assembling process as they dominate the monomers' spatial arrangement.

The characterization of the two different polydiacetylene states still opens room for a lot of discussion. The early attempt to assign the blue and the red state to the acetylene and butatriene electronic structure, respectively, was disproved by crystallographic studies and quantum chemical calculations. In both cases, the acteylene structure seems evident. The difference has to arise from other features.

Regarding the geometrical arrangement, a general consensus for the planar conjugated chain in blue state has been reached. However, the opinions differ for the non-planar red state of polydiacetylene. Various models like a segmented planar Kuhn chain model, a zig-zag shape or a continuous curved "worm-like" chain, called Pordo-Kratky chain, are proposed. The controversy in the model is linked to the explanation of the order and the electronic structure between the two states. Two different approaches are discussed here to explain the colorful nature of both states: The shortening of the effective conjugation length in Hueckel's theory versus the description by excitons.

To induce the red state, various stimuli like temperature, pH, solvents and peptides are discussed. Here, the importance of the hydrogen bond network between the hydrophilic head groups of adjacent repeating units of the polydiacetylene is highlighted. This is critical for developing reversible PDA-based sensors. However, the mechanism of an induced blue-to-red transition has not yet been addressed on a molecular level.

The following work aims at providing a deeper understanding of this transition in the case of an activation by peptides. As it is well known, the peptide melittin is able to penetrate lipid bilayers and form pores leading to cell lysis. But how much force is necessary to rupture a bilayer? Lipid-like PDA derivatives can be integrated into a model membrane to analyze this peptide-lipid interaction. Due to its extreme sensitivity, PDA is able to detect forces in a range down to $F \approx 50$ nN. This leads to the idea of developing a PDA-based force probe to detect these types of interactions. An external force converts PDA from the blue to the red state. As the latter state displays fluorescence, this transition can be followed by fluorescence microscopy. With a calibrated system, this signal can be calculated back into the originally applied force. As the blue-to-red conversion is proportional to the applied force, the sensor can not only detect but also quantify the force. Hence, PDA is an ideal candidate to develop a force probe sensor.

To do so, the diacetylene TRCDA monomer is incorporated into a soft lipid supported bilayer. After successfully growing monomer crystals and polymerization by UV light a blue-to-red transition can be induced. This environment simulates a typical peptide-lipid interaction, such as the interaction between the bee venom (melittin) and the host cell membrane.

Here, the mechanosensitive PDA is investigated by various microscopy techniques and

differential scanning calorimetry to shed light on the red state activation by the peptide melittin. Our hypothesis: The peptide-induced color change originates from the peptideinduced lipid phase transition.

Résumé

Les caractéristiques fascinantes du polydiacétylène (PDA) ont attiré les scientifiques du monde entier depuis sa découverte à la fin du XIXe siècle. En raison du mécanochromisme du polymère, il a été largement utilisé pour étudier l'interaction peptide-lipide dans les systèmes biologiques. Le PDA possède deux structures électroniques différentes décrites comme étant à l'état "bleu" et "rouge" selon son aspect optique. Divers stimuli sont capables d'induire une transition entre le premier et le second état. De plus, l'état rouge possède une voie de fluorescence entre l'état excité électronique et son état fondamental. Grâce à cette caractéristique, le PDA est capable de détecter différents types de peptides membranaires actifs. Malgré sa popularité, le mécanisme qui sous-tend l'interaction entre les dérivés du PDA de type lipidique et les peptides reste encore inconnu.

Wegner et. al ont publié (1969) une étude systématique de la polymérisabilité de différents dérivés du diacétylène.

Les conditions requises pour une réaction topochimique d'addition 1,4 à l'état solide réussie, l'espacement correct autour de $d \approx 5$ Å et le positionnement entre les monomères adjacents ont été clarifiés. Ils ont conclu que les liaisons hydrogène et les forces de Van der Waals jouent un rôle majeur dans ce processus d'auto-assemblage car elles dominent l'agencement spatial des monomères.

La caractérisation des deux états différents du polydiacétylène ouvre encore la voie à de nombreuses discussions. La première tentative d'attribuer l'état bleu et l'état rouge à la structure électronique de l'acétylène et du butatriène, respectivement, a été réfutée par des études cristallographiques et des calculs de chimie quantique. Dans les deux cas, la structure de l'actéylène semble évidente. La différence doit provenir d'autres caractéristiques.

En ce qui concerne l'arrangement géométrique, un consensus général a été atteint pour la

chaîne conjuguée plane à l'état bleu. Cependant, les opinions divergent pour l'état rouge non planaire du polydiacétylène. Différents modèles sont proposés, comme un modèle de chaîne de Kuhn planaire segmentée, une forme en zigzag ou une chaîne continue courbée "en forme de ver", appelée chaîne de Pordo-Kratky. La controverse sur le modèle est liée à l'explication de l'ordre et de la structure électronique entre les deux états. Deux approches différentes sont examinées ici pour expliquer la nature colorée des deux états : Le raccourcissement de la longueur effective de conjugaison dans la théorie de Hueckel par rapport à la description par excitons.

Pour induire l'état rouge, différents stimuli comme la température, le pH, les solvants et les peptides sont abordés. Ici, l'importance du réseau de liaison hydrogène entre les groupes de tête hydrophiles des unités répétitives adjacentes du polydiacétylène est mise en évidence. Ceci est essentiel pour le développement de capteurs réversibles basés sur les PDA. Cependant, le mécanisme de la transition induite du bleu au rouge n'a pas encore été abordé au niveau moléculaire.

Les travaux suivants visent à fournir une compréhension plus approfondie de cette transition dans le cas d'une activation par des peptides. Comme on le sait, le peptide melittin est capable de pénétrer les bicouches lipidiques et de former des pores conduisant à la lyse cellulaire. Mais quelle est la force nécessaire pour rompre une bicouche ? Des dérivés de PDA de type lipidique peuvent être intégrés dans une membrane modèle pour analyser cette interaction peptide-lipide. En raison de son extrême sensibilité, le PDA est capable de détecter des forces allant jusqu'à $F\approx 50$ nN. Cela conduit à l'idée de développer une sonde de force basée sur le PDA pour détecter ces types d'interactions. Une force externe fait passer le PDA de l'état bleu à l'état rouge. Comme ce dernier état montre la fluorescence, cette transition peut être suivie par la microscopie à fluorescence. Avec un système calibré, ce signal peut être calculé pour revenir à la force appliquée à l'origine. Comme la conversion du bleu au rouge est proportionnelle à la force appliquée, le capteur peut non seulement détecter mais aussi quantifier la force. Le PDA est donc un candidat idéal pour le développement d'un capteur de force.

Pour ce faire, le monomère diacétylène TRCDA est incorporé dans une bicouche supportée

par des lipides souples. Après avoir réussi à faire croître des cristaux de monomère et à les polymériser par la lumière UV, une transition du bleu au rouge peut être induite. Cet environnement simule une interaction peptide-lipide typique, telle que l'interaction entre le venin d'abeille (mélitine) et la membrane de la cellule hôte.

Ici, le PDA mécanosensible est étudié par diverses techniques de microscopie et de calorimétrie différentielle à balayage pour mettre en lumière l'activation de l'état rouge par la mélittine peptidique. Notre hypothèse : Le changement de couleur induit par le peptide provient de la transition de phase lipidique induite par le peptide.

Contents

A	ckno	wledge	ements	\mathbf{v}
Pı	ream	ble		vii
Sı	ımm	ary		ix
\mathbf{R}	ésum	ıé		xiii
1	An	introd	luction to (Poly)Diacetylene	1
	1.1	(Poly)	Diacetylene as a sensor	1
	1.2	Aim o	of this Work	2
	1.3	A sho	rt History of Polydiacetylene	4
	1.4	The S	tructure of (Poly)Diacetylene	5
	1.5	The P	Principle of the Solid-State Polymerization	6
	1.6	The T	Two States of Polydiacetylene	10
		1.6.1	Electronic Structure: Ground and Excited States	10
		1.6.2	Geometry of the Blue and Red Configuration	13
		1.6.3	The Problem of the Effective Conjugation Length	14
		1.6.4	Quantifying the Blue-to-Red Transition	18
	1.7	Differe	ent Stimuli for Inducing Chromism in Polydiacetylene	19
		1.7.1	Temperature:	
			Reversible and Irreversible Thermochromism	19
			Hydrogen Bond Network	20
			Environmental Changes	24
			Intercalation	25

		1.7.2 Macromolecules: Proteins and Peptides	28
		1.7.3 Solvents	33
		1.7.4 Surfactants	36
		1.7.5 pH	38
		1.7.6 Comparison of Different UV-Vis Spectra	40
2	The	Mechanism of Polydiacetylene Blue-to-Red Transformation Induced	
	by A	Antimicrobial Peptides	43
	2.1	Introduction	43
	2.2	Results and Discussion	45
		2.2.1 (P)DA Crystal Formation and Integration into a Lipid Bilayer	45
		2.2.2 Peptide-Lipid Interaction	50
	2.3	Conclusion	61
	2.4	New Experiments and Discussions	61
	2.5	Outlook	67
3	Mat	cerials and Methods	71
3	Mat 3.1	terials and Methods HEPES Buffer Solution	71 71
3			
3	3.1	HEPES Buffer Solution	71
3	3.1 3.2	HEPES Buffer Solution	71 71
3	3.1 3.2 3.3	HEPES Buffer Solution	71 71 72
3	3.1 3.2 3.3 3.4	HEPES Buffer Solution	71 71 72 73
3	3.1 3.2 3.3 3.4 3.5	HEPES Buffer Solution	71 71 72 73 73
3	3.1 3.2 3.3 3.4 3.5 3.6	HEPES Buffer Solution	71 72 73 73 74
3	3.1 3.2 3.3 3.4 3.5 3.6 3.7	HEPES Buffer Solution	71 71 72 73 73 74 74
3	3.1 3.2 3.3 3.4 3.5 3.6 3.7 3.8 3.9	HEPES Buffer Solution	71 71 72 73 73 74 74 74
3	3.1 3.2 3.3 3.4 3.5 3.6 3.7 3.8 3.9 3.10	HEPES Buffer Solution TRCDA / DOPC Suspension Preparation Polymerization Peptide Preparation UV-Vis Spectroscopy Calculation of Colorimetric Response TRCDA/DOPC Sample Preparation for Figure 2.7B,D-G and Figure 2.14. TRCDA Sample Preparation for Figure 2.7H,I	71 71 72 73 73 74 74 74 75
3	3.1 3.2 3.3 3.4 3.5 3.6 3.7 3.8 3.9 3.10 3.11	HEPES Buffer Solution TRCDA / DOPC Suspension Preparation Polymerization Peptide Preparation UV-Vis Spectroscopy Calculation of Colorimetric Response TRCDA/DOPC Sample Preparation for Figure 2.7B,D-G and Figure 2.14. TRCDA Sample Preparation for Figure 2.7H,I Gold-labeled Melittin TRCDA Sample Preparation for Figure 2.20	71 71 72 73 73 74 74 75 76

	xix
3.14 Isothermal Titration Calorimetry	 78
3.15 Dynamic Light Scattering	 78
3.16 Differential Scanning Calorimetry	 78
3.17 Plugin for ImageJ	 79
General Conclusion	83
A Appendix	87
A.1 Polymerizability Improvement by Soft Lipids	 87
B List of Publications	89
C List of Talks, Posters and Awards	91
C.1 Talks	 91
C.2 Posters	 92
C.3 Awards	 93
D List of Chemical Formulas	95
E List of Symbols and Abbreviations	101
Bibliography	103

List of Figures

1.1	Workflow of the (P)DA investigation in its different states: monomeric, blue-	
	and red polymeric state. The top row shows the employed techniques for bulk	
	analysis like UV-Vis spectroscopy and differential scanning calorimetry. Here	
	the average signal is captured. The bottom row shows techniques to get a	
	closer look at local behavior of (P)DA	3
1.2	10,12-Tricosadiynoic acid	6
1.3	Solid-state topochemical 1,4-addition reaction of diacetylene	6
1.4	PTS arrangement shown orthogonal to the backbone plane for monomer and	
	polymer	8
1.5	Schematic representation of the $2p_x$ and $2p_z$ orbitals of polydiacetylene back-	
	bone structure	9
1.6	Simplified backbone of PDA	11
1.7	Determination of the ground state symmetry for PDA	12
1.8	Important Energy States of PDA	13
1.9	Different models for the blue-to-red transition	14
1.10	Theoretical and experimental data for the absorption peak λ_{max} as a function	
	of the repeat unit	16
1.11	Characteristic UV-Vis Spectra of PDA	17
1.12	Colorimetric response of PDA	19
1.13	Urethane substitute for enhanced intramolecular hydrogen bonding	21
1.14	FTIR of poly(PCDA-mBzA) and poly(PCDA-NPA) and their schemes	21
1.15	Reversible colorimetric transitions of LS films	22
1 16	FTIR spectra of LS films	23

1.17	Color photographs of drop cast films of PCDA derivatives	24
1.18	Reversibility of HEEPCDA	25
1.19	Reversible PDA/PVP nanocomposite	26
1.20	Schema for DA molecules for various alkyl length	27
1.21	UV-Vis spectra of PDA/PVP10 nanocomposites	27
1.22	DMPC/PDA solution exposed to different peptides	28
1.23	Structure of Melittin and its incorporation into a bilayer	30
1.24	Fluorescence emission spectra for different lipid to peptide ratios for the native	
	L-melittin	31
1.25	Fluorescence emission spectra for Titration of PDA liposomes with LPS	31
1.26	Photograph of PDA solution exposed to different concentrations of surfactin	32
1.27	PDA as label-free bacterial detection system	33
1.28	CR of poly(PCDA)/1-but anol against THF	35
1.29	UV-Vis spectra of PDA8/12 exposed to ethanol)	35
1.30	CR of poly(PCDA) vesicles in aqueous solution exposed to SDS, Triton X-100	
	and CTAB	36
1.31	UV-Vis spectra of PCDA-HBA exposed to CTAC and DTAC	37
1.32	Deprotonation of a carboxylate head group in an aqueous environment	38
1.33	Comparison of exitonic and vibronic peaks of PCDA UV-Vis spectra for var-	
	ious stimuli.	41
2.1	Crystal growth of DA in a soft lipid BL environment	46
2.2	DA/PDA crystals embed into a DOPC soft lipid bilayer imaged by fluores-	
	cence and bright field microscopy	47
2.3	DA crystal growing with - and without a supporting DOPC bilayer	48
2.4	Polymerized TRCDA crystal self-assembled in a DOPC environment, dried	
	out and imaged by TEM	48
2.5	AFM measurement of DA/PDA embed into a DOPC soft lipid bilayer	49

2.6	Absorbance of polymerized DOPC/TRCDA suspension over time and growth	
	of the solution analyzed by UV-Vis and DLS	50
2.7	UV-Vis spectra of polydiacetylene (PDA) made of 60 mol $\%$ TRCDA and 40	
	mol % DOPC with and without melitti	52
2.8	TRCDA/DOPC ratio dependency on the colorimetric response upon adding	
	melittin	53
2.9	Atomic force microscopy of monomeric TRCDA	53
2.10	Differential scanning calorimetry of TRCDA monomer with and without melittin	54
2.11	Bright field microscopy image of PDNT-12-8-22Br assembled on a glass cov-	
	erslip before and after addition of different peptides	55
2.12	Isothermal titration calorimetry (ITC) performed with monomers and UV-	
	Vis spectroscopy with polymers during titration with different antimicrobial	
	peptides	56
2.13	Bright field microscopy images of TRCDA monomers assembled on a glass	
	coverslip before and after addition of different peptides	59
2.14	Incubation of the blue-state PDA with melittin imaged by fluorescence mi-	
	croscopy	60
2.16	Induced blue-to-red transition by UV light	63
2.17	Gold-labeled melittin inducing a blue-to-red transition of PDA imaged by TEM	64
2.18	Scheme of PDA exposed to Gold	64
2.19	Snapshots of polymerized TRCDA crystals exposed to melittin imaged by	
	bright field and fluorescence microscopy at different time points	65
2.20	Monomeric TRCDA crystals exposed to a continuously variable reflective neu-	
	tral density filter	66
A.1	Absorbance of DOPC/TRCDA suspension after polymerization	87

List of Tables

1.1	Crystal structure data for PTS for mono- and polymer	9
2.1	Comparison of different polydiacetylene (PDA) derivatives regarding the phase	
	transition (T_m) and the blue-to-red transition temperature (T_{PPP})	45

Listings

3.1	Source code for	the ImageJ	plugin to	correct th	he channel	order for	multidi-	
	mensional RGB	nd2 files						79

Chapter 1

An introduction to (Poly)Diacetylene

The first section (1.1) introduces Polydiacetylene (PDA) where section(1.2) motivates and sets this work into its scientific environment. The next section (1.3) outlines a short summary about the history of polydiacetylene (PDA): from its discovery, acknowledging important contributors, to its application as a sensor. In the following sections (1.4 - 1.6), a short overview of (P)DA's physical - and chemical properties is given. This sets the context for the investigation and applications presented afterwards. In this work DA and PDA refers to the monomeric and polymeric form respectively while (P)DA refers to both forms. Finally, section 1.7 discusses different stimuli which are causing the so-called blue-to-red transition. The subsection 1.7.1 provides, besides the stimulus "Temperature", also information about the reversibility of this transition.

1.1 (Poly)Diacetylene as a sensor

Due to the fascinating characteristics of Polydiacetylene it has attracted scientists around the world since its discovery in the late 19th century. After a successful polymerization of the monomeric form (diacetylene), the polymer is able to undergo a transition from its original blue state into its red state. This change can be employed to detect interactions similar to a switch. The red state has a fluorescence pathway and is therefore easily detectable by fluorescence microscopy. The blue-to-red transition can be triggered by external stimuli like temperature¹, solvents², pH change, bacteria³ and peptides⁴. Furthermore purely mechanical stimuli like surface-pressure at interfaces⁵ and friction forces⁶ are possible.

Especially in cell biology, studying the membrane tensions is still challenging but desired.⁷ The attributes of the PDA sensor led to applications in a variety of biological systems^{8–10}, but also found its application in a more general chemical environments, ^{11,12} besides the study of its intrinsic interesting electronic structure. ^{13–16}

Of course PDA is not the only approach to measure interactions and physical forces: With an atomic force microscope it is possible to study the adsorption/desorption behavior from a single macromolecule by single molecular force spectroscopy. ¹⁷ Due to the high sensitivity of the technique the range of measuring forces goes down to the piconewton region. Further methods include micropipette aspiration to study the surface tension of single cells, ¹⁸ and mechanosensitive so-called push-pull fluorophores ¹⁹ besides many more.

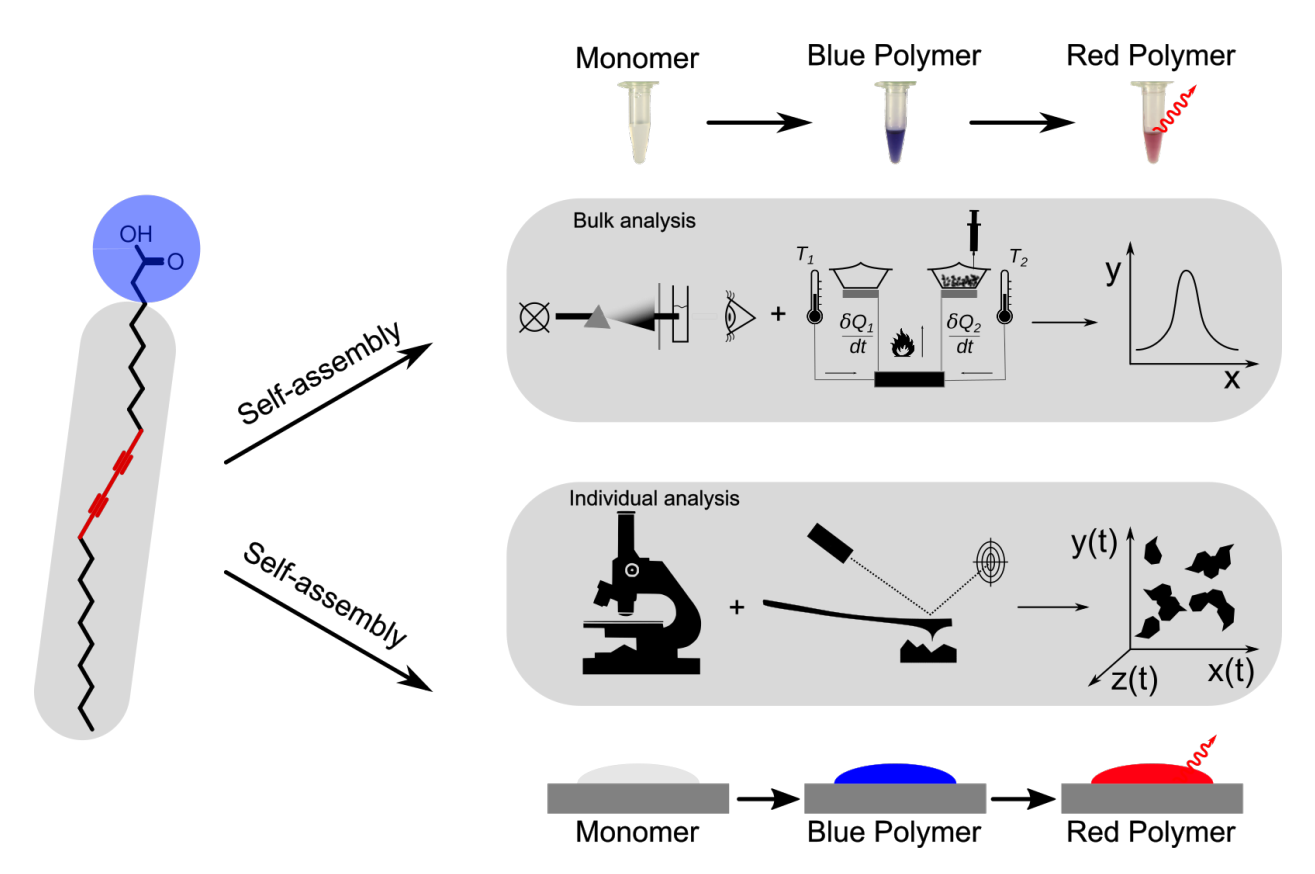
The push-pull fluorophores have been widely investigated and introduced into the market under the name Flipper-TR[®]. Due to its special design, a π donor at one end of the probe and a π acceptor on the other end these molecules can measure the membrane tension²⁰ as the planarity, and hence its electronic structure, is changing¹⁹. While the different states of PDA can be distinguished by fluorescence microscopy, these flippers need a more advanced technique (fluorescence lifetime imaging microscopy). The fluorescence lifetime²¹ is the crucial parameter for this probe. Therefore each system has its benefits and is worth to be investigated.

1.2 Aim of this Work

Great effort has been done to understand the blue-to-red transition and its interaction with lipid membranes.^{22–24} Nevertheless, its mechanism on a molecular level has not been addressed yet. Despite our general understanding of the mechanism of PDA, a clear picture of how a large variety of different stimuli causes this blue-to-red transition in each case is often lacking.

The aim of this project is to analyze the polydiacetylene-peptide interaction mechanism in mixed lipid systems and explain the transition more generally. The rough workflow is shown in Scheme 1.1.

1.2. Aim of this Work



SCHEME 1.1: Workflow of the (P)DA investigation in its different states: monomeric, blue- and red polymeric state. The top row shows the employed techniques for bulk analysis like UV-Vis spectroscopy and differential scanning calorimetry. Here the average signal is captured. The bottom row shows techniques to get a closer look at local behavior of (P)DA.

As it is well known, the peptide melittin is able to penetrate lipid bilayers and form pores.^{25,26} Therefore, the diacetylene TRCDA monomer is incorporated into a soft lipid supported bilayer. After successfully growing monomer crystals, these can be polymerized by UV light and a blue-to-red transition can be induced. This environment simulates a typical peptide-lipid interaction which occurs, when a bee injects its venom (melittin) into a host. The mechanosensitive PDA is investigated by various microscopy techniques and differential scanning calorimetry to shed light on the activation of the red state by the peptide melittin. It is hoped that the gained knowledge will establish the basis for the development of a microscopic force probe sensor.

This work is embedded into the context of a series of PDA related studies in our group. Infrared and UV-Vis studies has been performed on an amphipilic diacetylene derivative in its monomeric and polymeric form.²⁷ Therefore the UV-irradiation time ("UV dose") is determined to undergo from the monomer → polymer (blue state) → polymer (red state) to a final degradation state. The samples are further investigated by IR where the different bond vibrations of the double - and triple bonds are assigned and clarified according to the different states of the (P)DA. Another investigation is directed towards a deeper understanding of its mechanosensitive potential. PDA is studied by atomic force microscopy (AFM) and can be stimulated (converted from its blue to red form) by defined forces provided by the cantilever of an AFM. In a specific mode, called friction force microscopy, the AFM is able to distinguish between lateral and vertical forces. PDA reacts on the nanoscale quite anisotropically: only lateral forces seems to be responsible to induce the blue-to-red transition.⁶

The final group objective of our different PDA related research areas is to provide a calibrated force probe sensor integratable into biological membranes. In such an environment the peptide-lipid interaction can be studied by determining the increasing fluorescence signals in real time. These signals can be converted into forces after a successful calibration via AFM.

1.3 A short History of Polydiacetylene

In the year 1896 Alex Hébert described an unknown highly unsaturated fatty acid, which was found inside of the viscous orange green fluorescent oil of the Onguekoa Gore Engler tree seeds. When exposed to air, this new acid changed its color to pink over time. He suspected that light might also influence this process. The name isan acid was suggested for this acid.²⁸ The characteristics of this oil attracted other research groups, an another investigation was started by A. Steger and J. van Loon around 40 years later. After a series of fractionation processes (hydration, distillation in a high vacuum and recrystallization) of the oil, they confirmed the characteristics of this new acid. Furthermore, they concluded the presence of two unsaturated triple bonds and one double bond in the compound.²⁹

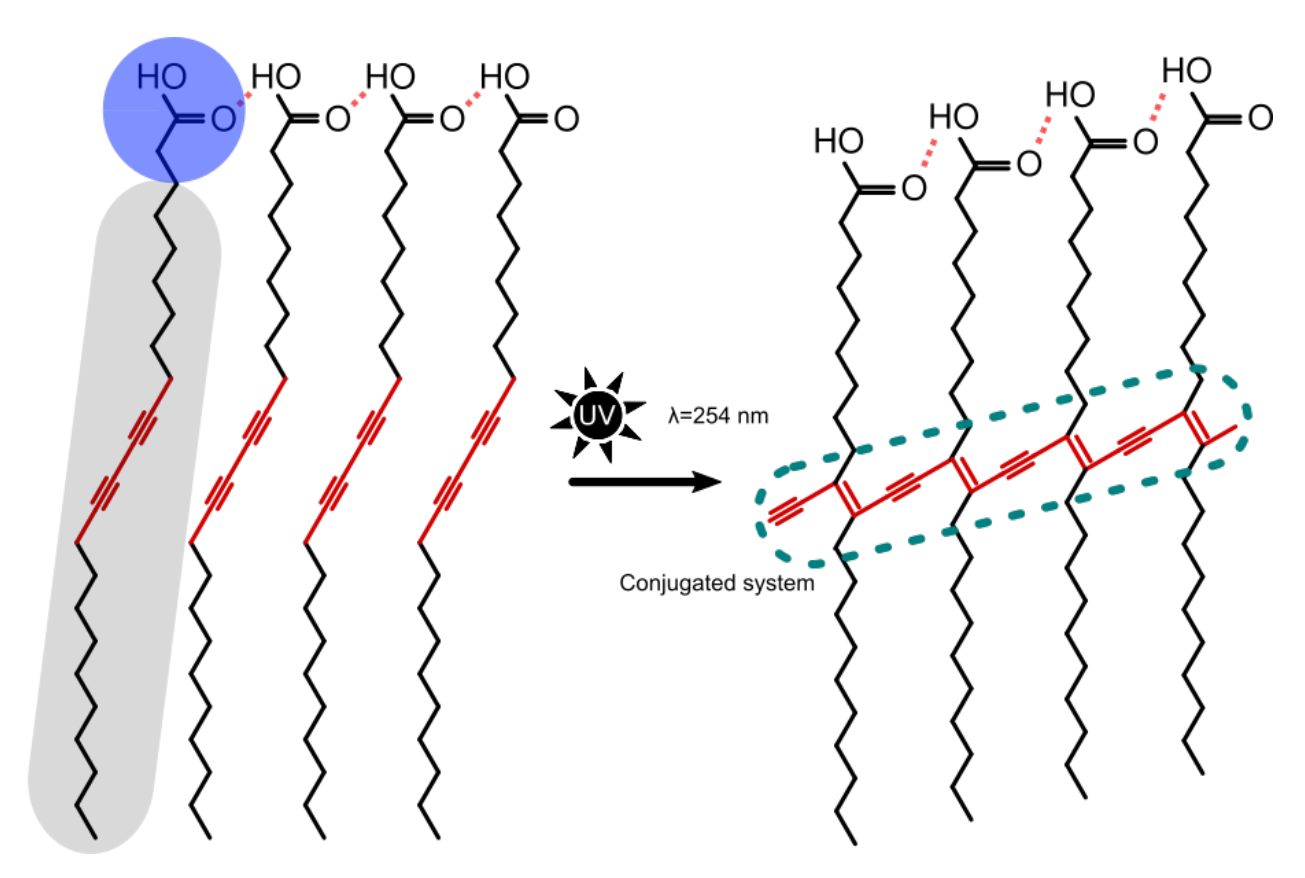
Gerhard Wegner et al. (1969) published a systematic investigation of these so-called conjugated diacetylenes. They studied the solid state polymerization of different diacetylene

derivatives by UV-light or heat below their melting point. Depending on the derivative, a strong change in color was observed for the monomer to polymer transition. For example the transparent crystals of 2,4-hexadiin-1,6-diol-bis-phenylurethane (Scheme D.1) developed quickly a deep blue color when exposed to light. Later the color shifted to a glossy copper red.³⁰

Schmidt et al. investigated the requirement for a successful solid state polymerization. The correct distance between the reactive centers of the adjacent monomers is the key element in this process. Due to the simplicity of the synthesis, self-assembling and electronic sensitivity towards environmental perturbations (pH change¹², mechanical stimuli³¹ and other biomolecules like peptides⁴ etc.) it was only a question of time till these highly-conjugated polymers were pursued for sensing applications.

1.4 The Structure of (Poly)Diacetylene

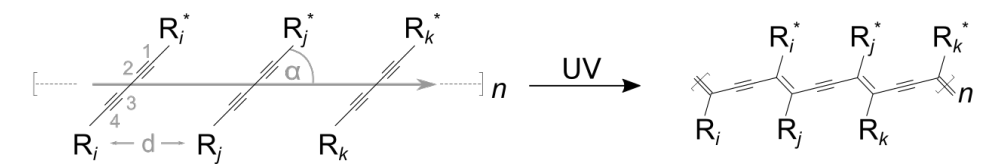
Diacetylene (DA, Scheme D.2) is an organic compound which comprises two ("di") triple bonds ("acetylene") separated by a single bond ($R_i-H-C\equiv C-C\equiv C-H-R_i^*$). This unit can be integrated into a variety of molecules. The following work discusses exclusively diacetylene with a conventional head/tail amphiphilic character: one part of the molecule is hydrophilic, composed e.g. by a carboxylic head group (typically attached via an alkyl chain spacer from the DA unit), while the rest of the molecule is hydrophobic. An illustration is provided for 10,12-Tricosadiynoic acid (TRCDA, Scheme D.4) in Scheme 1.2. The two acetylene groups ($R-C\equiv C-R$) are located at the 10th and 12th position of the aliphatic chain, while the overall length, counted as numbers of carbon atoms, is 23 (Tri:3, icosa:20). Due to its amphiphilic character and the ability to form hydrogen bonds between the carboxylic head group, the molecule is able to self-assemble in an aqueous solution into a highly ordered structure. After the irradiation of the monomer with UV light ($\lambda \approx 254$ nm), a solid-state topochemical 1,4-addition reaction converts the monomer into a polymer.



SCHEME 1.2: On the left side 4 aligned amphipilic diacetylene molecules are shown (10,12-Tricosadiynoic acid). For the first one, the hydrophilic head group is highlighted in blue and the hydrophobic part in grey. The diacetylene unit is colored in dark red. The hydrogen bonds of adjacent carboxylic head groups are indicated by the pink dotted line. After a successful polymerization by UV light, the polymer is shown on the right where the conjugated system is highlighted in green. This is responsible for PDA's colorful nature.

1.5 The Principle of the Solid-State Polymerization

The order and the distance between monomers after the self-assembly process is critical for an efficient polymerization.^{32,33} The basic chemical structure for the polymerization process is given in Scheme 1.3. The aligned monomer structure is shown on the left, while the right



SCHEME 1.3: Solid-state topochemical 1,4-addition reaction of diacetylene. The distance d between two adjacent monomers is around d = 4.7 - 5.2 Å, while the bond angle $\alpha \approx 45^{\circ}.^{34}$ Adapted with permission from [34, 35].

side represents the reorganized structure after the topochemical 1,4-addition reaction polymerization at the triple bonds. The symmetry of the space group for monomer and polymer crystal is maintained.³⁶ No polymerization can be observed for a melt due to the lack of order of the molecules' arrangement. 37 The distance between two adjacent monomers is around d = 4.7 - 5.2 Å for polymerizable diacetylenes, including non amphipilic derivatives, while the bond angle $\alpha \approx 45^{\circ}$ depends on the specific substituent.^{34,38} These distances are close to the values suggested by F. L. Hirsehfeld and G. M. J. Schmidt for a topochemical controlled solid state polymerization (d = 4 Å). For derivatives satisfying the spacing along two different directions, the polymerization occurs along the closer one matching $d.^{39}$ Diacetylene LB films can be spaced narrower: At the air-water interface 10,12-pentacosadiynoic acid (PCDA, Scheme D.7) starts to increase the from zero pressure of $25\,\text{Å}^2$. This would corresponds to a 2.5 nm distancing. Successful polymerization has been done in this study with overcompressed PCDA films at 8 Å^2 . But as trilayer formation is suggested by the authors, this would indicate similar spacing. In an earlier study of diacetylene LB films on water, the authors came to the result, that if the derivative is polymerizable, it could be done anywhere between the zero to the collapse pressure. 41 Typically at zero pressure clustered monomer domains are already formed, therefore the spacing cannot be determined under these circumstances.

In case of amphiphilic DA the substituents of the derivatives and their ability to form hydrogen bonds are a key factor for the polymerization because these hydrogen bonds determine the orientation and spacing in the crystal lattice.⁴²

The free radical chain reaction of the polymerization process includes three steps: initiation, propagation and termination. The initial free radicals are mostly created by UV-irradiation among others (γ - and x-ray ($h\nu$) or thermally (kT)).⁴³ Propagation and termination are competing processes. Polymerization can be divided into two different types: diffusion-limited and diffusionless. In the first case, the covalent bond between two adjacent repeating subunits in the polymer allows for a shorter spacing than the initial distance of the neighboring monomers. This increases the gap to the next monomer in the polymerization direction. Therefore the crystal structure has to rearrange or the oligomer will be

trapped and cannot be extended any further. In the second case, the distance between the two adjacent repeat units before and after the polymerization does not change. Schmidt et al.³² claimed that solid state polymerization falls into the diffusionless category. No linear contraction takes place, only a rotation of the monomer is necessary for a successful polymerization. The distance between the adjacent monomers has to be smaller than d=4 Å. They cited the DA crystal data for a diacetylenedicarboxylic acid dihydrate ($C_5H_2O_4$). This compound was investigated by J. Robertson et al. Here the distance is d=3.75 Å.⁴⁴ The authors claim that the crystal data corresponds to the monomer, however they report that the crystal turned black almost immediately after exposure to X-rays, which indicates transformation into a polymer. This raises concerns if this crystal data is actually free of doubt from the monomer. Wegner at al. later pointed out that the study of the monomer crystal structure was challenging: the x-rays already triggered the DA compound polymerization. XRD at low temperature (T=120 K) overcame the problem. The projection of the crystal structure onto the main chain plane is shown in Figure 1.4 for the monomer and polymer of polydiacetylene-bis(toluene-sulphonat) (PTS, Scheme D.23). The crystal data is

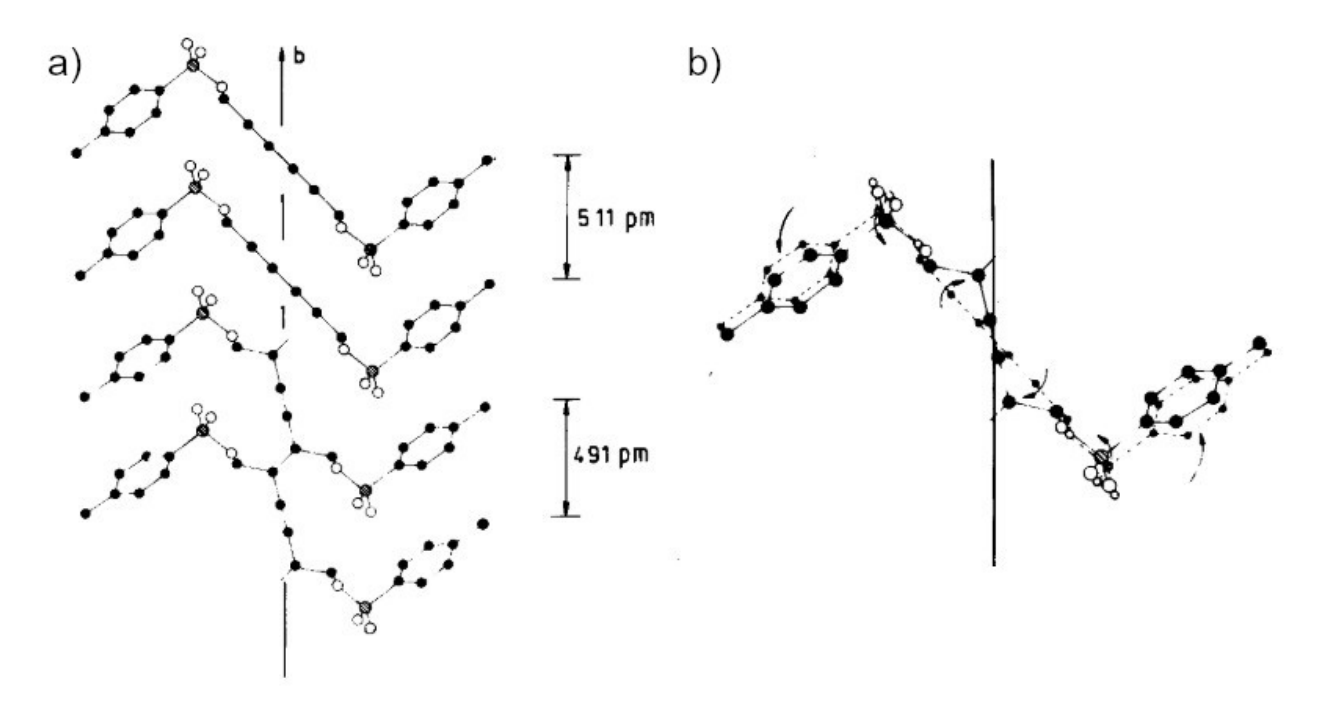


FIGURE 1.4: a) PTS arrangement shown orthogonal to the backbone plane for monomer (top) and polymer (bottom). b) Overlay of monomer structure (dotted) onto the polymer structure (continuous line). Adapted with permission from [38].

given in table Table 1.1.^{38,45} The backbone sequence alters between an acetylene (-C≡C-)

Table 1.1: Crystal structure	data for PTS	S for mono- and	l polymer.
------------------------------	--------------	-----------------	------------

	Monomer ³⁸	Polymer ⁴⁵
a(Å)	14.61	14.77
$\mathrm{b}(\mathrm{\AA})$	5.11	4.91
c(A)	25.56	25.34
β (°)	92	92
Space group	$P2_1/c$ (Monoclinic)	$P2_1/c$ (Monoclinic)

and ethylene group (>C=C<). This leads to a newly formed conjugated π system due to the hybridization into sp and sp² orbitals of the carbon atoms. The sp orbitals create σ -bonds to their adjacent carbon orbitals along the backbone, the remaining p_x and p_y orbitals of each C atom are responsible for the additional π -bonds (one π -bond in case of sp²). The new

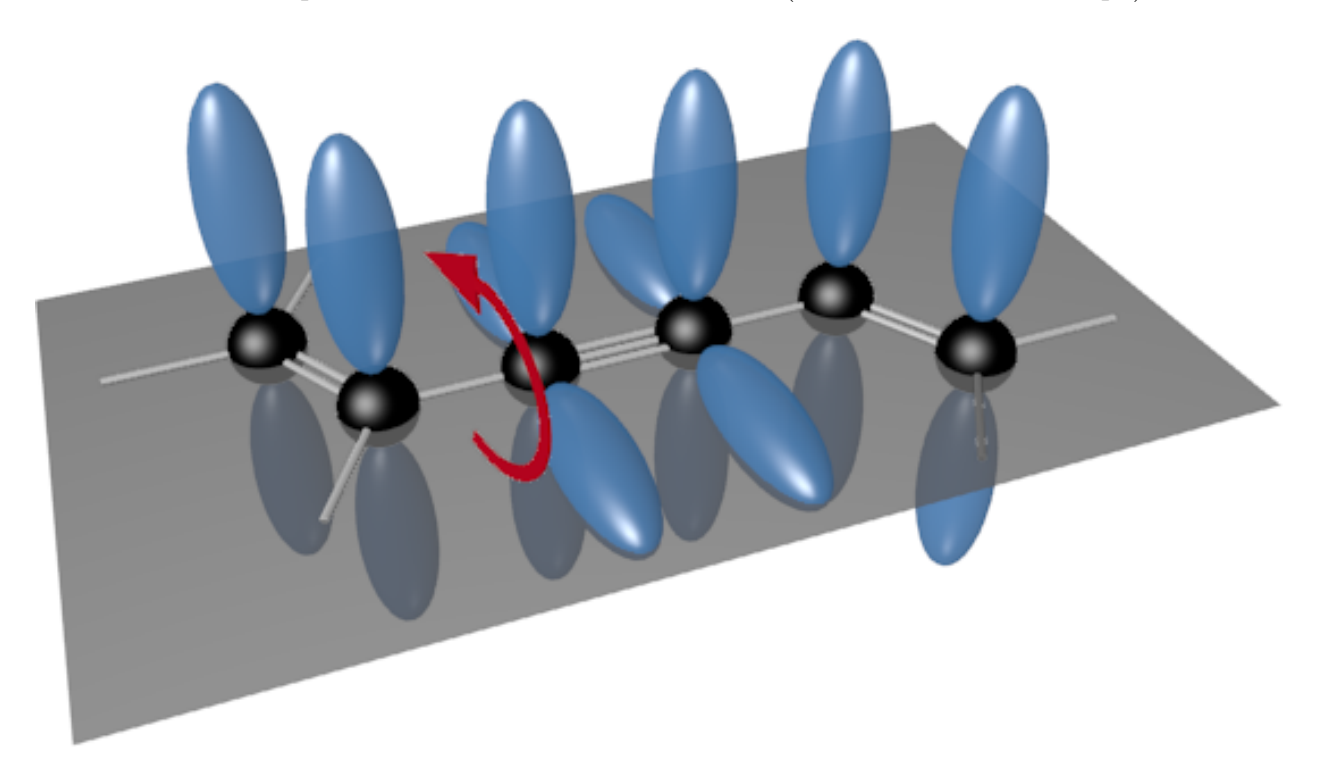


FIGURE 1.5: Schematic representation of the $2p_z$ and $2p_y$ orbitals of polydiacetylene backbone structure. σ -orbitals are not shown. The red arrow indicates the often used (too) simple picture to shorten the conjugation length.⁴⁶

electronic structure gives rise to the colorful nature of Polydiacetylene (PDA, Scheme D.5). Furthermore, every stimuli influencing the conjugated π network (e.g. mechanical stress³¹, pH¹², peptides²³ etc.) will alter the electronic structure and therefore the optical appearance.

1.6 The Two States of Polydiacetylene

PDA is a great candidate for sensing applications due to the circumstance that the polymer has two different states. By external stimuli it is possible to induce a shift from one state into the other. In general, the polymerized diaceylene initially appears in a strong blue color in reflectance or transmission. When exposed to e.g. sufficient heat, the sample reaches a characteristic temperature and changes its color to red. Hence, these states are called blue state and red state.⁴⁷ It is worth mentioning that this convention is counterintuitive in the field of spectroscopy. It describes the reflectance/transmission characteristics unlike the common view on the absorption.

The absorption peaks are around $\lambda_{max} = 640$ nm and $\lambda_{max} = 540$ nm at room temperature respectively.³⁷ Besides these colors, others like violet, orange-red, purple, etc.^{30,48} and even additional states^{49,50} can be found. In this work *blue* and *red* will be generalized for the two main states. Besides the chromism, the red state has an allowed fluorescence pathway, which can be detected by fluorescence microscopy, making PDA an ideal candidate as a sensor.

For clarity reasons, in this work PDA is considered to have only two states. However, it is worth mentioning that in PDA's UV spectra the isosbestic point (at this wavelength the absorbance is invariant, compare e.g. Figure 1.15) cannot always be determined, indicating that the blue-to-red transformation is not a simple transformation between only two absorbing species. 47,51,52

1.6.1 Electronic Structure: Ground and Excited States

The electronic states of PDA can be well-described by the Pariser-Parr-Pople-Peierls (PPPP) model.⁵³ This model is a tight-binding model (Hueckel model in chemistry based on linear combination of atomic orbitals for π -systems) of the π -electrons taking the electron-electron interaction (Pariser-Parr-Pople) for long range $(V \sim \frac{1}{r})$ and the electron-lattice (Peierls) coupling of the π -electron system into account.

The PDA backbone is spatially centrosymmetric and belongs therefore to the $C_{2h}^{36,54}$ point group: it has a rotation symmetry for 180° along the principal axis and a center of

inversion (for every point p_1 at \vec{r} exists another indistinguishable point p_2 at $-\vec{r}$). The normal of this mirror plane lies parallel to the main principal axis and is therefore called horizontal mirror plane (compare Figure 1.6). In group theory, this combination makes the

$$X \rightarrow X$$
 $X \rightarrow X$
 $X \rightarrow$

FIGURE 1.6: Simplified backbone of PDA. The grey dot shows the principal axis which points in the same direction as the surface normal for the mirror plane ("h" - horizontal). A rotation around this axis by 180° or an inversion at the middle point results in the original structure. Therefore PDA belongs to the C_{2h} point group.

molecule a member of the point group which is denoted C_{2h} . C indicates the proper rotation for the point group symmetry operation, while the subscript index n indicates a rotation by an angle of $\frac{2 \cdot \pi}{n} = 180^{\circ}$ for n = 2. h indicates a horizontal mirror plane. When applying a rotation operator around the principle axis, the sign of the WF (wave function, describes the molecular orbital) for a C_{2h} symmetry can end up either symmetric (+) or antisymetric (-), labeled as a and b respectively. This system also has an inversion symmetry, (invariant to an inversion operator $\vec{r} \rightarrow -\vec{r}$), denoted as g (gerade) and u (ungerade) for the symmetric and antisymmetric case respectively. The WF ψ_1 e.g. is symmetric under rotation around the principal axis and antisymmetric under inversion and therefore labeled as a_u (compare Figure 1.7)a). In order to determine the symmetry for the states (notation: $a \to A, b \to B$), the symmetries of the participating orbitals have to be multiplied. In the ground state (S_0) , the 6 electrons fill the orbitals $\psi_{1...3}$. Completely filled orbitals lead to symmetric and gerade states: $a_u \cdot a_u = b_g \cdot b_g = A_g$. Therefore the ground state (S_0) is labeled as $1^1 A_g^{56}$ (compare Figure 1.7b). The first number (1) is an index for this symmetry increased by 1 with each higher state with the same symmetry (here A). The B states have their own index. The superscript (1) is the multiplicity of the energy level. It is calculated from the total spin angular momentum by the following formula: $m = 2\sum_i s_i + 1$ (here $2 \cdot \left(\frac{1}{2} - \frac{1}{2}\right) + 1 = 1$). This state is called *singlet state*. For exited states, the symmetry can be either A_g or B_u .

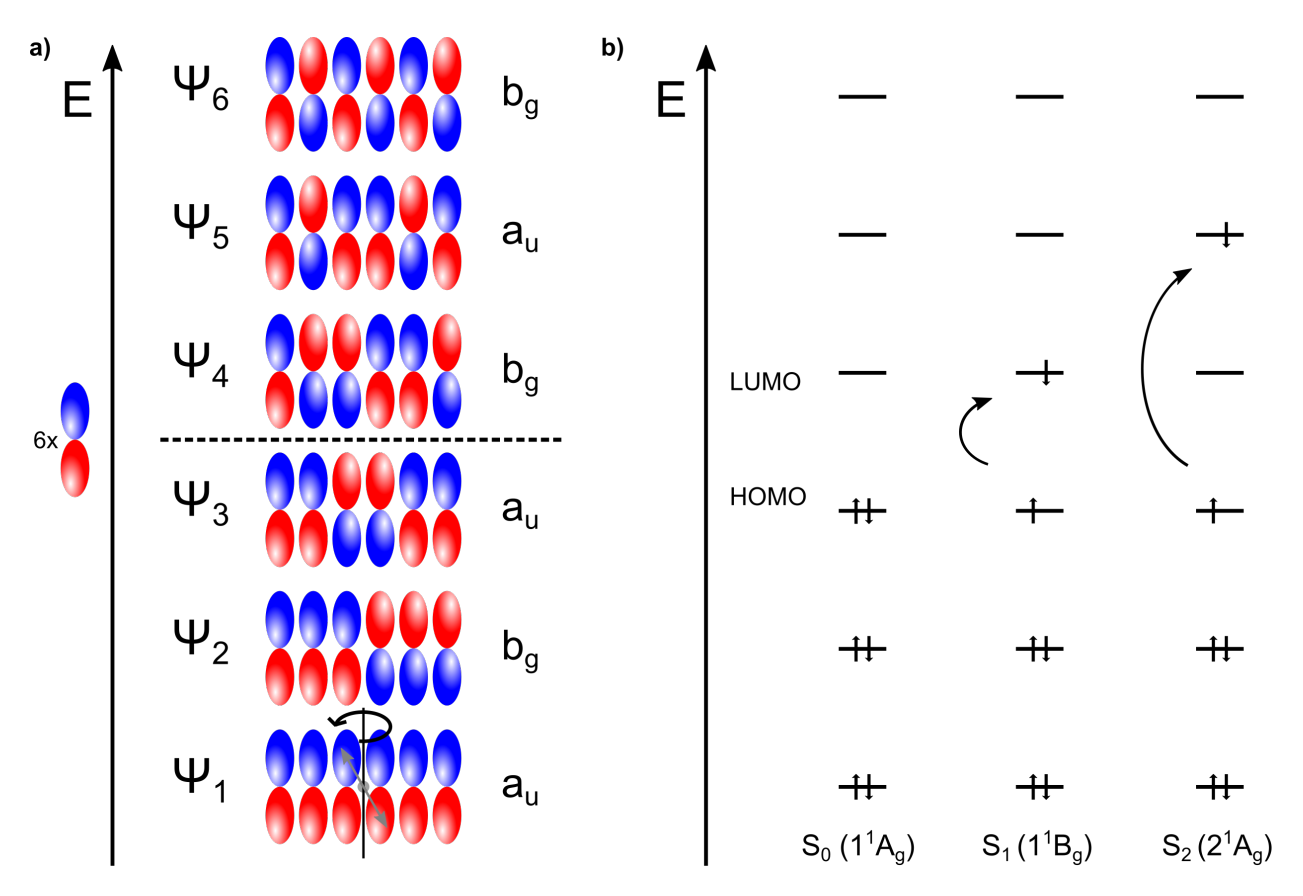


FIGURE 1.7: a) Determination of the ground state symmetry for PDA. The 6 p atomic orbitals are linearly combined building up the molecular orbitals $\psi_{1...6}$, each with an increased energy level and number of nodes (between a lateral color change of the p orbitals). For the first WF, the principal axis (bar) and the center of inversion (grey dot) are shown. Applying the symmetry operations of the C_{2h} point group (Identity, rotation, mirroring and inversion) the symmetry of the WF can be identified as either a_u or b_g . b) After filling the orbitals with the 6 electrons, the HOMO orbital (ψ_3) in the ground state (S_0) can be determined. For one-photon absorption and no interaction between electrons also the next two energy levels S_1 and S_2 are shown. If the electron-electron interaction is considered, $1B_u$ and $2A_g$ are inverted in blue state.⁵⁵

The symmetry is determined by multiplying the symmetry of the participating orbitals (half filled with an electron) eg. for S_1 : $a_u \cdot b_g = 1^1 B_u$ and for S_2 : $a_u \cdot a_u = 1^1 A_g$. For one-photon absorption and no interaction between electrons, the first excited free exciton state excited state (S_1) is labeled as $1^1 B_u$ while the following would be $2^1 A_g$. But in case of a long polymer chain, the order of the excited states $1^1 B_u$ and $2^1 A_g$ are exchanged. The case of blue PDA the $2^1 A_g$ state is 0.1 eV below the antisymmetric state.

For centrosymetric molecules the Laporte rule dictates that a transition is only allowed between states with different parity. As these two states have the same symmetry (A_q) , the transition is optically (dipole-) forbidden. Therefore, only red PDA shows strong fluorescence (where the 1^1B_u state lies below the 2^1A_g). The energy level diagram for the blue and red form of PDA is shown in Figure 1.8.

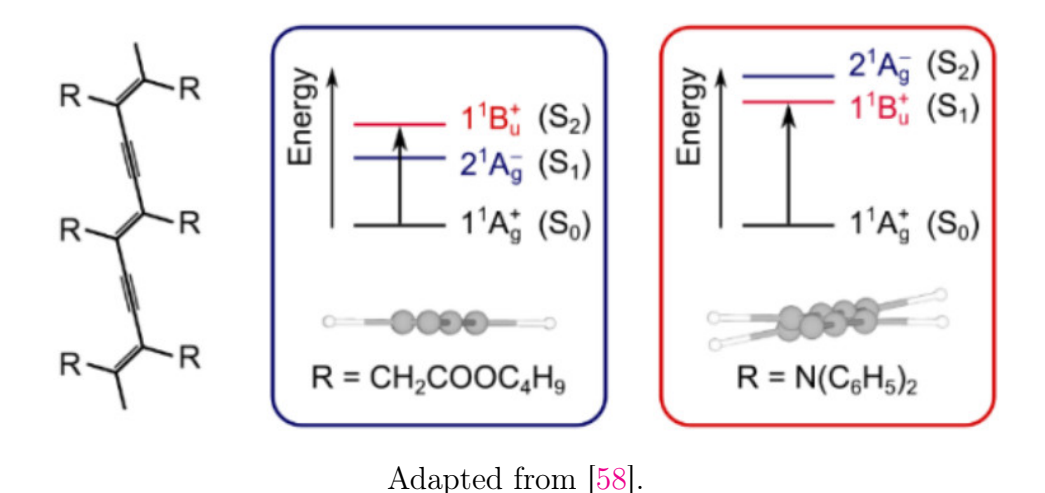


FIGURE 1.8: Arrangement of the different states in blue and red PDA. For blue PDA, the 2^1A_g lies below the 1^1B_u state and an optical decay (fluorescence) is forbidden unlike in the case of red PDA. The "+" and "-" refers to the reflection symmetry along an arbitrary plane containing the internuclear axis and not discussed here further.

1.6.2 Geometry of the Blue and Red Configuration

A certain PDA derivative backbone structure can be represented as an intermediate state between two extreme electronic configurations but at riene

 $(-RC=C=C=CR=)_n$ and acetylene structure $(=RC-C\equiv C-CR=)_n$.⁶² For both types, representative PDA derivatives can be found e.g. poly(5,7-dodecadiyne-1,12-diol-bis pheny-lurethane $(TCDU)^{63}$ and PTS^{64} respectively. The total length of the repeat unit is nearly the same (4.89 Å vs 4.87 Å).⁶²

In the case of TCDU, it has been shown by a Raman spectral study that it adopted an acetylene electronic structure at low temperature or high pressure (e.g. T < 100 K and p > 5 kbar). At high temperature or low pressure a butatriene structure was observed. Hence, it was suggested that the blue state is presented by an acetylene electronic configuration while the red state is described by the butatriene structure. This theory could not be generalized and was later disproved by a crystallographic study supported by quantum

chemical calculations⁶⁷. Solid state nuclear magnetic resonance spectroscopy studies on several PDAs ruled out the presence of the butatriene structure.^{66,68} In the ground state, the acetylene structure is energetically favored. Only for very short polymers (n < 6) the butatriene structure occurred.⁶⁹ Therefore the difference between the blue and the red state has to arise from other characteristics.

Different models were proposed for the blue-to-red transition. It was suggested³⁴ that the planar conjugated chain transforms to a segmented planar (Kuhn chain model⁷⁰) or a continuous curved "worm-like" chain⁷¹ (Porod-Kratky chain^{72,73}) but also a zig-zag shape was considered⁷⁴. The different models are shown in Figure 1.9. An uniform model hasn't been accepted yet.

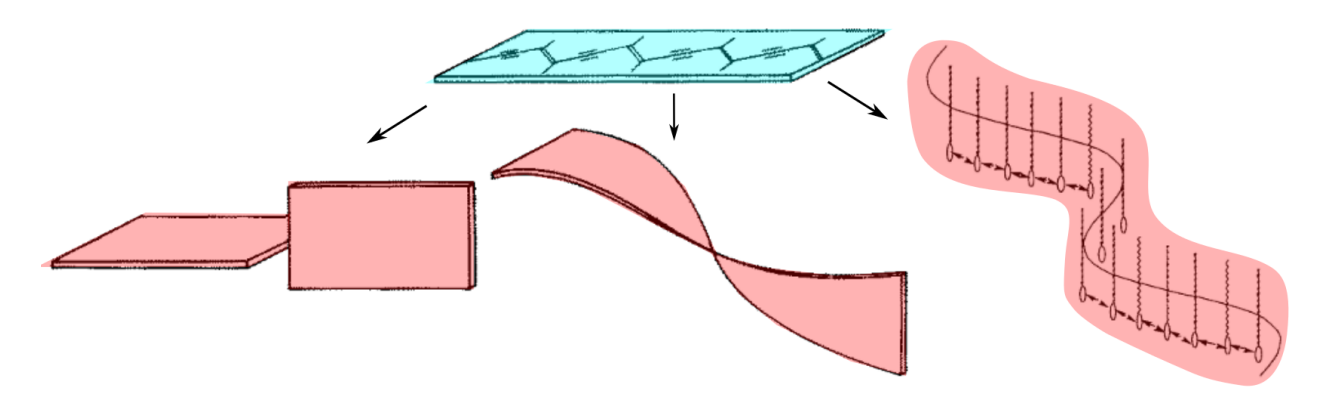


FIGURE 1.9: Different models for the blue-to-red transition: a) fully conjugated planar chain, b) segmented planar Kuhn chain model, c) worm-like Porod-Kratky d) zig-zag model. Figure adapted from [34, 74].

1.6.3 The Problem of the Effective Conjugation Length

Even though the concrete geometric structure is still an ongoing discussion, the general trend from a blue planar to a non planar red structure^{68,75} is accepted. In case of hydrogen bond forming PDA derivatives this is supported due to a less distinct hydrogen bonding network of the side chains in the second case.⁷⁶ It is argued that the *effective conjugation length* (ECL) is shortened by twisting of the backbone or other defects when a transition from blue to red PDA takes place.^{77,78}

The energy difference between the ground and the first excited state depends on the length of the conjugated π system: the larger the system, the smaller the gap. Similar to the particle in a box principle, the HOMO and LUMO energy level would approach each other (ΔE decreases) when the distance between the two potential walls increases. This gap can be calculated as a function of the conjugated system repeat unit by the modified free electron Kuhn model.⁷⁰ ΔE can be expressed by the empirical equation $\Delta E = E_1 + A/n$ where E_1 is the band gap energy of the monomer, A a constant and n the number of repeat units.⁷⁹ To measure the band gap experimentally, a series of compounds with increasing repeat units can be synthesized. The gap between the ground and excited state can then be measured by UV-Vis spectroscopy. A comparison is shown in Figure 1.10. A shortening of the π conjugated system results in an absorption at lower wavelength.⁸⁰

In general the electronic structure of matter can be described as follows: starting from individual atoms and combining them into a more complex system (atomic orbital theory extended by the linear combination of atomic orbitals: LCAO). Extending the theory to bulk material (crystals) the ansatz of solid state physics considers the whole crystal structure as the system taking the periodicity (e.g. Bloch wavefunctions) into account. The problem is that the ECL in a perfect quasi 1-D crystal of a PDA chain is not a precisely defined. In the literature the concept of the ECL is assumed to be a certain sub length of the whole polymer chain, an oligomer, which would have the same electronic characteristics as the whole PDA. 15 The ECL is rather described as "some undefined orbital related property that somehow determines the wavelength of maximum absorption λ_{max} ". ⁵⁴ Especially in case of the worm-like chain model it is impossible to define the ECL quantitatively^{54,81} and there is strong evidence for this continuous and smoothly curving model.⁸² Therefore the concept of the ECL was disputed in 1973 and an excitonic concept was proposed.⁸³ The allowed transition for blue PDA between the ground state $({}^{1}A_{q})$ and the lowest excited state $({}^{1}B_{u})$ with an excitation energy of around 1.9 eV (650 nm) is suggested to be exciton-related and therefore called excitonic transition.^{84,85} This exciton, a coupled electron-hole quasi particle bound by the Coulomb force, can be formed by absorbing a photon with an energy higher than the band gap. An electron from the valence band is promoted to the conduction

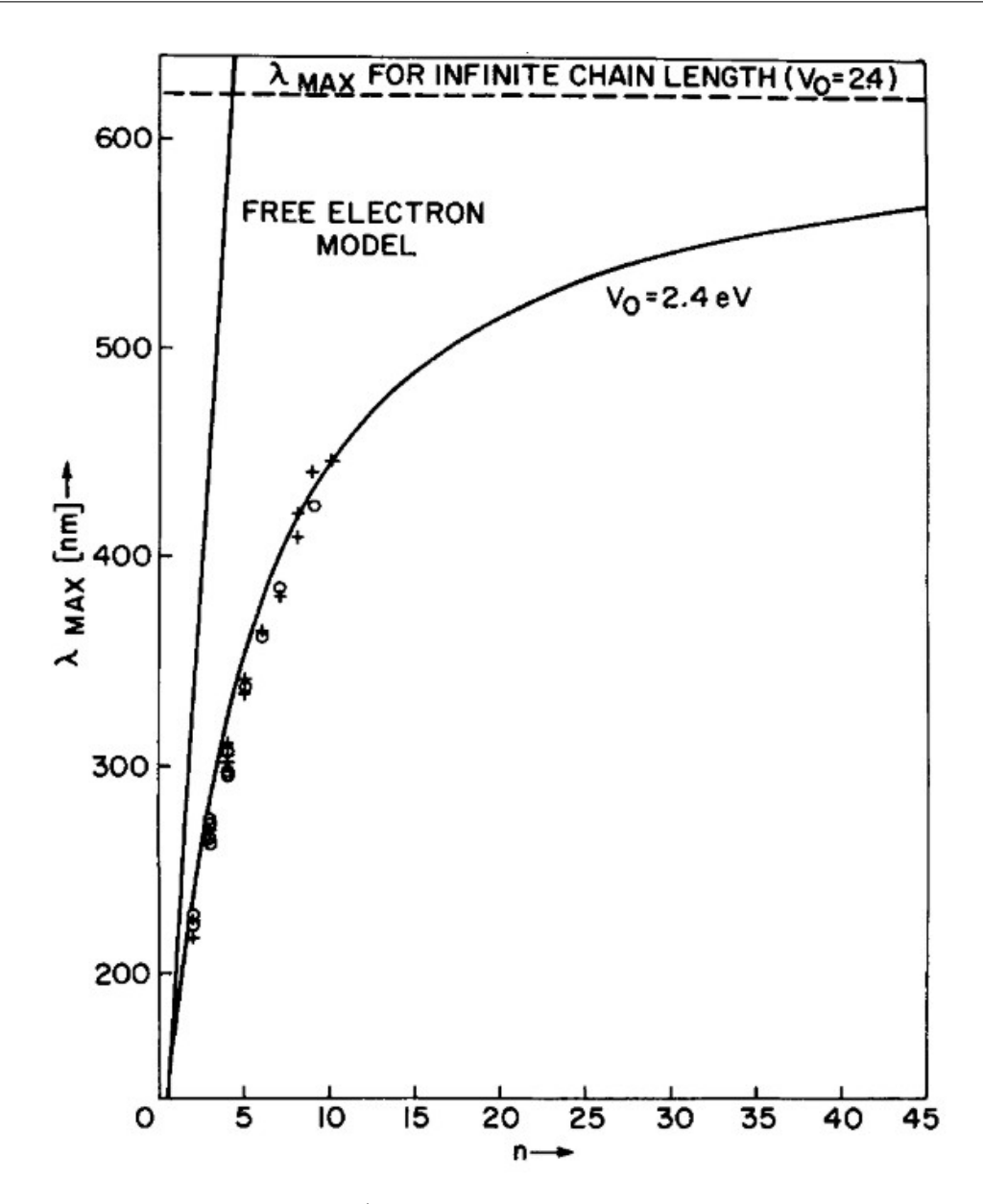


FIGURE 1.10: Theoretical (free electron model and modified free electron model of Kuhn⁷⁰) and experimental data for the absorption peak λ_{max} as a function of the repeat unit, "+" for polyenes (alternating double and single bond), "o" for polyenynes (alternating triple, single and double). Adapted with permission from [80].

band and leaves a hole behind. This transition is often coupled with vibronic sidebands, which are multiples of vibrational excitations for $C=C/C\equiv C$ and therefore called vibronic transitions.^{54,85} A typical UV-Vis spectra for the transition is shown in Figure 1.11. Both spectra show the characteristic main peak (excitonic transition) and a energetically higher side peak (vibronic satellite). For the blue state (continuous line) the peaks are at 620 nm and 580 nm while for the red state (dashed line) the peaks are located at 540 nm and 490

nm. The shift was induced by the Phospholipases A2 enzyme.²⁴

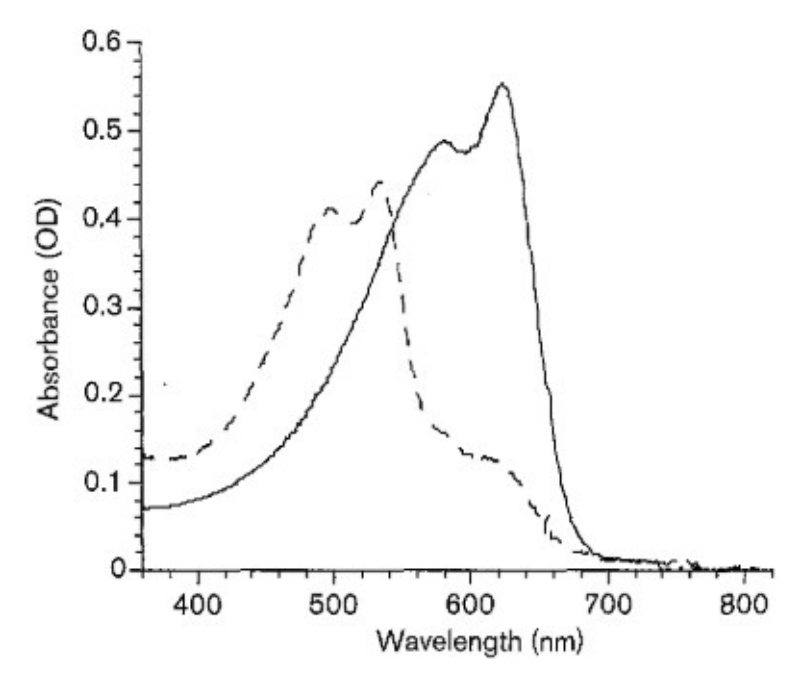


FIGURE 1.11: Characteristic UV-Vis Spectra of PDA (TRCDA mixed with DMPC) before (continuous line) and after inducing the blue-to-red transition by the enzyme Phospholipases A2. Adapted with permission from [24].

The exciton has a typical length of around 1 nm (around 5 unit cells). This was derived by the Stark shift (energy level splitting similar to Zeeman effect but for electric fields) for PTS and several other PDAs.^{83,86} Besides its small Bohr radius, this exciton is an excitation of the whole crystal chain: it has been experimentally shown that the emission of a single exciton can be extended up to 20 µm implying that the wave function of the exciton has a macroscopic coherence length.⁸⁷

The length of an ECL is normally much longer than the length of the exciton. Therefore, the ECL does not affect the excitonic state. For example, the order in the red state for the PDA 4BCMU should be different for various systems. But the absorption spectra for 4BCMU do not differ much between its crystal⁸⁸- and gel⁸⁹ form.¹⁵

Besides the structure and their planarity, the order-disorder of the different PDA states is an ongoing discussion. Originally, it was thought that the blue state is more ordered than the red state but recent findings showed almost perfect order in red crystals which behaved as a perfect quasi 1-D electronic system.^{87,90} Further experiments demonstrated an even higher order in the red state compared to blue state.⁹¹ As the bond length between the two states

does not necessarily shift much, the general theory explaining the two states includes a twist in the backbone and it is therefore determined by the attached side group. ^{15,68}

1.6.4 Quantifying the Blue-to-Red Transition

To quantify the blue-to-red transition, the colorimetric response⁹² (%CR) is defined as follows:

$$\%CR = \frac{RA_0 - RA_1}{RA_0} \cdot 100$$

where the relative intensity RA_i is defined as

$$RA_i = \frac{A_i^{blue}}{A_i^{blue} + A_i^{red}}$$

 A_i^{blue} and A_i^{red} are the absorbances at the wavelength $\lambda_{blue} \approx 650$ nm and $\lambda_{red} \approx 550$ nm respectively. The index i = [0, 1] refers to the absorbance before and after inducing the transition. Applying Beer's Law $(A = \varepsilon \cdot c \cdot l)$ and the definition of the molar concentration $(c = \frac{n}{V})$ where n is the number of moles of blue or red PDA, the relative intensity RA_i can be expressed as:

$$RA_{i} = \frac{n_{i}^{blue}}{n_{i}^{blue} + \frac{\varepsilon_{i}^{red}}{\varepsilon_{i}^{blue}} n_{i}^{red}}$$

When assuming similar extinction coefficients within one state of PDA (blue and red respectively) at both wavelengths ($\lambda_{blue} \approx 650$ nm and $\lambda_{red} \approx 550$), RA_i is equal to the mole fraction of blue PDA before and after the transition respectively. Extinction coefficients for the blue form of PDA could not be found, but for the red form, the values are within a similar range: $\varepsilon_{535} = 1.50 \cdot 10^4 \frac{1}{\text{nm}}$ and $\varepsilon_{500} = 1.61 \cdot 10^4 \frac{1}{\text{nm}}$.³⁷ Please note that the deviant wavelengths (535 nm and 500 nm) arise due to different prominent peaks for blue and red of the studied PDA ($C_{12}H_{25}-C\equiv C-C\equiv C-(CH_2)_8-COOH$ LB multilayer treated by ethanol). Hence the colorimetric response %CR describes the amount of PDA migrating from the blue into the red state expressed in percent. An example is given in Figure 1.12 where the CR was calculated for the transition shown in Figure 1.11.

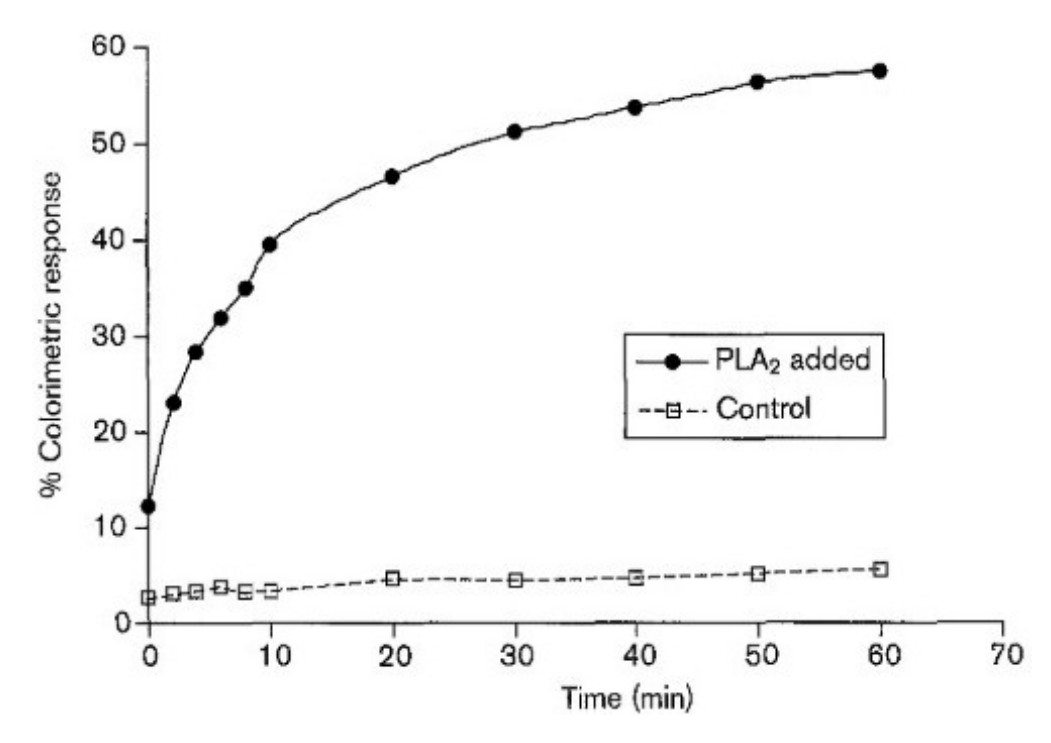


FIGURE 1.12: Colorimetric response of PDA (TRCDA) mixed with a soft lipid (DMPC) exposed to Phospholipases A2. Adapted from [24]

1.7 Different Stimuli for Inducing Chromism in Polydiacetylene

Polydiacetylene can be stimulated by a wide range of external influences. The following section will give an overview about common techniques employed to induce a transition of the polymer and how chemical modification is able to tune its characteristics.

1.7.1 Temperature:

Reversible and Irreversible Thermochromism

Numerous crystal structures undergo phase transition upon thermodynamic parameter (e.g. pressure or heat) changes. ⁹³ Therefore it is not surprising that this behavior also applies to polydiacetylene crystals. These phase transition coincide with a color change. If the crystal changes its spectra with temperature, it is commonly named thermochromic. ⁴³ Two types of thermochromic transitions are possible: the reversible and the irreversible transition.

By altering the system's temperature, the crystal structure will adapt to its new environment. Hence, a change in the electronic structure is possible. As the temperature change is one of the simplest external stimulus to induce a blue-to-red transition, it has been widely employed to study PDA systems.

There are many examples in the literature of PDA derivatives that cannot undergo a reversible transition, among which TRCDA and PCDA. 94–96 For sensing applications, a reversible detector would be desirable. As it has been pointed out in section 1.5 the intramolecular hydrogen bonding network is important for the geometric structure which leads finally to its electronic configuration. Therefore, it was suspected that altering the intramolecular forces could influence the reversibility behavior. It could be shown that thermochromatic reversibility is possible up to 200 °C with a temperature change rate of 5000 Ks⁻¹ by peptide-based amphipilic polydiacetylene (10,12-pentacosadiynoic acid (PCDA), Scheme D.7). 97 Different approaches to achieve reversibility are discussed in the following section.

Hydrogen Bond Network

A direct control over the hydrogen intramolecular forces was achieved by increasing the number of hydrogen bonds per unit. Urethane-substituted polydiacetylene are able to undergo reversible thermochromic transition. For example Poly3BCMU (substituent group is $(-(CH_2)_3OCONHCH_2COOC_4H_9)$, shown in Figure 1.13) was analyzed by UV-Vis spectroscopy. The Poly3BCMU was investigated as a polymer film (evaporated from chloroform) with a thickness of ≈ 0.5 µm). After polymerization, the UV-Vis spectrum of the crystal showed a peak at $\lambda = 633$ nm at 26 °C while the sample appeared blue in transmission. By heating the sample up to 160 °C, the first peak decreased while another appeard at $\lambda = 476$ nm. By cooling down to 28 °C the blue peak reappeared. The film showed a yellow appearance around 120 °C, similar to the polymer dissolved in chloroform. The authors concluded that the urethane's intramolecular hydrogen bond network between the N-H and C=O stabilizes the planar PDA conformation which is disrupted while heating but restored while cooling (compare Figure 1.14 (c)). Further investigation showed that the thermochromic

$$O O U = CH_2$$
 $-(CH_2)_mOC-N-CH_2-C-O-C_4H_9$
 $+$

FIGURE 1.13: Urethane substitute which is responsible for the intramolecular hydrogen bonding between C=O and N-H. Adapted with permission from [50].

reversibility is completely destroyed upon heating above the melting point. In this case, the hydrogen bond network, parallel to the backbone, is disrupted irreversibly.⁷⁶

Another example is PCDA. As the carboxylic head group of PCDA does not create strong enough H-bonding between the side chains in order to maintain a reversible structure between the blue-to-red transition, the head group was functionalized to add another H-bonding group. The molecular structure of 10,12-pentacosadiynoic amino meta-benzoic acid (PCDA-mBzA, Scheme D.8) is shown in Figure 1.14 (c).

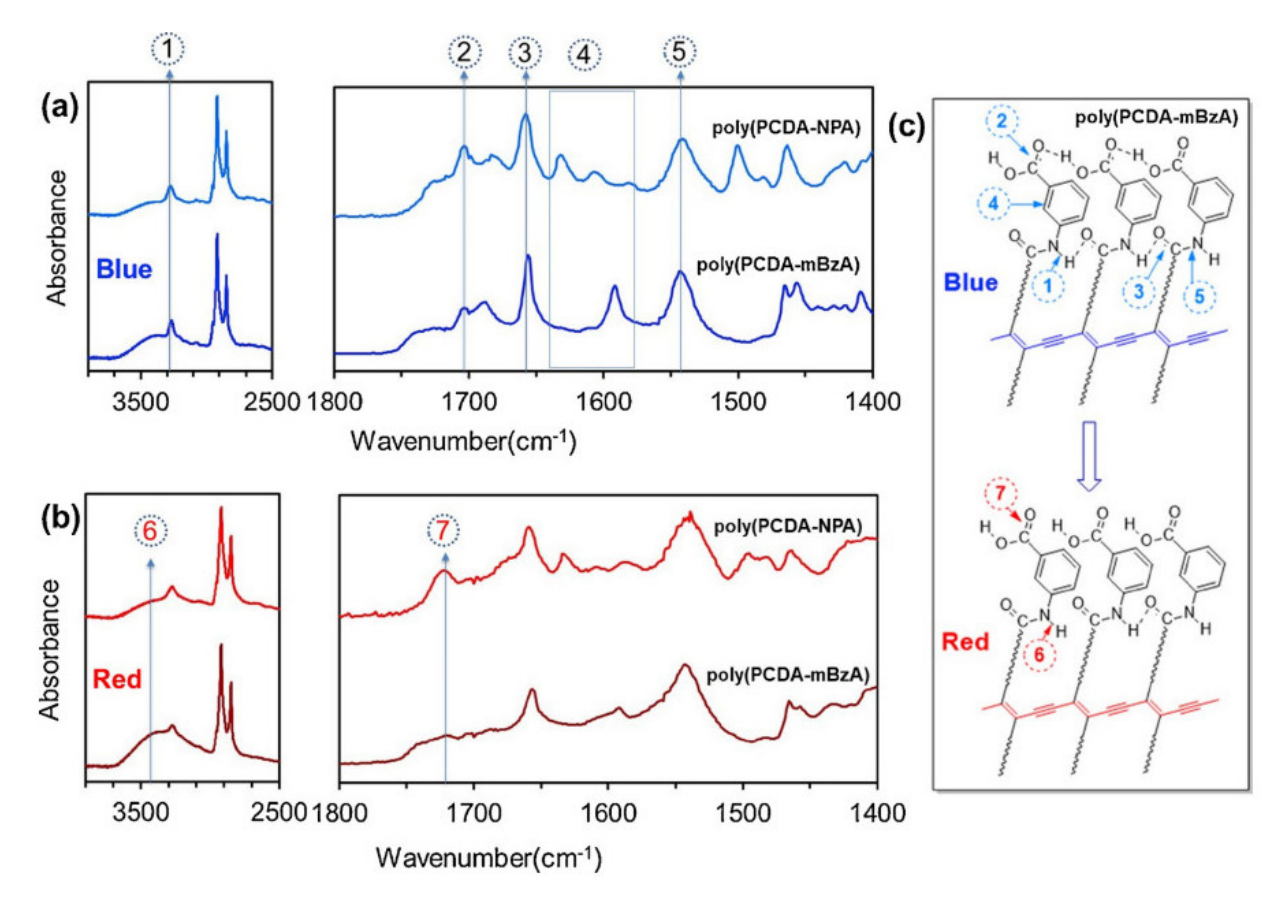


FIGURE 1.14: FTIR spectra of poly(PCDA-mBzA) and poly(PCDA-NPDA) films in blue (a) and red phase (b). The assigned peaks are shown in the molecular structure in (c). Adapted with permission from [98].

Fine tuning of the second H-bonding partner could be done by positioning a carboxyl group at the ortho-, meta- or para position of an attached aniline group (amino group attached to a phenyl ring) to PCDA. Polymerized Langmuir-Schaefer (LS) films of the meta derivative showed prominent reversibility after heating or increased pH. After polymerization, the typical blue- (here 640 nm) and red (here 580 nm, purple appearance) peaks were visible. But unlike a common transition where the intensity of the blue peak decreases while the intensity of the red peak increases, the blue peak was shifting towards the red peak while heating. The results are summarized in Figure 1.15. This continuous transition was

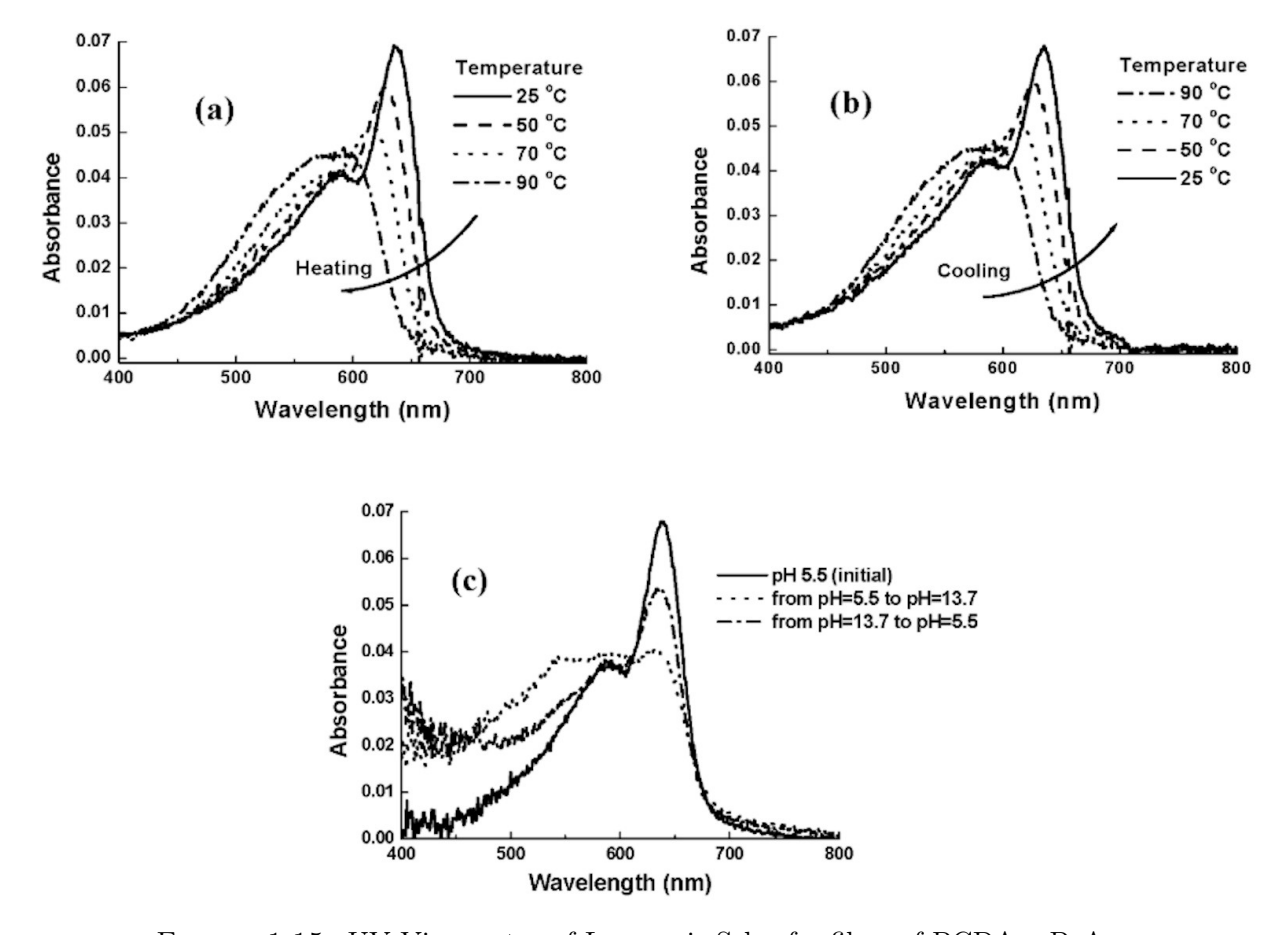


FIGURE 1.15: UV-Vis spectra of Langmuir Schaefer films of PCDA-mBzA show reversible blue-to-red transition behavior. a) Heating b) cooling c) pH variation. Adapted with permission from [99].

interpreted as a steady change in the average conjugation length of the π system.

By measuring at the specific vibrations for the H-bonds (ν (C=O) 1689 cm⁻¹ for the carboxyl group and ν (C=O) 1657 cm⁻¹ for the amide group) via Fourier transform infrared spectroscopy (FTIR), it was shown that the initial frequency was not shifted by increasing

the temperature up to 100 °C (see Figure 1.16 (b)). Therefore, the original supramolecular structure was able to restore to its initial state after cooling down to room temperature recovering the original average conjugation length of the π system. In case of PCDA, which is unable to recover back from the red to the blue state, a permanent shift to higher frequency is observerd (see Figure 1.16 (a)). Similar FTIR data was recorded 16 years later for the same compound (Figure 1.17), furthermore the different peaks were assigned to its corresponding position in the molecular structure. Increasing the aromatic head group fur-

Wavenumber (cm⁻¹)

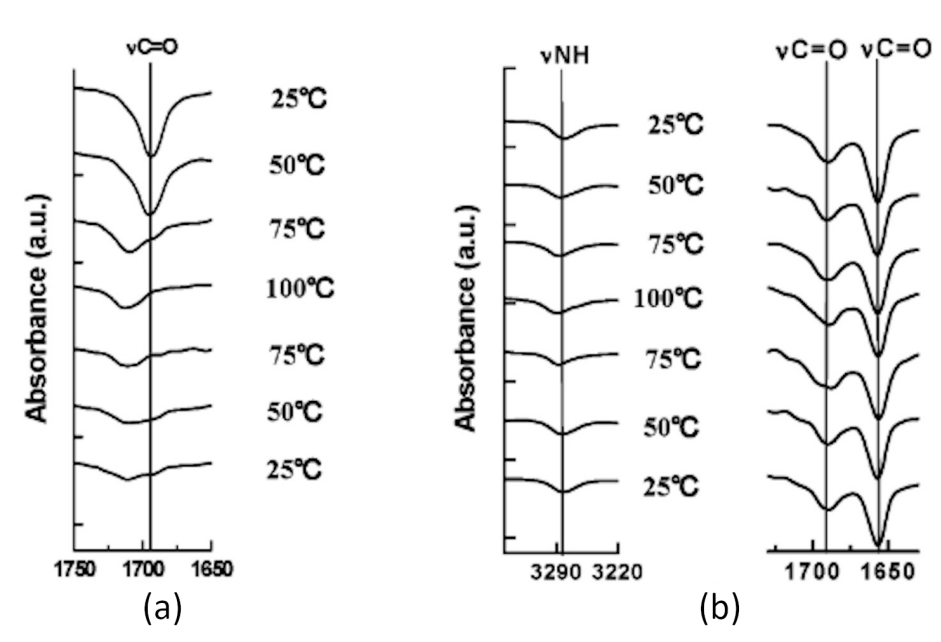


FIGURE 1.16: In situ external reflection FTIR spectra of polymerized PCDA (a) and PCDA-mBzA (b) on hydrophobized glass. Adapted from [99].

ther by adding a naphthoic acid (two benzene rings, PCDA-NPA, Scheme D.9) had several effects. The monomer molecular structure was investigated by X-ray powder diffraction (XRD). The spacing in the lattice increased, which results in a less effective polymerization. The d-spacing, the head-to-head distance in a bilayer, increased from 4.72 nm over 5.87 nm to 6.35 nm for PCDA, PCDA-mBzA and PCDA-NPA respectively while also the tilting angle θ increased from 47.9° over 50.9° to 52.2°. Besides the molecular arrangement, two other properties vary with bulkier head groups: (1) the temperature of the reversible color transition range is reduced by 40 °C from 230 °C to 190 °C (compare Figure 1.17 (d) and (e)) and (2) the color relaxation back to its blue state is speed up by a factor of 2. The

authors believe that steric effects are the reason for the increased tilt angle θ and the less stable H-bonding.⁹⁸

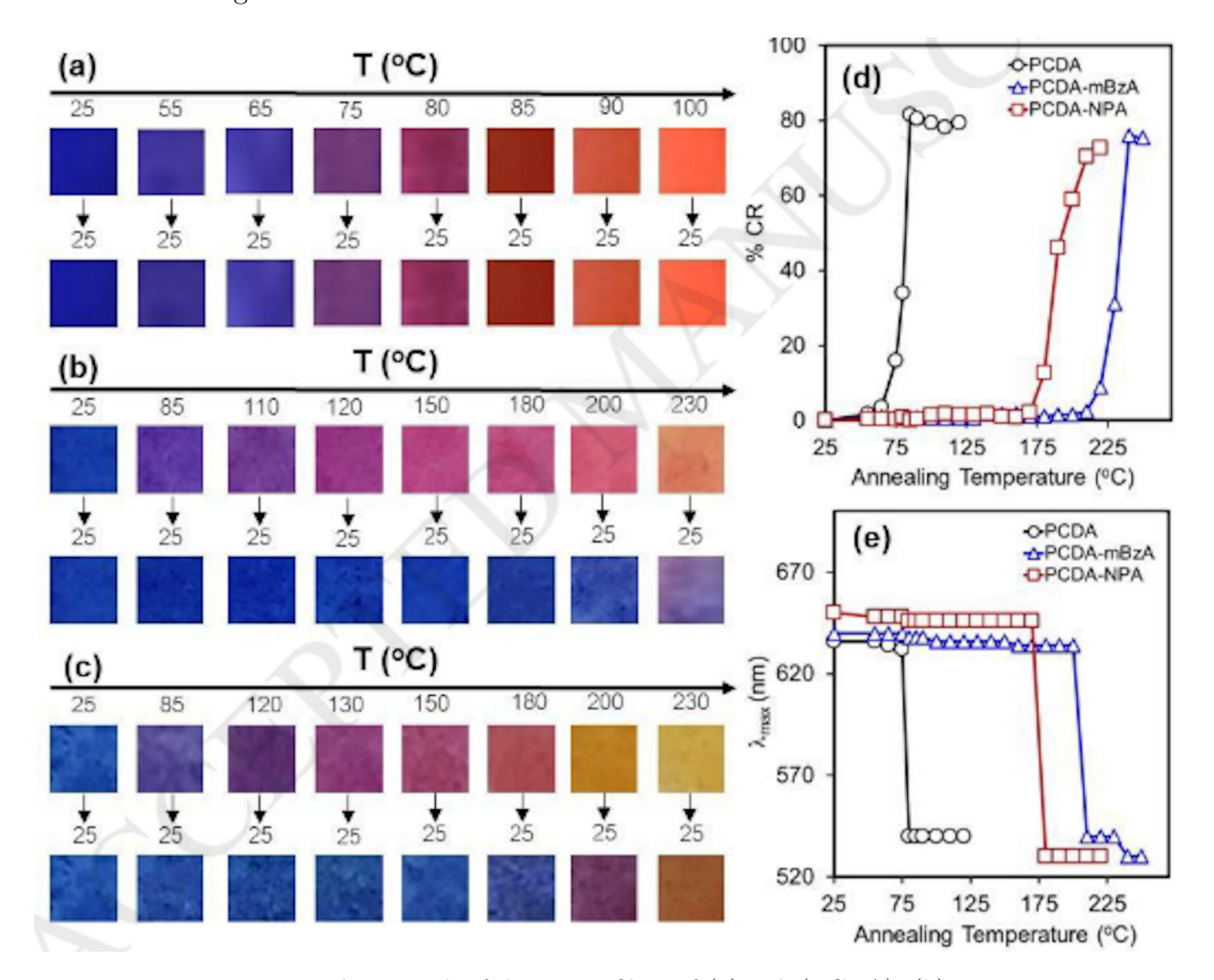


FIGURE 1.17: Photograph of drop cast films of (a) poly(PCDA), (b) poly(PCDA-mBzA), and (c) poly(PCDA-NPA) for cycled temperatures. (d) The %CR and (e) λ_{max} of absorption spectra after heating the samples to different annealing temperatures and cooling back down to room temperature. The temperature for the irreversible color transition is indicated due to the sudden change. Adapted with permission from [98].

Environmental Changes

It has been shown that changing the solvent can affect intermolecular forces. N-[2-(2-Hydroxyethoxy)ethyl]pentacosa-10,12-diynamide (HEEPCDA, Scheme D.6) was not able to recover back to its blue form after heating above 60 °C when dissolved in H_2O but was able to recover in D_2O (compare Figure 1.18).⁹⁶ The author's argumentation proposed that

hydrogen bonds are stronger in heavy water compared to pure water.¹⁰⁰ Therefore, the intermolecular forces are greater, thus the geometry withstands higher temperatures. But a recent study came to the opposite conclusion¹⁰¹, therefore this argument has to be taken carefully.

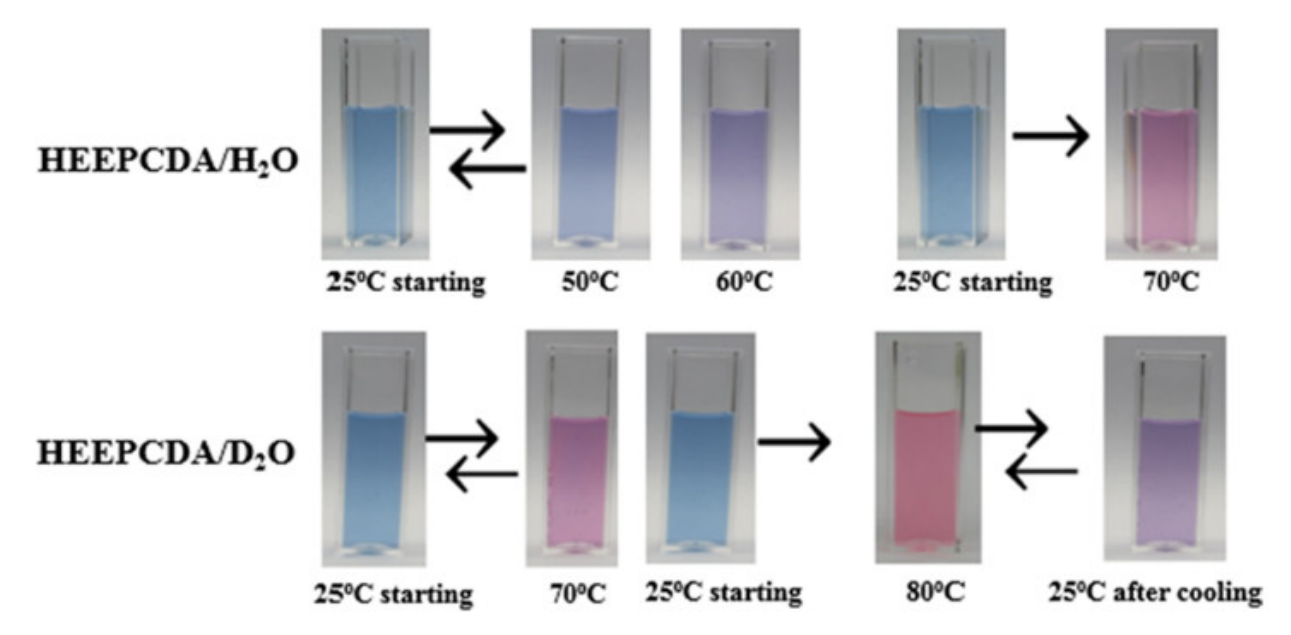


FIGURE 1.18: HEEPCDA dissolved in D₂O shows reversibility unlike in the case of H₂O. Adapted with permission from [96].

Intercalation

By adding cadmium ions (Cd²⁺), the reversibility of the PCDA-mBzA could be modulated. After adsorption of the metal ions (1 mM) at the carboxyl acid, the hydrogen bond of the terminal carboxyl group disappears as the negative-charged deprotonated carboxyl group is screened by the metal ion. Only the hydrogen bonding of the amide group stays intact which does not provide sufficient interchain interaction for a reversible behavior resulting in an irreversible transition. Partial desorption of the cadmium ions from the head group was achieved by submerging the films in an aqueous solution for 24 hours at a pH of 2.0. Afterwards the reversibility of the films was restored as demonstrated by UV-Vis and FTIR.¹⁰²

Another study intercalated polyvinylpyrrolidone (PVP10, Scheme D.18) into PCDA to form nanocomposites in order to archive a reversible behavior. PCDA in its pure form has an irreversible blue-to-red transition but when integrated as a "brick and mortar" morphology ¹⁰³

(PVP acts as a mortar between the PDA bilayer bricks, compare Figure 1.19 B1), thermochromic reversibility could be shown between 20 - 85 °C (compare Figure 1.19 A1-3). 85 °C was the maximum temperature of the UV-Vis spectrophotometer.

To establish these reversible nanoaggregates it was important to anneal the sample slightly over the melting point of PCDA ($T_m = 62 - 63$ °C) so that PVP chains could diffuse into DA crystal. This hydrogen-bonding-assisted process resulted in stable PVP/DA composite with an increased melting point $T_m = 72$ °C.

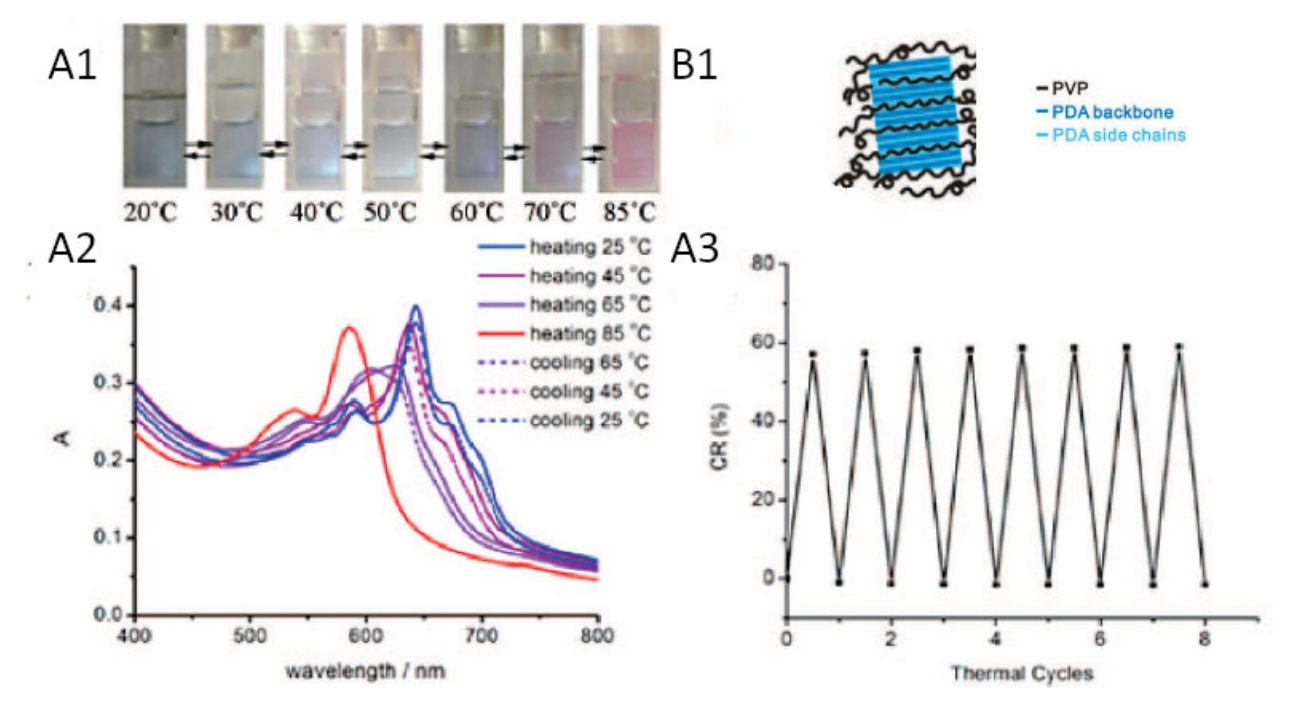


FIGURE 1.19: Photograph (A1) and UV-Vis spectroscopic data (A2) of thermochromic reversible PDA/PVP nanocomposites. The CR is calculated in A3) demonstrate the chromic reversibility. A "brick and mortar" morphology scheme is presented in B1). Adapted with permission from [104].

The blue-to-red transition was followed by UV-Vis spectroscopy as shown in Figure 1.19.

The calculated CR demonstrates the complete reversibility.

Fine tuning of the transition temperature for these intercalated nanocomposites could be done by varying the position of the DA unit and the overall chain length. Different PDA derivatives (PDA(X,Y), where X is the number of R-CH₂-R units between the backbone and the head group while Y the one towards the other side (shown in Figure 1.20) were synthesized and their thermochromism was analyzed by UV-Vis spectroscopy.

FIGURE 1.20: Schema for DA molecules for various alkyl length before (x) and after (y) the moiety.

Varying the distance between the PDA backbone and the carboxylic head group changed the transition temperature in a non systematical manner, but shortening the alkyl tail facing away from the head group lowered it by 10 °C. Not only the transition temperature was affected, but also the UV-Vis spectra itself as it lead to a shift of the blue absorption peak: $\lambda_{max} = 655$ nm for PDA(3,7)/PVP10 compared to $\lambda_{max} \sim 635$ nm for PDA(8,9)/PVP10 (compare Figure 1.21). It is generally believed that for the complex with the shorter distance to the head group (PDA(3,7)/PVP10) the molecular packing is optimized. This results in a longer conjugation length of the π system. Consequently, the peak shifts to higher wavelength. The lowering of the transition temperature for shorter chains is explained by a reduced dispersion interaction (virtually excited dipoles) of the nanocomposite.¹⁰⁵

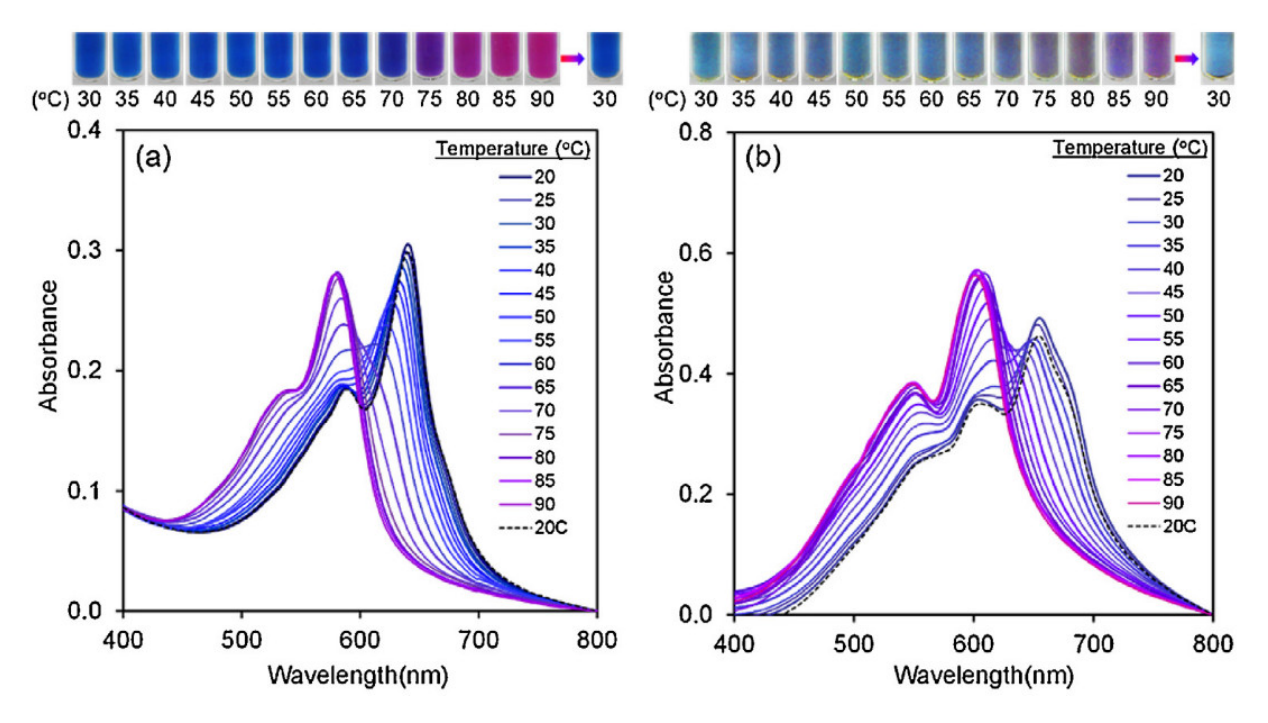


FIGURE 1.21: UV-Vis spectra of PDA/PVP10 nanocomposites for different PDA derivatives: (a) PDA(8,9) and (b) PDA(3,7). The thermochromic transition for the shorter derivative is shifted by 10 °C towards lower temperature. Adapted with permission from [105].

1.7.2 Macromolecules: Proteins and Peptides

Peptide-lipid interactions are fundamental for the function of all biological systems including human beings. Peptides are not only a part of the innate host defense system (grouped as antimicrobial peptides, AMP) to eliminate pathogenic microorganisms^{106,107} (causing a disease) but also play a major role in protein transport, signaling peptides or in the secretory pathway (movement of the protein).¹⁰⁸AMPs can trigger the blue-to-red transition of PDA. Therefore, they are valuable tools to study the peptide-lipid interaction.

Bacteria can develop resistances against most antibiotics. Penicillin was released in 1940 as a promising candidate to kill various types of bacteria and only two years later the first penicillin-resistant staphylococci appeared. The peptide melittin, the main component of the toxic bee venom, is able to kill bacteria by lysis: it penetrates the phospholipid membrane of the cell causing its disintegration. Previous studies showed that PDA integrated into a phospholipid matrix can be triggered by various peptides. The CR was peptide- and concentration dependent (compare Figure 1.22).

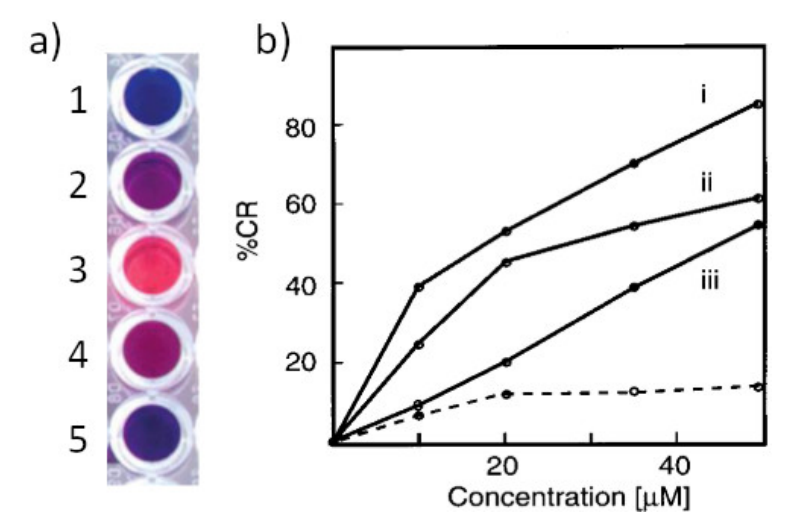


FIGURE 1.22: a) shows a photograph of a DMPC/PDA solution at 27 °C for different peptides: 1) control, 2) melittin at c=0.1 mM, 3) magainin at c=1 mM, alamethicin at c=0.1 mM and 5) M2 domain of the δ subunit of the acetylcholine receptor. b) shows the colorimetric response for the peptide magainin (i), melittin (ii) and alamethicin (iii) titrated with a DMPC/PDA vesicle solution (2:3 mole ratio, 1 mM lipid concentration). The dashed line shows the result for melittin exposed to pure PDA. Adapted with permission from [23].

Furthermore it was even possible to gain insight into the mode of action of the peptidemembrane interaction. The atomic crystal structure of melittin (net charge +6 at neutral pH)¹¹¹ showed that the monomer forms a two segmented α -helix which is roughly connected at the middle (between the 11th and 12th amino acid out of 26) with a bend angle of $\approx 120^{\circ}$. The non-polar side chains are facing inwards of the bend while the hydrophilic chains are situated at the outside (compare Figure 1.23 a) and c)).

Due to its amphipilic character it can interact with negatively charged and neutral bilayers. 112 When interacting with a phospholipid bilayer (negatively charged when deprotonated), it is thought that at low concentration the monomer lies parallel to the bilayer surface with the hydrophobic inner part towards the alkyl chain. The outer leaflet of the bilayer is increased to fill the "empty" space of the inner side of the bilayer. The bend structure leads to an unfavorable configuration for the lipid membrane called $wedge\text{-effect}.^{113,114}$ At higher peptide concentrations, and at increased salt concentrations, melittin forms a tetramer. 115 This tetramer can penetrate the lipid bilayer and form pores as the outer side of the new formed structure is hydrophobic while the inner part is hydrophilic. The radius of the pore is estimated to be ~ 5 nm depending on the peptide concentration, lipid composition and incubation time. 116 This model is called toroidal pore model (compare Figure 1.23). When the membrane is disintegrated further into sheets, the peptide is able to stabilize the edge. This is called the $edge\text{-effect}.^{26,116-118}$

Melittin has a single tryptophan residue that can be deployed to measure the peptides surrounding. When this residue is exposed to an aqueous solution, the intrinsic fluorescence is quenched. On the other hand the emission is increased and the peak shifts to lower wavelength when surrounded by a hydrophobic environment.

The intensity of the fluorescence and the peak shift was investigated for the native L-melittin compared to the non-native D-melittin. Only the L-melittin showed a change in both values (compare Figure 1.24) which indicated that only the native melittin is able to penetrate the hydrophobic bilayer²³. This result is consistent with the established model for D-melittin which is not able to completely fold into a helical structure. Consequently, it is unable to penetrate fully into a bilayer.¹¹⁹

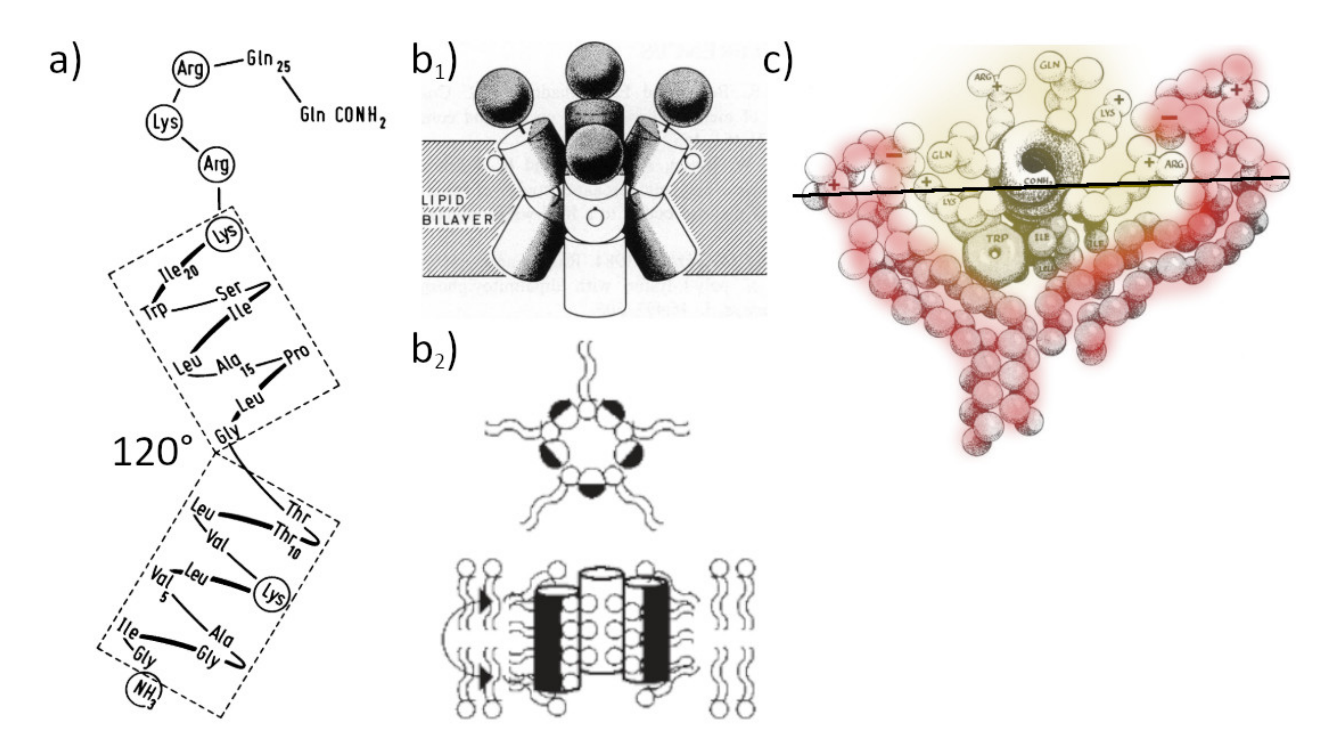


FIGURE 1.23: a) shows the secondary double α -helix amino acid sequence for melittin. The bend angle between the two α helices is $\approx 120^{\circ}$. b₁) represents a schematic model of the tetrameric form of melittin embed into a lipid bilayer at higher concentrations. The positive c-terminal is visualized by the black sphere, the hydrophobic outer part of the helices in white, the hydrophilipic part dotted in black and the Trp residue, employed as a fluorescence donor and acceptor as a white sphere. b₂) shows the toroidal pore model for antimicrobial peptide actions. The wedge-model is shown in c), where the bilayer is highlighted in red and melittin in yellow. The black bar separates roughly the hydrophilic upper region and the hydrophobic lower region. Adapted from [112, 117, 118].

A good example of PDA application is the method for bacterial identification.¹²⁰ The membrane of gram negative bacteria consists of lipopolysaccharide (LPS). LPS is toxic for humans at high concentrations and can produce a septic shock and even death. Two different DA-based peptide amphiphiles were synthesized, connecting TRCDA with either pentalysine oligopeptide (five lysine AA connected) (1a) or a histidine (another AA) (1b). 1a was furthermore equipped with a naphthalic acid fluorophore. When 1a and 1b are mixed in a molar ratio of 1:9, they self-assemble into highly fluorescent vesicles when exposed to aqueous solution. After polymerization of the transparent liposomes, they appear red in reflectance. It is not specified if this appearance is related to the typical blue and red state of PDA. As shown in Figure 1.25 the fluorophore is completely quenched by an energy transfer from the naphthalic acid fluorophore (em. max. 540 nm) to the cross-linked polymer (abs. max. 536

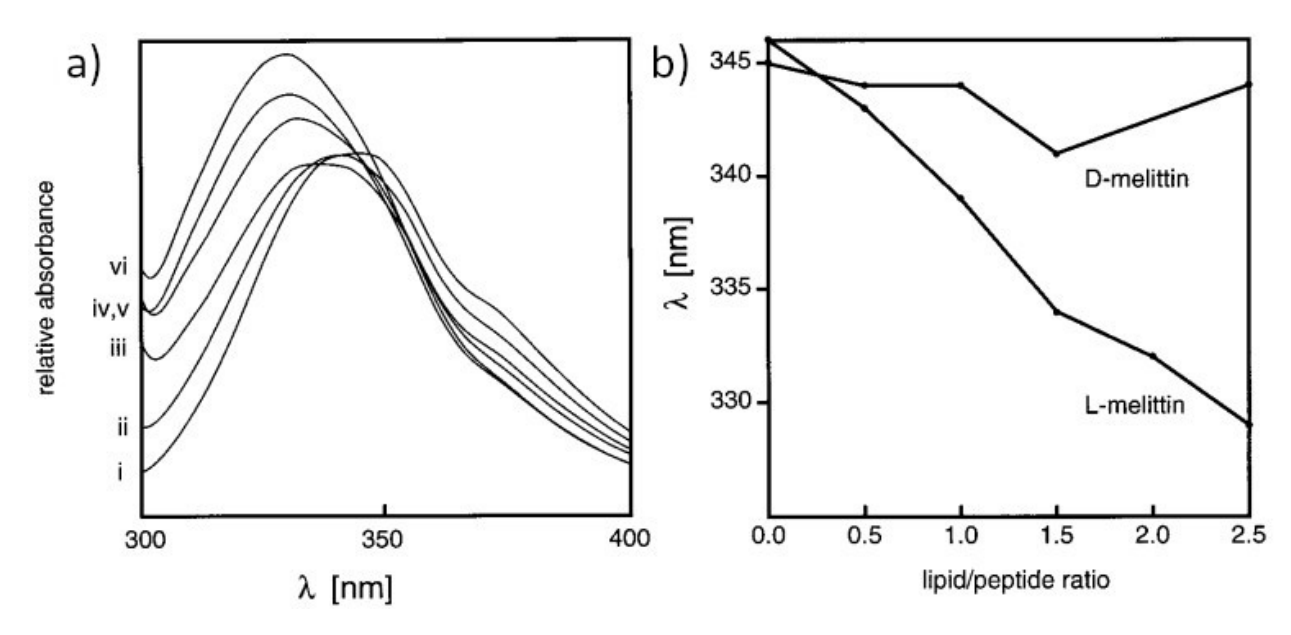


FIGURE 1.24: a) Fluorescence emission spectra for different lipid to peptide ratios for the native L-melittin: (i) 0, (ii) 0.5, (iii) 1, (iv) 1.5, (v) 2 and (vi) 2.5. (b) shows the emission peak shift for D- and L-melittin for different ratios. Adapted from [23].

nm).

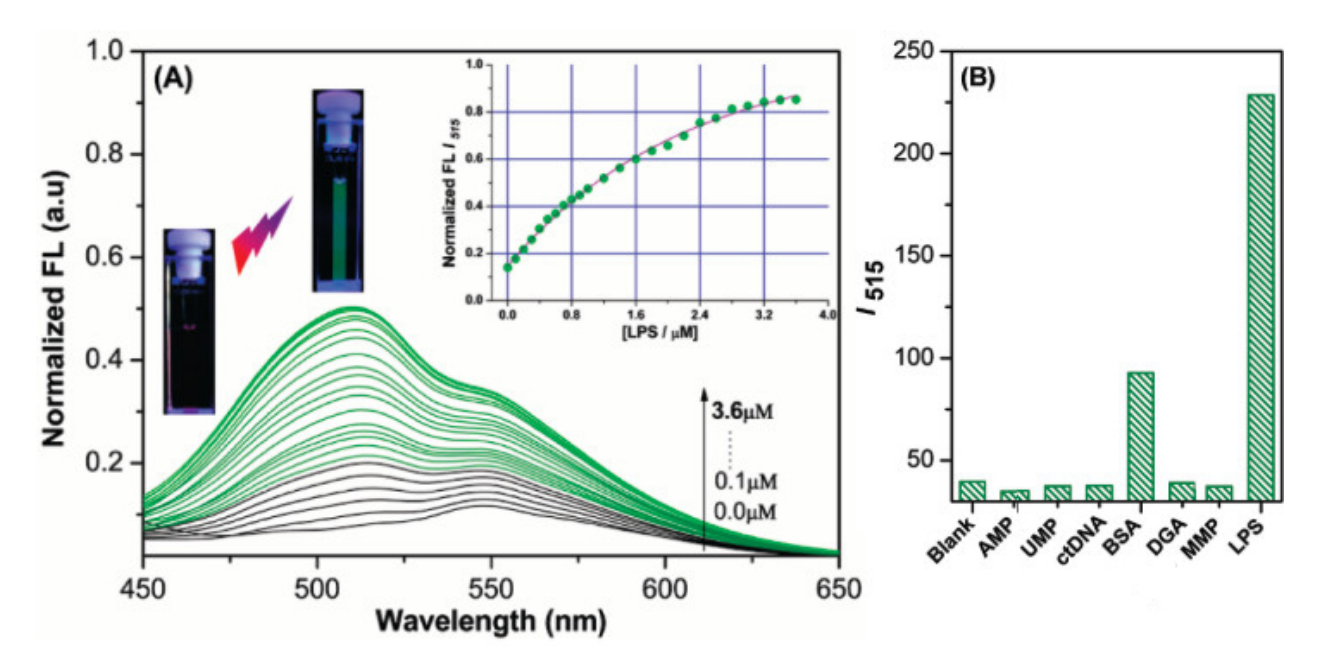


FIGURE 1.25: (A) Fluorescence emission spectra ($\lambda_{ex} = 400$ nm) for Titration of PDA liposomes with LPS. The insert shows the normalized intensity at 515 nm for the different LPS concentrations. The liposomes are tested against different biologically important species but only for LPS (and BSA) the fluorescence increased (B). Adapted with permission from [120].

When modified PDA liposomes are exposed to LPS, the fluorescence is restored even at

very low concentrations (compare Figure 1.25). Other important species have been tested but only for LPS (and BSA) an increase of fluorescence could be observed resulting in a highly selective LPS probe.

As in this approach the bacteria or a compound of the bacterial membrane (LPS) has to interact directly with the sensor, another group focused on a label-free detection system.¹²¹ The idea was not to detect the bacterium itself but the released chemicals it produces. Among other bacterial strains, the Bacillus subtilis SSB466 and NCIB3610 were chosen where the second one is a surfactin-producing strain. Theoretical calculations suggest that surfactin can penetrate into a charged bilayer due to its amphiphilic character.¹²² First PDA liposomes were tested directly against surfactin which resulted in a strong induced shift (compare Figure 1.26).

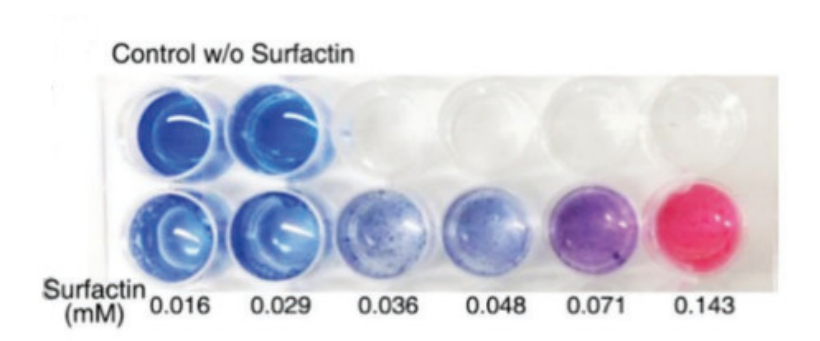


FIGURE 1.26: Photograph of PDA solution exposed to different concentrations of surfactin. At higher concentrations a strong blue-to-red transition is visible. Adapted from [121].

The PDA liposomes were then incorporated into a Luria-Bertani-agar and then injected with the chosen bacteria. Only the surfactin-producing strain induced a blue-to-red transition. The UV-Vis spectra was measured over the growth of 25 hours and revealed a similar outcome. Even though the control and the non surfactin-producing strain changed their spectra slightly (most likely due to the increased grow temperature at T=37 °C) NCIB3610 showed a dramatic two-fold color change (compare Figure 1.27).

The growth of both strains was furthermore examined ensure sure that an indirect surfactin-PDA interaction mechanism has been observed. The bacterial growth rate for both strains was similar, implying an indirect detection.

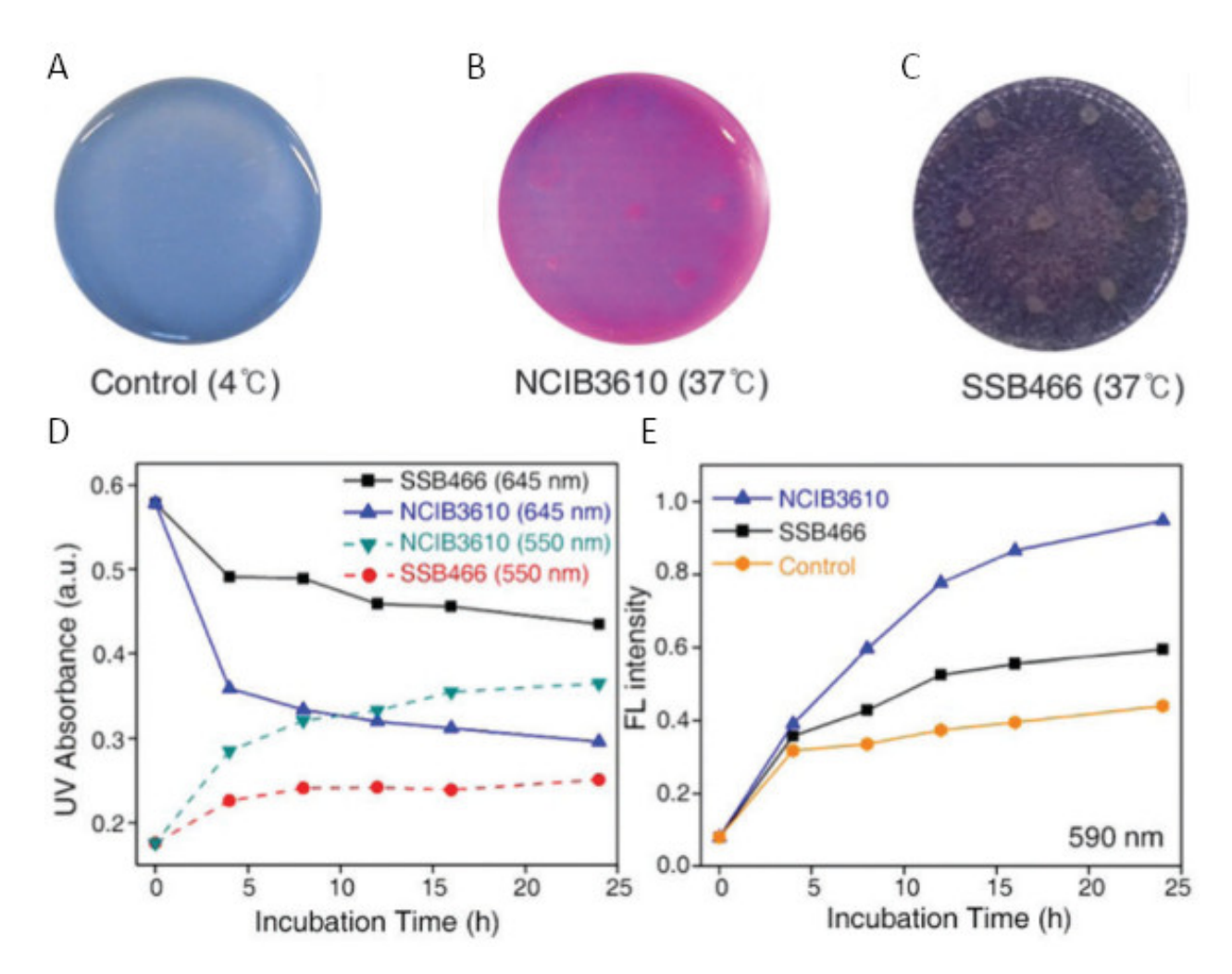


FIGURE 1.27: PDA as label-free bacterial detection system. A-C Photograph of PDA-LB-agar plates after incubation for 16 hours with different bacterial strains. D and E shows the UV-Vis and fluorescence spectrum change for different strains over time. NCIB3610 indicates the strongest change. Adapted from [121].

1.7.3 Solvents

PDAs can be assembled in many different ways (mono-/multilayer via LB¹²³, colloidal dispersion in solutions¹²⁴, spin coating¹²⁵ etc.) which influences the molecular organization during the self-assembly process of the monomer.

The rather different DA derivative N,N'-ethylenebispentacosa-10,12-diynamide (EBPCDA-2DA, Scheme D.19) was synthesized for the investigation of molecular packing in different solvents. Typically, the DA derivative consists of a non-polar hydrocarbon chain tail and a polar head group. EBPCDA-2DA is a symmetric molecule with its polar amide groups in the

middle surrounded by two carbon chains facing away from each other. Both chains accommodate a diacetylene structure. The morphology (XRD), the thermochromism (UV-Vis spectroscopy/drop casting) and variation of crystalline fraction (Differential scanning calorimetry (DSC) of EBPCDA-2DA in the two different solvents water and butanol (Scheme D.20) was investigated. It could be demonstrated that the EBPCDA-2DA formed only in butanol a well-defined structure compared to irregular-shaped particles in water. Furthermore the polymerizability improved 2-3 times and the color transition temperature increased by 55 °C when butanol was used as a solvent.

It is assumed that due to the apolar tail of butanol, the monomer with its long alkyl chain can self-assemble more effectively compared to the polar solvent. A better packing results in a better polymerization degree and also a more rigid supramolecular structure which influences the thermal stability.¹²⁶

By addition different alcohols into an aqueous solution of TRCDA and PCDA, the transition temperature and the sensitivity for chemical stimuli could be fine-tuned. PCDA, a PDA with a longer alkyl chain compared to TRCDA, showed a lower color stability when alcohol was added. However, increasing the concentration of the alcohol too much (e.g. $c_{\frac{76v}{v}} > 5$ for 1-butanol in PCDA) led to a shift from blue to purple at room temperature (T = 25 °C). Upon increased volume percentage of 1-butanol the irreversible blue-to-red transition could be lowered from 55 °C to 35°C.

The sensitivity towards chemical stimuli was tested e.g. against Tetrahydrofuran (THF, Scheme D.21). Upon increased concentration of butanol ($c_{\frac{\%v}{v}} = 0-6$) in the butanol/PCDA solution the EC_{50} for the CR after adding THF could be shifted by around 15% (compare Figure 1.28).

It was concluded that the alcohol disrupts the hydrogen bond network of the PDA's carboxylic acid groups by penetrating between the linked polymer subunits.

When polymerized multilayers (up to 32) of PDA8/12 (compare Figure 1.20) prepared by the LB technique, were treated with chloroform, ethanol or similar non-solvents they turned irreversible bright red. The UV-Vis spectra, shown in Figure 1.29, contains the characteristic peaks around 638 nm in the blue state and 500 nm in the red state after

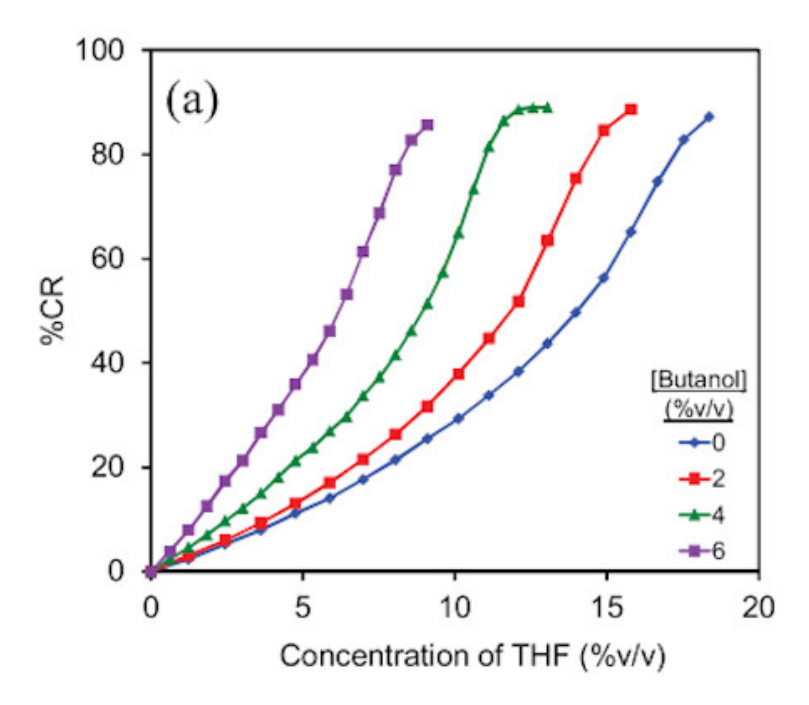


Figure 1.28: CR of poly (PCDA)/1-butanol suspension against THF. Adapted with permission from $^{127}\,$

treating the multilayer with ethanol. A similar spectrum was obtained when heating the film over 90 °C.¹²⁸ It is further mentioned that the intensity of the two peaks in a certain state (e.g. blue: $\lambda_1 = 638$ nm and $\lambda_2 = 585$ nm) is drastically dependent on the temperature. With decreasing temperature, the right peak decreases, while the left peak increases.

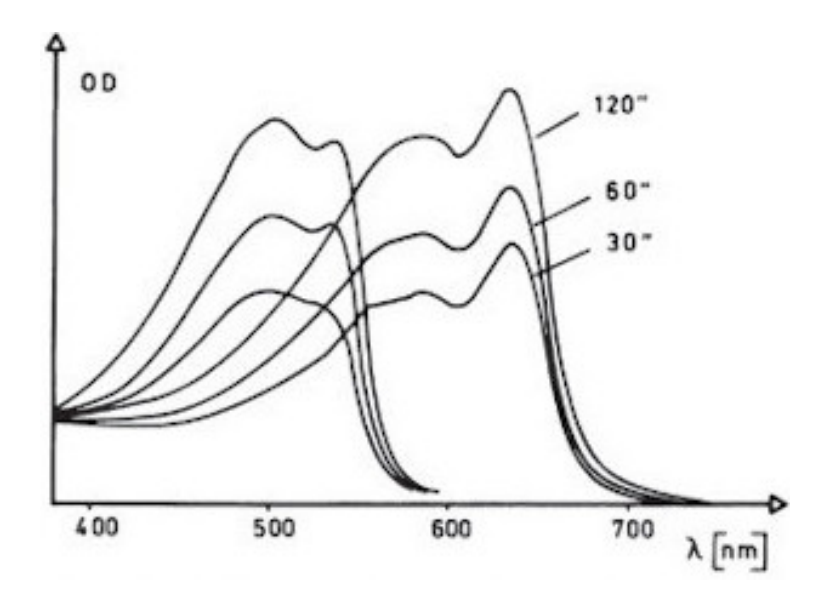


FIGURE 1.29: UV-Vis spectra of PDA8/12 exposed to ethanol for different irradiation times. Adapted from [128].

1.7.4 Surfactants

Surfactants are able to perturb the molecular structure of PDA and are therefore eligible to induce a blue-to-red transition. When adding cetyltrimethylammonium bromide (CTAB, Scheme D.12) to an aqueous solution of PCDA vesicles at pH = 6.88, a strong CR could be observed. CTAB is a cationic surfactant, hence it should be attracted to the negatively-charged carboxylic head group of PCDA. The long hydrophobic alkyl chain could then be incorporated into the hydrophobic part of the vesicle weakening the intramolecular interaction and shortening the conjugation length of the π -system. On the other hand, the anionic surfactant sodium dodecyl sulfate (SDS) is impeded by the electrostatic interaction which results only in a very minor CR. The nonionic surfactant p-(1,1,3,3-tetramethylbutyl) phenoxypolyoxyethyleneglycol (Triton X-100, Scheme D.14), shows a mild CR between the two extreme (compare Figure 1.30).¹²⁹

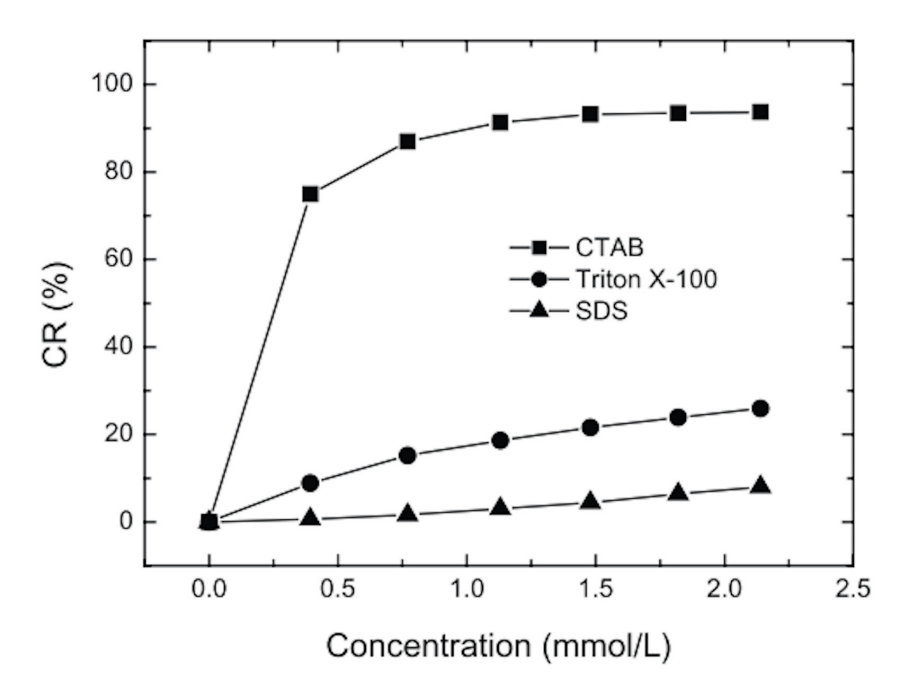


FIGURE 1.30: Calorimetric response of poly(PCDA) vesicles in aqueous solution titrated against SDS, Triton X-100 and CTAB. Adapted with permission from [129].

By varying the chain length of the applied surfactant, the one with a longer chain length like cetyltrimethylammonium chlorid (CTAC, Scheme D.15) changed the color from blue to a light-yellow while the shorter dodecyltrimethylammonium bromide (DTAB, Scheme D.16)

induced a purple-to-red CR. ¹³⁰ These surfactants were added to an aqueous solution of 4-(pentacosa-10,12-diynoyloxy)benzoic acid (PCDA-HBA, Scheme D.10). The spectra are shown in Figure 1.31. To get insights into the spacial positioning of the PCDA-HBA - CTAC/DTAB complex, time-dependent density functional theory (TDDFT) was performed which allowed the calculation of the geometrical structures and UV-Vis spectra. Both CTAC and DTAB showed strong electrostatic interaction between the deprotonated carboxyl group of the PDA and the cationic heads of the surfactants. Furthermore, the van der Waals forces between the aliphatic chains of each part were confirmed which explains the integration. The PCDA-HBA - CTAC showed a deeper penetration down to the PDA backbone compared to the PCDA-HBA - DTAC. It is worth mentioning that when DTAB was exposed to 4-pentacosa-10,12-diynamidobenzoic acid (PCDA-ABA), a PDA derivative which forms H-bonds to neighboring side chains (PCDA-HBA does not), a CR could not be observed. This implies that in this case the surfactant could not disturb the conjugated length of the PDA backbone because the H-bonds stabilized the intermolecular structure sufficiently.

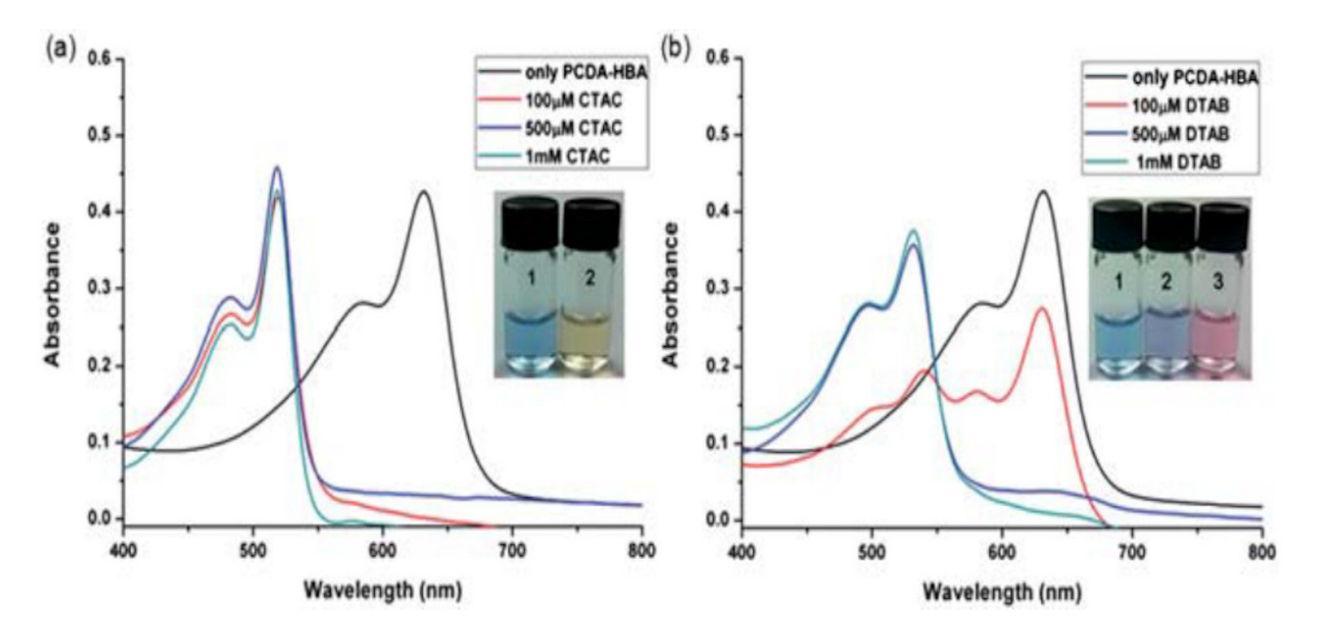
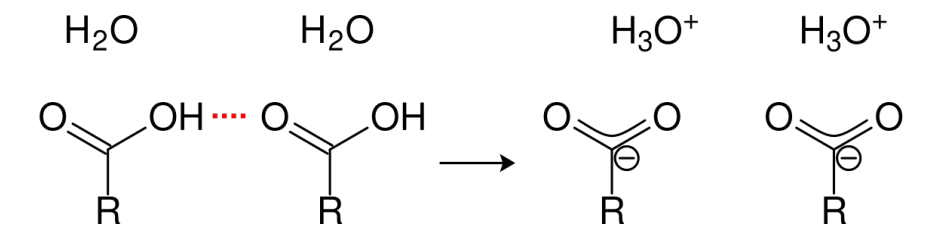


FIGURE 1.31: UV-Vis spectra of PCDA-HBA liposomes in HEPES exposed to CTAC (a) and DTAB (b) for different concentrations. The inset shows a photograph of the solution for the control (1), 500 μ M (2) and 1 mM (3). Adapted from [130].

1.7.5 pH

Several papers have proven that an increased pH leads to a PDA chromic transition^{131–133}. At pH ~ 11 a blue-to-red transition for TRCDA vesicles could be observed,¹² while the exact pH for the shift depends on the type of PDA and its environment. When DMPC, which has a transition temperature of $T_m = 24$ °C, is mixed with PCDA in a vesicle complex, the color transition was triggered at pH ~ 9.131 However, in earlier studies involving phospholipids, it was shown that adding soft lipids (a lipid, whose transition temperature is around room temperature such as DMPC) can increase the sensitivity by its own at a constant pH.²³

To understand the effect of pH in the PDA aqueous solution, it is important to point out that the PDAs discussed in this work contain a carboxylic acid (R-COOH) head group. The pH dependent deprotonation leads to a negative-charged carboxylate head group as shown in scheme Scheme 1.32.



SCHEME 1.32: Deprotonation of a carboxylate head group in an aqueous environment. Red dotted line represents hydrogen bonding.

The acid-base reaction in an aqueous solution is:

$$R-COOH + H_2O$$
 \Longrightarrow $R-COO^ + H_3O^+$ acid + base \Longrightarrow conjugated base + conjugated acid

After introducing the acid dissociation constant $K_a = \frac{[R-COO^-][H_3O^+]}{[R-COOH]}$ ([x] is the concentration of compound x), the expression $pK_a = -log_{10}K_a$ and the definition of $pH = -log_{10}([H_3O^+])$, the Henderson-Hasselbalch equation can be derived:

$$pK_a = pH + \log_{10} \left(\frac{[R-COOH]}{[R-COO]} \right)$$

With the degree of ionization $\alpha = \frac{[R-COO^-]}{[R-COOH]+[R-COO^-]}$, the equation can be expressed as:

$$pK_a = pH + \log_{10}\left(\frac{1-\alpha}{\alpha}\right) \tag{1.1}$$

The degree of ionization α can be experimentally determined by FTIR spectra looking at the carbonyl absorption at 1691 cm^{-1} before and after altering the pH.¹² Using equation 1.1 the pK_a can be calculated and ranges between 9.5-9.9.¹² In contrast to common carboxylic acids which have a much lower acid dissociation constant ($pK_a \sim 5$). This explains that the CR takes place at the basic region ($pH = pK_a$ for [R-COO⁻]=[R-CCOH]).

Upon increasing pH, more carboxylic acids will be deprotonated and therefore not available for hydrogen bonding anymore. Furthermore the electrostatic repulsion between the negative-charged carboxylate disturbs the structure's morphology and can induce a twist in the backbone. This can even lead to a complete change in the micro structure from a helical ribbon/flat sheet structure into nanofibers observed by transmission electron microscopy (TEM) and circular dichroism (CD, a spectroscopic method to study the chirality of a compound via polarized light). The destabilization of the hydrogen bond network by increased pH results in a higher sensitivity of microorganism detection. 133

Adding a salt to the aqueous solution e.g. NaCl (c > 50 mM) resulted in a reduction of the pH by two units for the blue-to-red transition. After testing various cations with different sizes, it was shown that the bigger ones (Na⁺,K⁺) induce a stronger CR compared to smaller ions (Li⁺, Mg⁺).¹² On the other hand, increasing the acidity does not induce any colorimetric transition but leads to a higher degree of precipitation in a TRCDA vesicle mixture after incubation at pH ~ 4 .

An interesting study focused on how to achieve a reversible blue-to-red chromic transition.

PCDA, which by itself has an irreversible transition, was co-assembled with $\mathrm{Zn_2}^+$ and OH^- ions in an aqueous medium. Adding zinc ions with a molar ratio 2:1 for PDA: $\mathrm{Zn_2}^+$ by its own did not show reversibility¹³⁴ in an aqueous phase. But by increasing the pH to 8 and beyond, the PCDA/ $\mathrm{Zn_2}^+$ complex showed complete reversibility. Due to the deprotonation of the carboxylic head group, the zinc ions intercalated between the PDA units at the self-assembling process promoting the head group - head group interaction between adjacent neighbors.¹³⁵

In order to reverse the sensitivity towards pH it could be shown that positively-charged ZnO particles could be intercalated between the negative-charged PDA head group. Decreasing the pH led to the dissociation of the ZnO nanoparticles within the composite. This changed the packing due to steric forces and resulted in a blue-to-red transition. ¹³⁶

1.7.6 Comparison of Different UV-Vis Spectra

The research around PDA is highly focused on the blue-to-red transition. Therefore the colorimetric response plays an important role in most of the scientific literature. The following study aims to review the recent publications in the field including the PDA derivative PCDA. The excitonic and vibronic blue and red peaks of the collected UV-Vis spectra are compared. These peaks are the basis to calculate the CR (compare subsection 1.6.4). The data is presented in Figure 1.33.

The number on the ordinate indicates the number of papers considering each stimulus. E.g. the stimulus "alkene swelling" is extracted from one paper, the stimulus "temperature" from 6. Often the exact wavelength of the peak is not pointed out specifically. In these cases, the value was estimated in steps between 10 nm and 5 nm. The less common stimulus myristoylcholine (MC) in combination with acetylcholinesterase and dichlorvos were included as they were all performed under similar conditions by one group.

The maximum peak spread is around 20 nm. The absolute wavelength is not critical for the calculation of the CR unlike the absorbance. Even so, this uncertainty evidences the gap of a complete theoretical understanding of PDA's electronic structure.

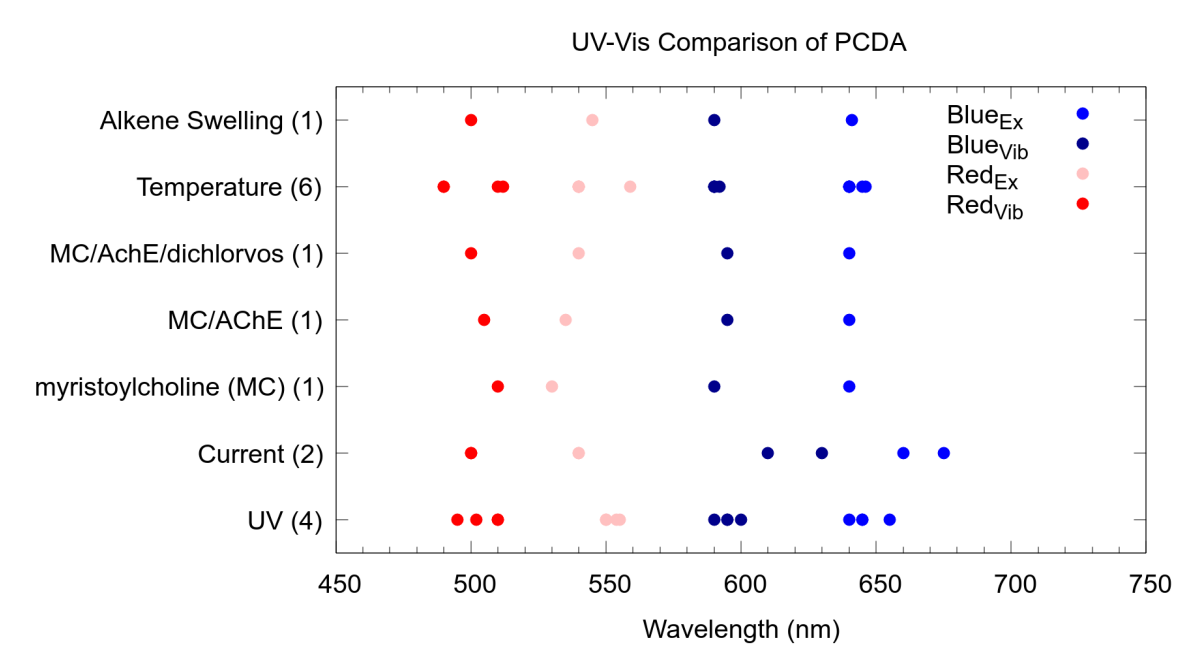


FIGURE 1.33: Comparison of excitonic and vibronic peaks of PCDA UV-Vis spectra for various stimuli. Data extracted from [91, 131, 137–143]

Chapter 2

The Mechanism of Polydiacetylene Blue-to-Red Transformation Induced by Antimicrobial Peptides

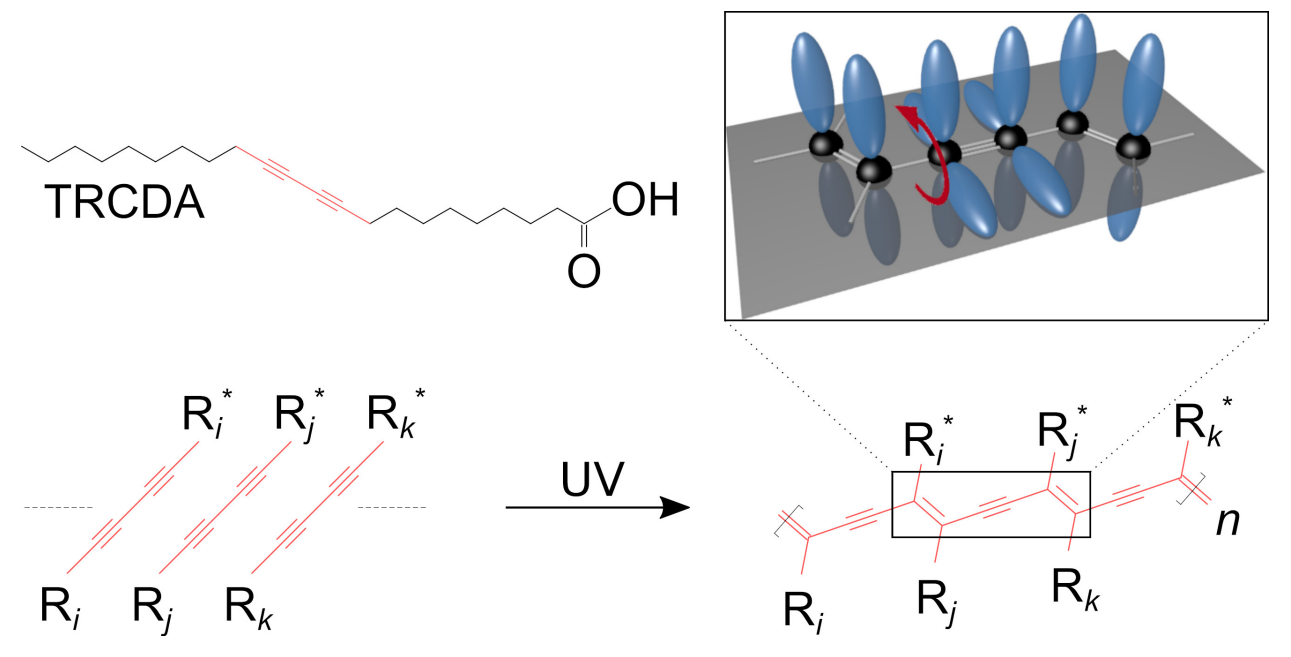
This chapter is adapted from the following publication and supported with additional yet unpublished data.

Nuck, J. & Sugihara, K. Mechanism of Polydiacetylene Blue-to-Red Transformation Induced by Antimicrobial Peptides. *Macromolecules* **53**, 6469–6475. ISSN: 15205835 (2020)

2.1 Introduction

A mechanochromic polymer, polydiacetylene (PDA),³⁰ has garnered attention due to its unique force-sensing mechanism and its potential for applications in chemo-/bio-/mechanosensing for the detection of temperature,¹⁴⁴ pH change,¹² mechanical stimuli,³¹ ions,¹⁴⁵ solvents,² light,¹⁴⁶ surfactants,¹⁴⁷ bacteria,³ and other biomolecules,¹⁴⁸ such as peptides.^{4,149} Synthetic efforts^{150–152} and the recent introduction of a differential approach² have improved its specificity for developing a convenient colorimetric and fluorescence sensor. X-ray crystallography,¹⁵³ nuclear magnetic resonance (NMR),¹⁵⁴ and many other experimental studies^{27,95,137,149,155–160} have been combined with theoretical works¹⁶¹ for providing a mechanistic model. The torsion induced in the backbone is believed to be the origin of the color change and the activation of the fluorescence pathway, where this twist reduces the π conjugation and thus broadens the

HOMO-LUMO energy gap (Scheme 2.1). Despite our general understanding of its mechanism, a clear picture of how a large variety of different stimuli causes this torsion in each case is often lacking.



SCHEME 2.1: Chemical Structure of 10,12-Tricosadiynoic Acid (TRCDA) Monomers, Their Polymerization by UV Light and a 3D Scheme, where the p-Orbitals of the Carbon Atoms (Black) are shown in Blue. Adapted by [46].

Among different stimuli, temperature has probably been studied the most due to its experimental simplicity. Many groups have reported that the thermochromic blue-to-red transition temperature $T_{\rm B2R}$ of PDA is correlated with the solid-to-liquid phase transition temperature $T_{\rm m}$ (the melting temperature) of their lipidic monomers (Table 2.1). ^{162–168} This suggests that the blue solid-state polymer turns into red when its side chains "melt" (crystal-to-amorphous transition). Previous studies by X-ray, ¹⁵³ NMR, ²⁴ infrared (IR), ²⁷ and Raman spectroscopy techniques ¹⁵⁷ have measured an increased disorder during the blue-to-red transition, which agrees with this picture, although a local increase of order has also been reported. ^{15,153}

If the solid-to-liquid phase transition of the lipidic monomers is linked to the blue-tored transition of the polymer, can anything that influences the lipid phase potentially alter the color? Antimicrobial peptides such as melittin that are known to induce the blueto-red transition⁴ have been previously reported to modulate the melting temperature of

TABLE 2.1: Comparison of different polydiacetylene (PDA) derivatives regarding the phase transition $(T_{\rm m})$ and the blue-to-red transition temperature $(T_{\rm B2R})$

molecule	$T_{ m m}$	$T_{ m B2R}$	ref
8,10-Heneicosadiynoic acid	51-52	52	[162]
10,12-Tricosadiynoic acid	54-56	55	[162]
10,12-Pentacosadiynoic acid	62-63	65	[162]
4,4'-(5,7-Dodecadiyn-l,12-diyldioxy)dibenzoic Acid	1st: 113, 2nd: 132	120-130	[163]

lipids. ^{169–172} Can we extrapolate the lesson learnt from thermochromism and interpret the peptide-induced color change by the peptide-induced lipid phase transition? In this work, we study the hypothesis that the peptide-induced color change in PDA is a peptide-assisted chromism, where the direct role of peptides is to induce a phase transition. This color change is analogous to a thermochromic process where temperature is the stimulus which induces the phase change associated with a color change of the compound investigated.

2.2 Results and Discussion

2.2.1 (P)DA Crystal Formation and Integration into a Lipid Bilayer

DA crystals can be prepared by various techniques like LB¹²³, spin coating¹²⁵ etc. For amphipilic derivatives like TRCDA a DA solution is often mixed with other soft lipids like 1,2-dioleoyl-sn-glycero-3-phosphocholine (DOPC,Scheme D.24) (DOPC) or DMPC and prepared in an aqueous solution. This mixture is kept in a vial over night at a temperature T=2 C°. ^{23,24,173} This step is necessary for the self-assembling process and subsequent polymerization. ⁴⁸

To quantify the degree of polymerization and the blue-to-red transition, these solutions are then analyzed by UV-Vis spectroscopy. This approach does not allow a local view as the whole solution gives rise to an average signal. Hence, besides the common technique employed for UV-Vis spectroscopy (Scanning a filled cuvette), we modified this process by injecting the solution on a supported glass coverslip confined by PDMS. The detailed protocol is described in 3.2 and 3.7. Afterwards the solution is studied by an optical microscope. By this method

it is possible to gain insight into the self-assembly mechanism, the polymerization process and the blue-to-ted transition.

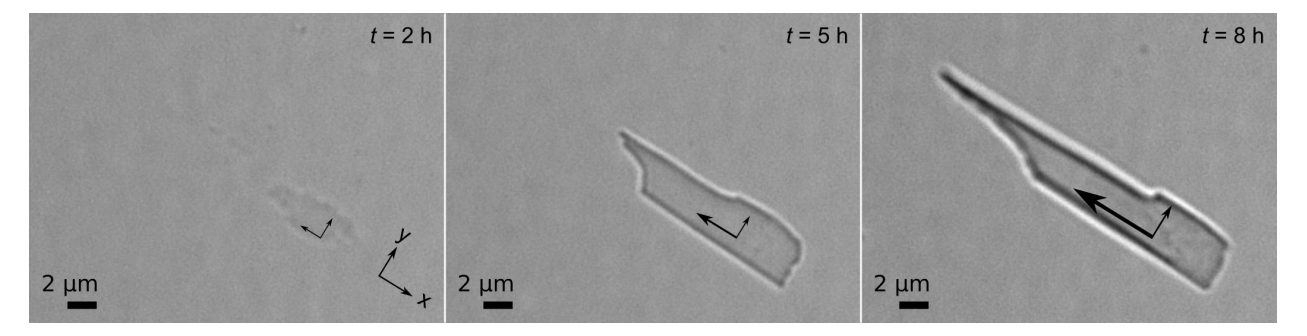


FIGURE 2.1: Crystal growth of DA in a soft lipid BL environment over 8 hours. Between the frames, the sample was stored at T=2 °C. An anisotropic growth is clearly visible.

These TRCDA domains grew anisotropic (grew much faster in one direction of the crystal than the other, see snapshots in Figure 2.1 from a bright field movie). The growth speed v depends on the temperature and concentration. But even more important seems to be the molecular orientation. The direction with the higher growth speed is named v_x while the slower one v_y . For the above crystal, the following parameters were measured: $|v_x| = 1.46 \frac{\mu m}{h} \pm 0.51 \frac{\mu m}{h}$ and $|v_y| = 0.16 \frac{\mu m}{h} \pm 0.02 \frac{\mu m}{h}$. We hypothesize this difference is due to the alignment of the molecules. The overall formation results in a tree-like structure with branches. This morphology has also been reported for TRCDA crystals prepared via LB.¹⁷⁴

Taken together, the formed structure on glass consists of fluidic DOPC bilayers, as seen by the fluorescence recovery after photobleaching of NBD-PE mixed at 1 mol %, and TR-CDA domain structures (Figure 2.2 top row) that are visible also in bright field microscopy (Figure 2.2 bottom row). When the TRCDA domains are polymerized they form blue PDA.

In order to understand the role of the soft lipid DOPC (Transition temperature T = -17 °C) a direct comparison of a self-assembling process of TRCDA with and without DOPC is shown in Figure 2.3. In both cases agglomeration of TRCDA is visible in the solution after several hours at T = -2 °C. Only in the presence of the soft lipid the crystals are forming on the bottom of the glass coverslip. This data indicates that the soft lipid contributes to the DAs self-assembling process. DOPC forms a bilayer on the bottom of the glass coverslip within seconds after the mixture is injected. The BL provides a viscid support while the DA

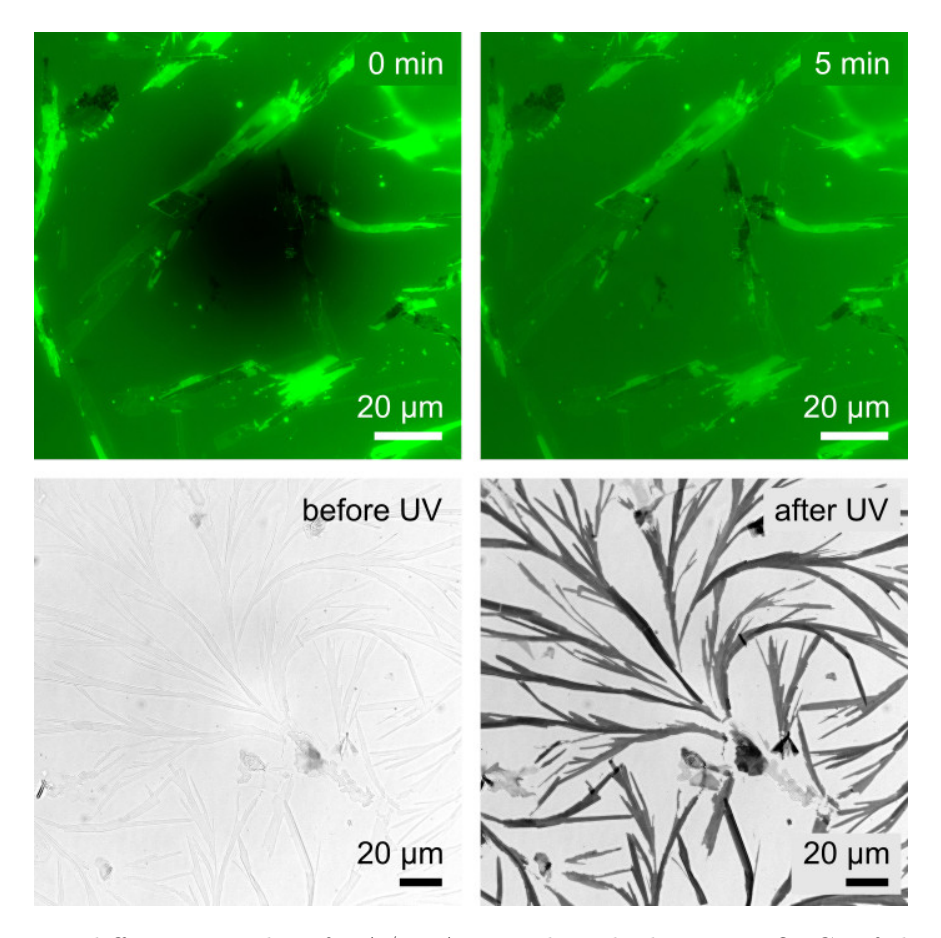


FIGURE 2.2: Two different samples of DA/PDA crystals embed into a DOPC soft lipid bilayer imaged by fluorescence and by bright field microscopy respectively. The top row shows the existence of the bilayer by FRAP (a dye has been added to the DA/DOPC mixture). The bottom row presents the DA crystals (monomer, left) and PDA (polymer, right) after applying UV light. Due to the black and white camera, the blue structure appears in black.

molecule starts forming irregular structures in the solution and regular shapes within the BL. This leads to a more homogeneous crystal structure of the crystals and finally a better polymerization yield (compare also Figure A.1).

An even closer look on the topology of the (P)DA crystals is archived by TEM. The DA solution is incubated directly on the TEM grid. The dried out structures are shown in Figure 2.4. The crystal growth on the silicon nitride TEM grid looks similar to crystals grown on the glass coverslip (compare Figure 2.1). At a high magnification (Figure 2.4B), an alternating contrast pattern is visible. This indicates the crystal structure ¹⁷⁵ where the backbone of PDA follows the regions of higher contrast (along each line).

UV-Vis - and transmission electron microscopy are great methods to characterize the

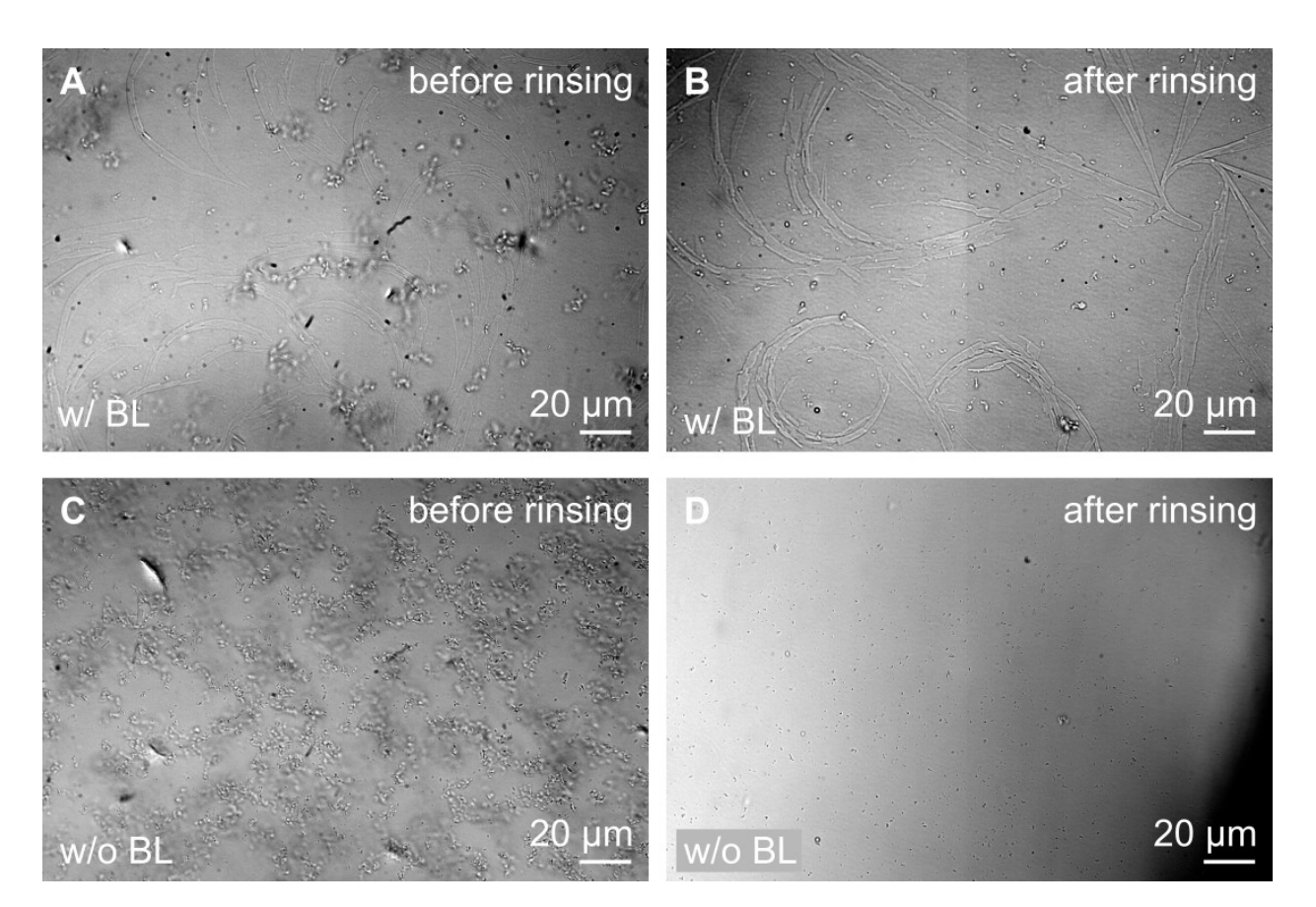


FIGURE 2.3: DA crystal growing with (A,B) and without a supporting DOPC bilayer (C,D). In both cases, an agglomeration formation in the solution is visible (A,C). However, after rinsing, only in the sample with supporting bilayer, a clean crystal growth is evident (B). The presence of the BL is confirmed by FRAP but not shown (similar to Figure 2.2 top row). Unpublished data.

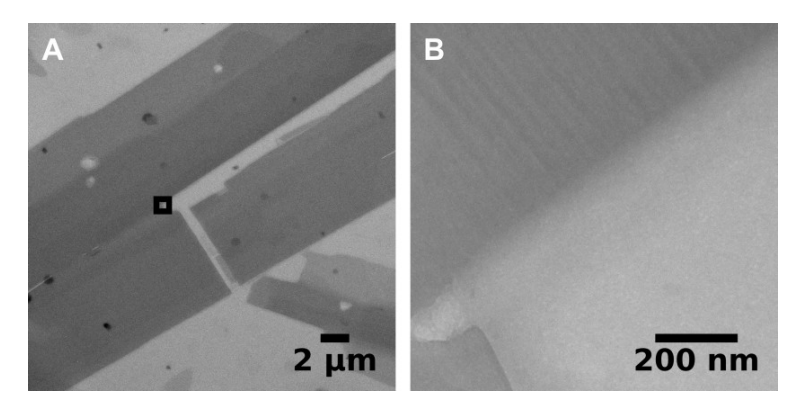


FIGURE 2.4: (A) Polymerized TRCDA crystal self-assembled in a DOPC environment, dried out and imaged by TEM. A higher magnification of the black square is shown in B. The alternating contrast pattern indicates the crystal structure.¹⁷⁵ The backbone is oriented along the dark lines. Unpublished data.

topology in two dimension. But in order to get a complete picture of the crystal structure, atomic force microscopy (AFM) measurements were performed. Thereby it was revealed that these TRCDA domains are multilayers with a height up to 100 nm (Figure 2.5),

which roughly corresponds to 40 monolayers, assuming a thickness of 2.5 nm for a single monolayer.⁹⁵ The formation of supported lipid bilayers with TRCDA is not trivial, because the integration of diacetylene in lipid mono-/bilayers is notoriously difficult as they prefer non-lamellar phases such as helix and tubes.¹⁷⁶ When a TRCDA monolayer assembled at a water-air interface is compressed, TRCDA protrudes from the layer, forming a segregation or a multilayer structure.¹⁷⁷ These TRCDA multilayer domains slightly alter their shapes during polymerization, detected by AFM (Figure 2.5).

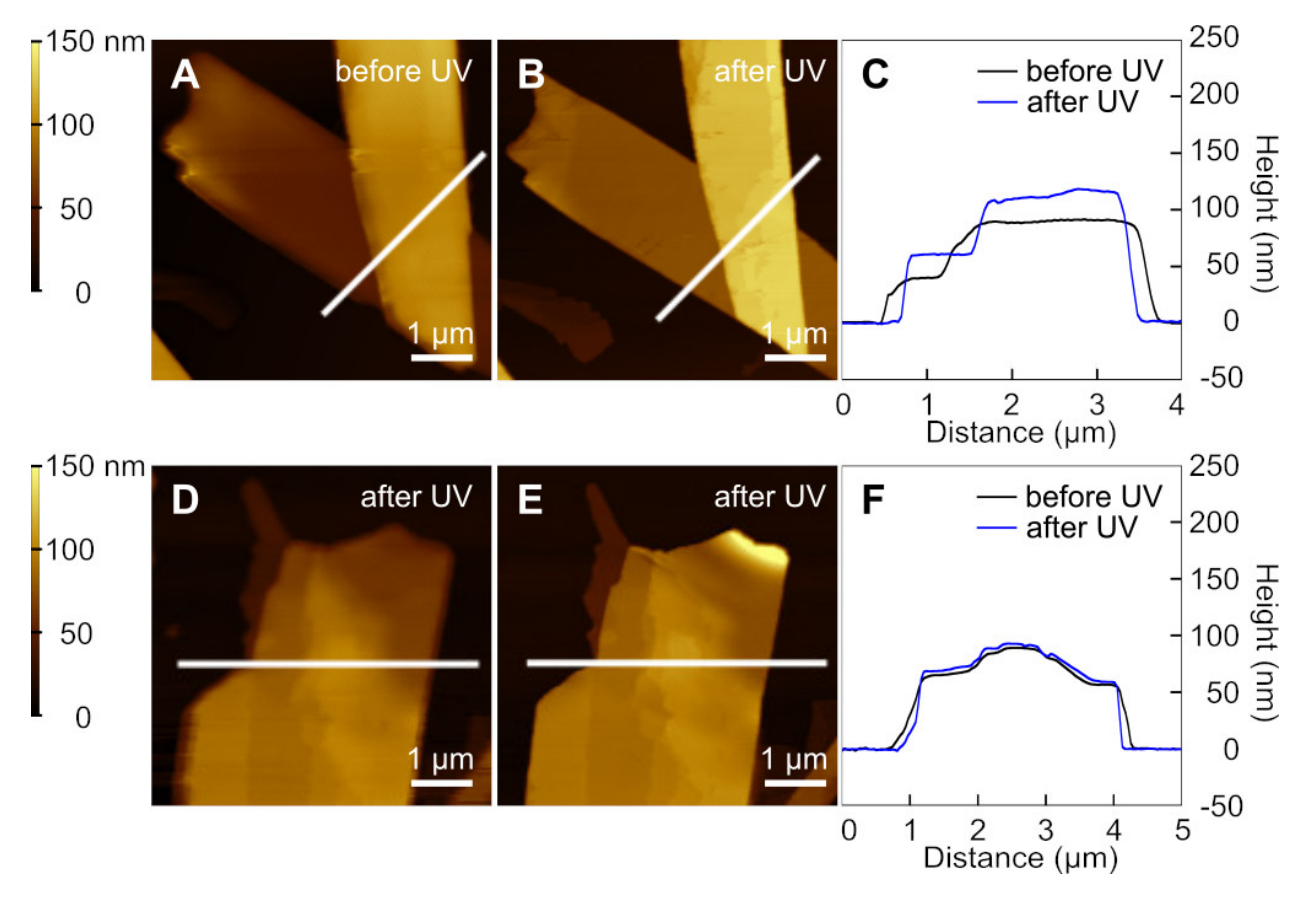


FIGURE 2.5: AFM measurement of DA/PDA embed into a DOPC soft lipid bilayer. Topography of two different regions before (A,D) and after (B,E) polymerization with their cross-sections (C,F).

Many TRCDA structures increase in their height by 5-33%, while the width tends to become narrower after the polymerization by 8-13%. This contraction of TRCDA in the direction parallel to the backbone during the polymerization has been previously reported in other AFM studies for mono- and trilayers, 40,178 and also in investigations by infrared (IR) spectroscopy^{27,179} and electron diffraction analysis. This phenomenon is explained by the

conjugated backbone formation, where the bond length that connects two monomer units is shorter compared to the original monomer-monomer distance determined by the hydrogen bonds at the TRCDA head group.¹⁷⁸ In addition, the angle of the monomers relative to the substrate is known to change during the polymerization^{40,179} which can affect the thickness and the width of the PDA.

The crystal growth occurs not only inside a supporting bilayer, but also in the DA/-DOPC suspension. Tracking the particle size of assembling monomers via dynamic light scattering (DLS) reveals an increase over time. DLS assumes a spherical particle moving in the suspension and determines hence a radius. However, it does not classify the shape of the particle in any way. When these samples are polymerized and the absorbance is quantified via UV-Vis spectra, the intensity of the blue polymers is also enhanced in a time-dependent manner (Figure 2.6).

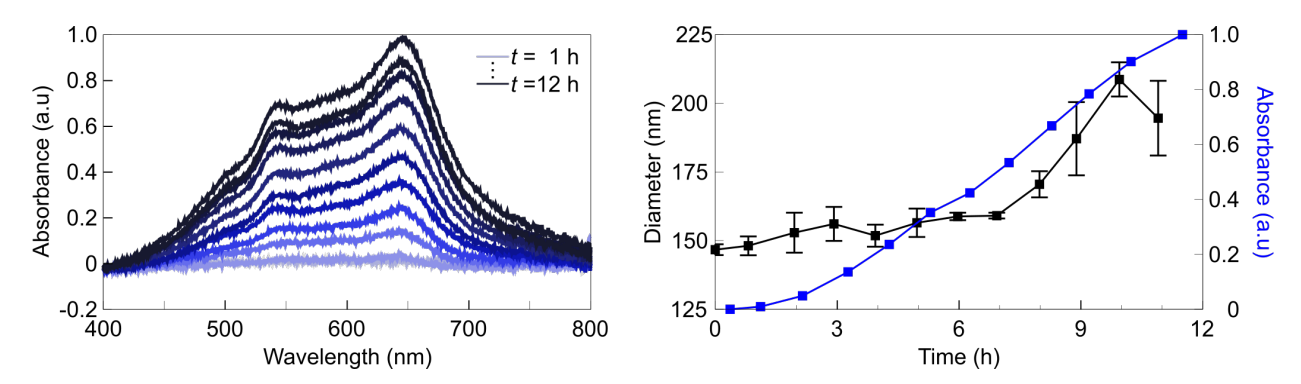


FIGURE 2.6: Absorbance of polymerized DOPC/TRCDA suspension over time (left). The same solution is analyzed by DLS prior to its polymerization. The virtual radius and its absorbance at the blue peak is plotted over time on the right. The growth of the structures in the solution is evident.

Taken together this leads to the following model: the TRCDA monomer self-assemble in the aqueous solution over time forming larger structures. When polymerized, the absorbance increases in a linear manner.

2.2.2 Peptide-Lipid Interaction

50

We selected melittin as a model antimicrobial peptide as it has been previously shown multiple times to induce blue-to-red transformation in PDA. Melittin is the main active component of bee venom. Is a bar-type peptide, which adsorbs on lipid bilayers with

various orientations such as surface, transmembrane, and pseudotransmembrane orientations, while it forms a channel as an oligomer at high concentrations. ^{181–184} As reported, addition of melittin into a PDA suspension made of 10,12-tricosadiynoic acid (TRCDA) induced a blue-to-red transition (Figure 2.7A). ^{2,146} The backbone of PDA is considered to be centrosymmetric (C_{2h}) . ¹⁸⁵ The allowed transition for blue PDA between the ground state (1¹Ag) and the lowest excited state (1¹Bu) with an excitation energy of around 1.9 eV (\sim 650 nm) is suggested to be exciton-related ⁸⁴ and therefore called the excitonic transition. This transition is often coupled with vibronic side bands, which are multiples of 1500/2100 cm⁻¹ vibrational excitations for C=C/C=C and hence called vibronic transition. ⁵⁴ Previously, the efficiency of the blue-to-red transformation (colorimetric response) upon addition of peptide has been shown to increase by adding dimyristoyl phosphatidylcholine (DMPC). ¹⁴⁷

The result was roughly reproduced with DOPC, which showed the maximum local colorimetric response at around 40% DOPC (Figure 2.8).

When we monitored this melittin-induced blue-to-red transition by optical microscopy, a morphological change in PDA was observed, where droplets formed mainly on red (fluorescent) PDAs (Figure 2.7D-G), which can also be confirmed by atomic force microscopy (AFM) images (Figure 2.7B,C). These snapshot images suggest that the droplet formation and the chromism coincide spatiotemporally. First, a similar droplet formation occurred when TR-CDA monomers, which are in a solid state at room temperature ($T_{\rm m}=56~{}^{\circ}{\rm C}$), were exposed to melittin (Figure 2.7H), indicating that these droplets are made up of monomers that are left unpolymerized within the PDA crystals. These droplets resemble liquid TRCDA when it is heated up above the melting temperature (Figure 2.7I), implying that melittin causes a solid-to-liquid phase transition of TRCDA. This was further confirmed by the decrease in Young's modulus measured by force spectroscopy (Figure 2.9) and the drop in the melting temperature after addition of melittin, characterized by differential scanning calorimetry (DSC, Figure 2.10).

Previously, studies using DSC^{54,169,171} have shown that some antimicrobial peptides modify the lipid melting temperature due to their ability of inducing disorder in bilayers. This

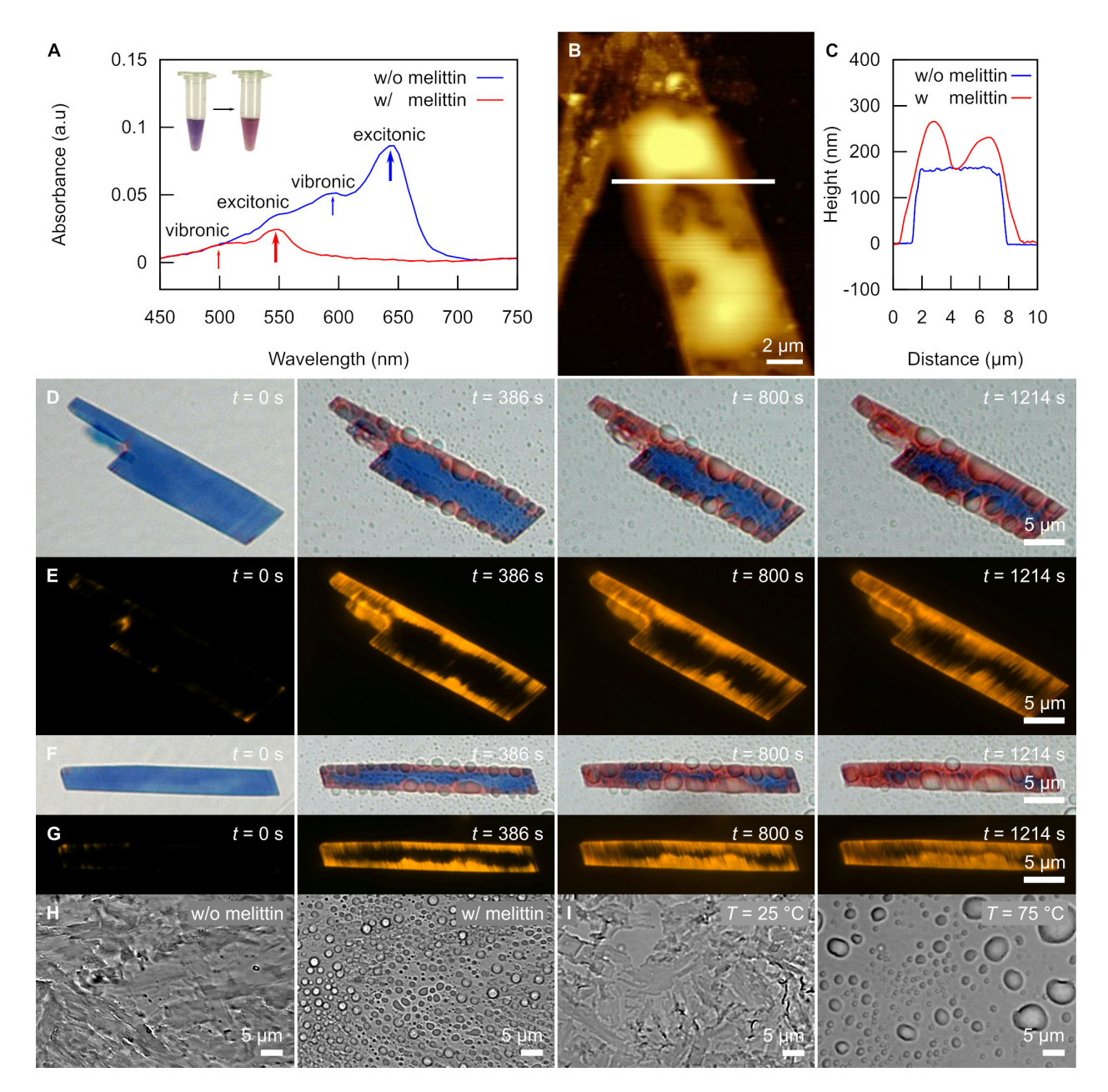


FIGURE 2.7: (A) UV-Vis spectra of polydiacetylene (PDA) made of 60 mol % TRCDA and 40 mol % DOPC with and without melittin at a peptide-to-lipid molar ratio (P/L) of 0.03. (B) AFM topology of a PDA crystal after addition of melittin. (C) Cross sections before and after adding melittin to the crystal. (D, F) Bright field and (E, G) fluorescence microscopy snapshots of PDA during the incubation with melittin. (H) Bright field microscopy images of TRCDA monomers assembled on a glass coverslip before and after addition of melittin at a molar ratio (P/L) of 0.03. (I) Bright field microscopy images of TRCDA monomers before and after heating to T = 75 °C.

explains the data shown in Figure 2.7H, where at a high peptide-to-lipid molar ratio melittin can melt solid phase lipids at room temperature. Anionic TRCDA and cationic melittin (net charge +6) interact via both electrostatic and hydrophobic interactions. The function of melittin in TRCDA layers may not be exactly the same as the known actions in phospholipid

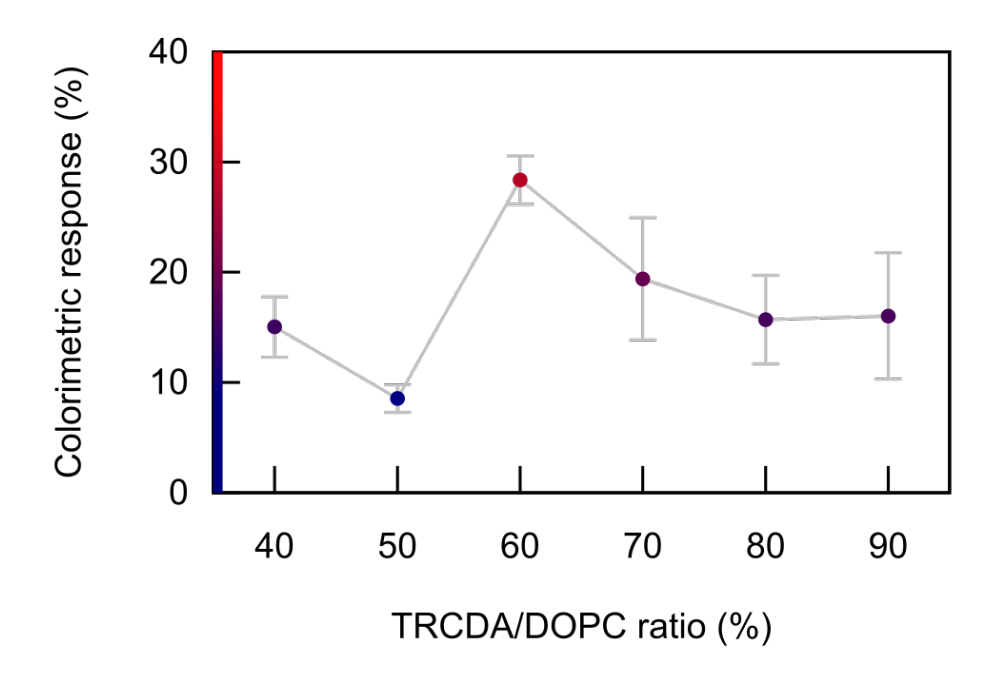


FIGURE 2.8: TRCDA/DOPC ratio dependency on the colorimetric response upon adding melittin at a peptide-to-lipid molar ratio of 0.03.

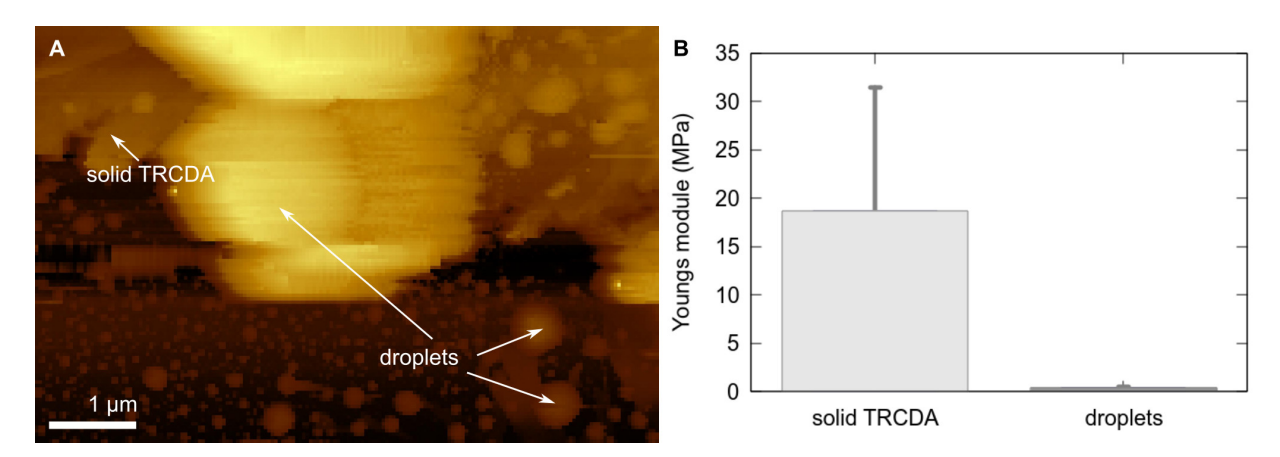


FIGURE 2.9: Atomic force microscopy of monomeric TRCDA in HEPES buffer solution after adding melittin. Amorphous and crystalline structures are indicated by the arrows. Via force spectroscopy the Young's moduli for the different areas were determined (B). The Young modulus is 414 ± 126 kPa and 18.7 ± 12.7 MPa for the droplets and the solid TRCDA respectively. The elasticity of the droplets is comparable to soft gelatin and too soft for solid-state TRCDA. This supports that the "droplet" is TRCDA in a liquid state.

bilayers such as pore formation, yet a strong interaction is expected as both of them are amphiphilic. Alteration of the monomer to N-[2- (ethylamino)ethyl]-10,12-pentacosadiyneamide hydrogen bromide qualitatively presented similar results (Figure 2.11).

These observed droplets spatiotemporally coincide with the red polymer in Figure 2.7D-G. By connecting these dots, we think that the melting of the crystal induced by melittin is

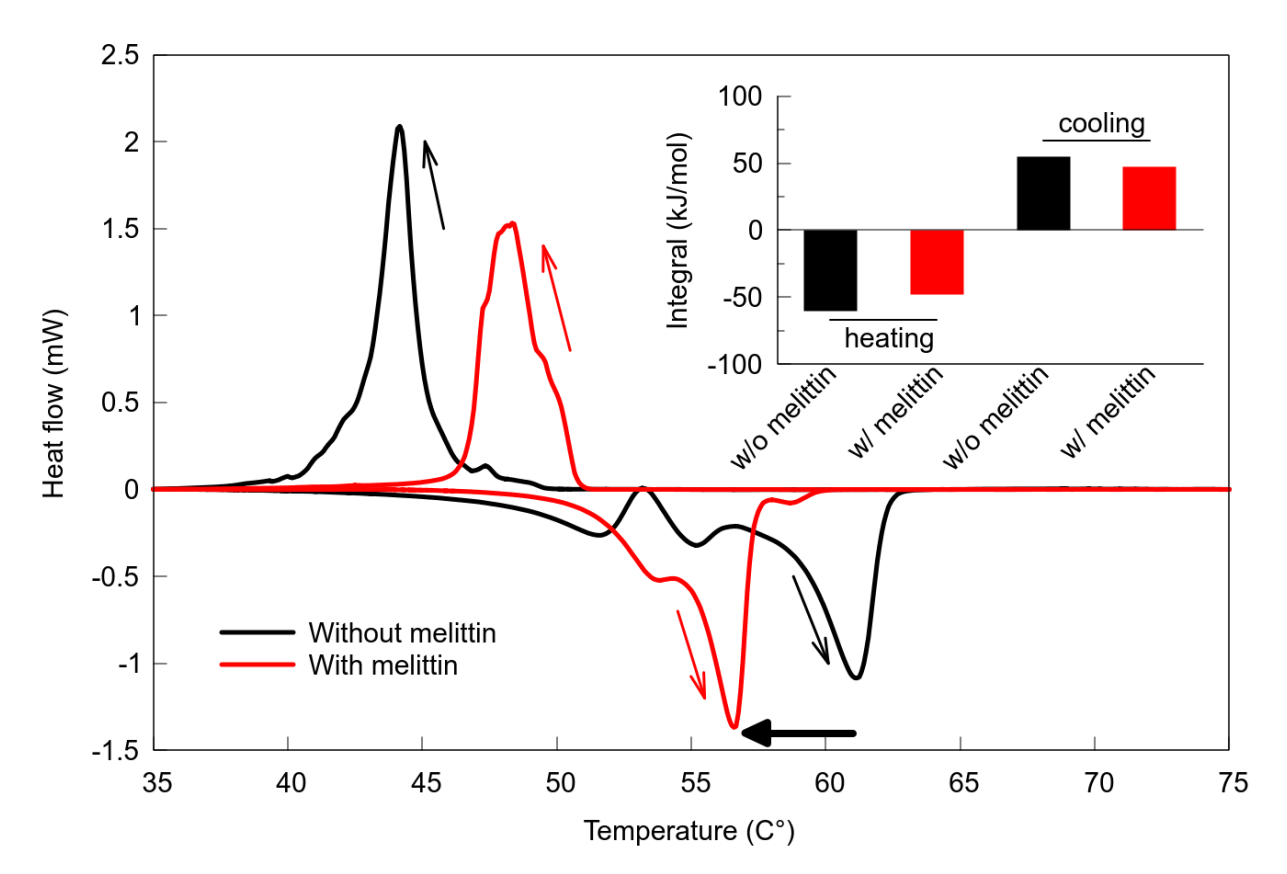


FIGURE 2.10: Differential scanning calorimetry of TRCDA monomer with and without melittin at a (P/L) ratio of ~ 0.15 . In the presence of melittin, the transition temperature decreased by ~ 4.4 °C while heating. The inset shows the integrated (total) normalized heat transferred at the transitions. The total heat for the phase transition is reduced by $\sim 20\%$ with melittin. This is because the addition of melittin had partially transformed the solid TRCDA into liquid, thus less solid-state TRCDA was left in the chamber for the further phase transition when the temperature was being scanned. Both suggest that melittin triggers the solid-to-liquid transformation of TRCDA. Interestingly the crystallization temperature increased when melittin was added, presented by the peak temperature shift from 44.2 °C to 48.3 °C during cooling. A possible explanation is that the addition of melittin acted as an impurity, which may have helped with the solidification as more nucleation centers were available compared to pure TRCDA. Note that the signals with melittin contain salts in the chamber due to the NaCl in the melittin solution, yet the control experiments confirmed that salts yield no significant signals.

the origin of the blue-to-red transformation in PDA.

This interpretation has a striking similarity to thermochromism. 62,144,163,186 A previous work 162 and our literature review in Table 2.1 show that the melting temperature (the solid-to-liquid phase transition temperature) $T_{\rm m}$ of the diacetylene monomer and the blue-to-red thermochromic transition temperature $T_{\rm B2R}$ of its polymer form (PDA) coincide ($T_{\rm m} = T_{\rm B2R}$). This suggests that the thermochromism of PDA originates from the melting of the crystal structure, which induces torsions in the backbone and therefore shortens the conjugation

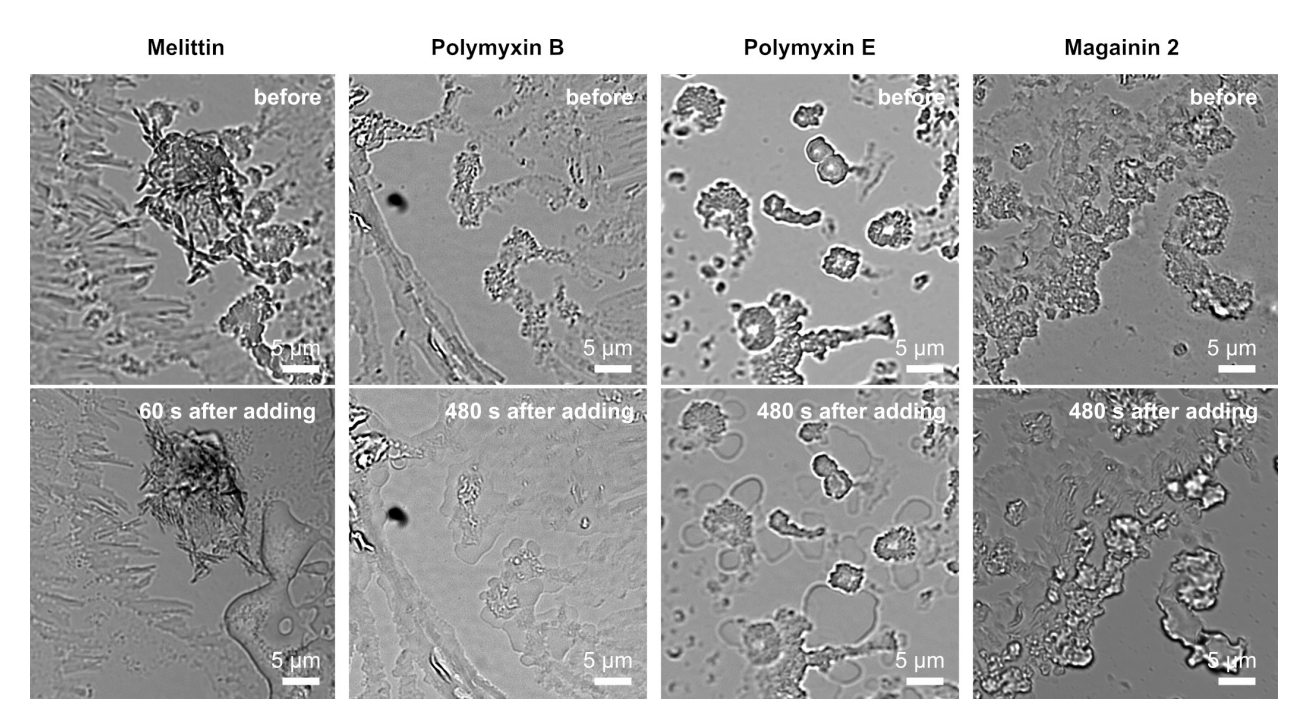


FIGURE 2.11: Bright field microscopy image of N-[2-(ethylamino)ethyl]-10,12-pentacosadiyneamide hydrogen bromide assembled on a glass coverslip before and after addition of different peptides. The concentration of the added solution was 1 mM for melittin and 2 mM for polymyxin B, polymyxin E and magainin 2.

length. This is in agreement with IR spectroscopy studies, where alkyl chains in red PDAs were more disordered than those of blue PDAs.²⁷ In other words, thermochromism and peptide-induced chromism can be universally explained by the lipid phase transition, where its cause is elevated temperature in the former case and the interactions with peptides in the latter case.

To study the thermodynamics of this phenomenon, we performed titration of TRCDA with peptides and monitored this process by isothermal titration calorimetry (ITC). We carried out a reverse titration, where peptides were injected into lipids. This is the opposite of the typical ITC experiments, where lipid vesicles are injected into peptides. When 1 μM melittin solution was injected into the TRCDA suspension (always 2 μM, 11 times), no significant peak was observed (Figure 2.12B, first column: *). After the completion of 11 injections, the solution in the chamber was replaced with a new TRCDA suspension and the next melittin solution (10 μM) was injected, where no significant heating was observed either (Figure 2.12B, first column: **). When 100 μM melittin solution was injected, injection-number-dependent endothermic peaks started to appear (Figure 2.12B, first column: ***).

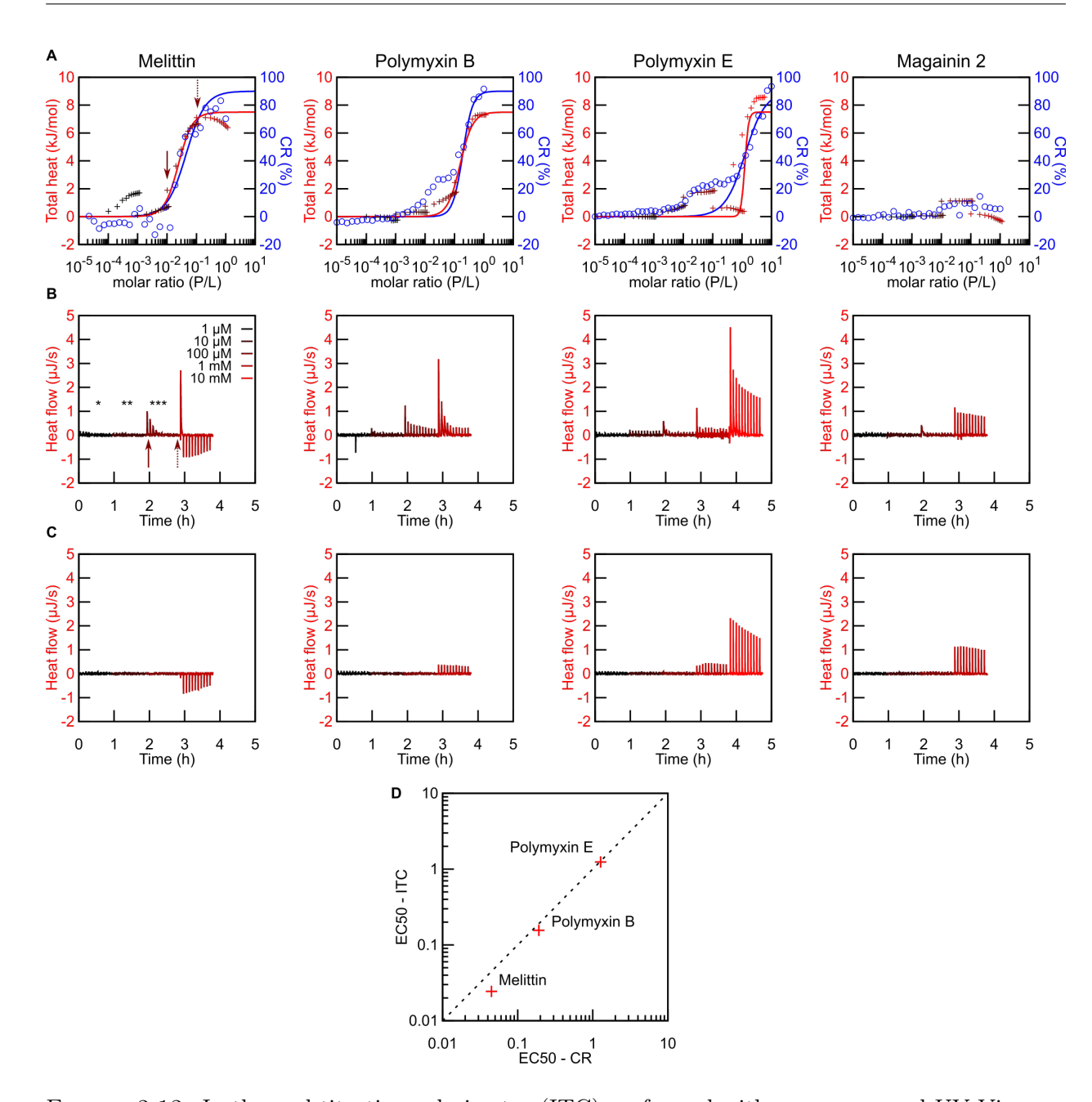


FIGURE 2.12: Isothermal titration calorimetry (ITC) performed with monomers and UV-Vis spectroscopy with polymers during titration with different antimicrobial peptides: melittin, polymyxin B, polymyxin E and magainin 2. (A) The cumulative integration of titration peaks in (B) after the subtraction of the control signal in (C) on the left axis and the colorimetric response on the right axis. To cover the titration over several orders of magnitude of peptide-to-lipid ratios, the titration was performed with four to five different concentrations of peptide solution as described in the text in details. (C) The control experiment, where peptides are injected into buffer solution. (D) Comparison between the EC_50 from ITC and CR for each peptide.

Such endothermic peaks have been previously associated with a solid-to-liquid phase transition of 1,2-dipalmitoyl-sn-glycero-3- phosphocholine (DPPC, $T_{\rm m}=41.3$ °C) caused by the

titration with ethanol. 187 Nevertheless, in the case of titration with peptides, the signal corresponds to the heat from binding and peptide conformational changes in addition, ¹⁸⁸ which are difficult to separate. The peptide-to-lipid ratio of around 10-2 was required for these endothermic peaks to appear, which is consistent with our bright-field microscopy observation, where droplets as an indicator of melting started to appear at a similar peptide-to-lipid ratio (Figure 2.7H). Integration of these peaks was plotted as "total heat" in Figure 2A after subtracting the heat of dilution shown in Figure 2.12C (control experiment where melittin is injected into 4-(2- hydroxyethyl)-1-piperazineethanesulfonic acid (HEPES) buffer). Here, the integration is a cumulative integration of peaks from one concentration of melittin (not the integration of each individual peak like in the standard ITC analysis). For example, the integration of the first peak when 100 µM melittin solution was injected is indicated as the first dark red marker, as shown in Figure 2.12A (see the solid line marked by an arrow in Figure 2A,B), while the cumulative integration up to the 11th peak is indicated as the 11th dark red marker in Figure 2.12A (see the dotted line marked by an arrow in Figure 2.12A,B). The unit, kJ/mol, is defined as the total heat divided by the amount of TRCDA (not peptides). The result suggests that there is a critical peptide-to-lipid ratio $(\alpha_{\rm melt} \sim 0.02 \text{ as EC}_{50})$ at which TRCDA interacts with melittin and melts (Figure 2.12A, first column); although the simple sigmoidal curve fitting is an approximation, the actual ITC data is more complex. At high peptide-to-lipid ratios, where the total heat starts to saturate because all TRCDA accessible to melittin has already melted, ΔH (total heat per mol of TRCDA) is in the range of ~ 7.5 kJ/ mol, although this value fluctuated in each experiment. Next, the TRCDA suspension is exposed to UV irradiation to form the PDA suspension, which is similarly titrated with melittin and monitored by UV-Vis spectroscopy. Colorimetric response (CR), which is a ratiometric analysis between the blue peak at 645 nm and the red peak at 546 nm to quantify the color (see Materials and Methods), was calculated and is plotted in Figure 2.12A on the right axis. The result shows that there is also a threshold peptide-to-lipid ratio ($\alpha_{\rm B2R} \sim 0.04$ as EC₅₀) at which peptides induce the blue-to-red transition in PDA. The orders of magnitude of these peptide-to-lipid ratios required to interact and melt monomers (α_{melt}) and to change the color of the polymers

To study whether this is a general phenomenon in antimicrobial peptides, these experiments were repeated with polymyxin B, polymyxin E, and magainin 2. First, bright-field microscopy images confirmed that polymyxin B and polymyxin E melt TRCDA similarly to melittin, whereas little effect was observed with magainin 2 (Figure 2.13). The results of ITC experiments with these peptides were fitted with a sigmoidal curve with a maximum value of 7.5 kJ/mol for all of them (Figure 2.12A-C, the second, third, and fourth columns). Note that magainin 2 did not show a significant response in both ITC and UV-Vis spectroscopy under our experimental conditions (e.g., 10 mM HEPES, 150 mM NaCl, pH = 7.4); thus, fitting was omitted. In an earlier study,²³ magainin 2 induced a strong colorimetric response with PDA mixed with DMPC without the salt. The correlation between EC₅₀ from ITC and EC₅₀ from UV-Vis fell onto the unity line (dotted line in Figure 2.12D), suggesting that the orders of magnitude of α_{melt} and α_{B2R} match for all of the antimicrobial peptides ($\alpha_{\text{melt}} \sim \alpha_{\text{B2R}}$).

An open question is whether the cause of the blue-to-red transition in PDA is associated with the solid-to-liquid transition of leftover monomers in PDA or the phase transition of the alkyl chains in the polymer, which is rather a crystal-to-amorphous transition. Previously, PDA with 99% polymerization efficiency, where leftover monomers were negligible, was used to answer this question with respect to thermochromism and it was concluded that it is the latter. This suggests that the presence of the leftover monomers is not required for the color change in the case of thermochromism. Nevertheless, in the case of peptides, monomers may have an additional role of facilitating the penetration of peptides inside PDA crystals.

To study the penetration of melittin inside PDA crystals, we correlated the height of the PDA crystals and the fraction of PDA that was activated by melittin by combining fluorescence microscopy and AFM. Melittin stimulated blue-state PDA flakes in a time-dependent manner (Figure 2.14A).

This fluorescence increase started from the edge of the structure, while it penetrated

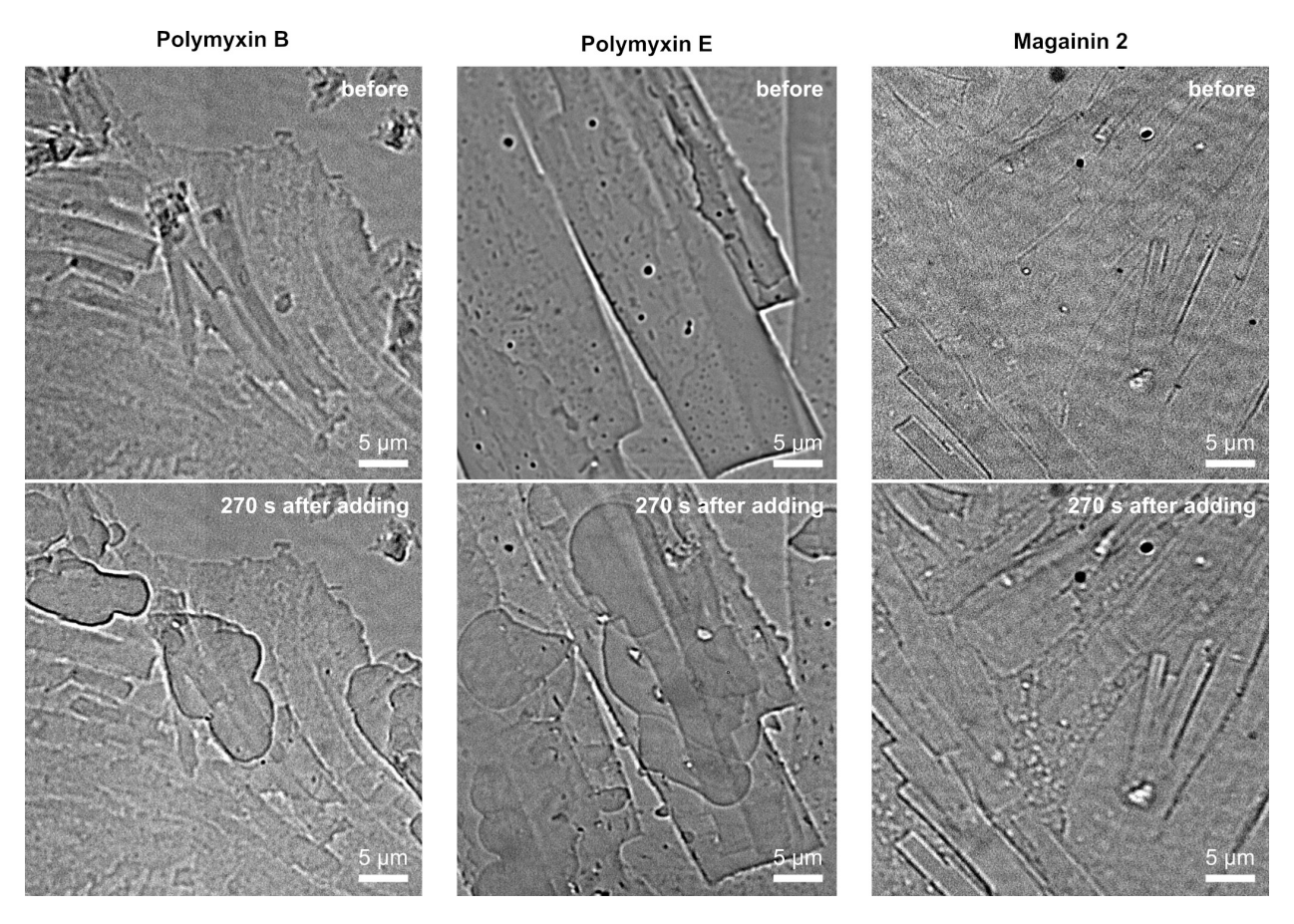


FIGURE 2.13: Bright field microscopy images of TRCDA monomers assembled on a glass coverslip before and after addition of different peptides (polymyxin B, E and magainin 2) at a molar ratio (P/L) of 10.

inside the PDA flakes over time (Movie M1 is shown in the Supporting Information online). After 20 min of incubation, the system roughly reached equilibrium and the fluorescence signals saturated. We analyzed the changes in the fluorescence intensity of PDA before and 20 min after melittin addition and their AFM topology in five different regions of interests (ROIs, Figure 2.14 G). These values are normalized by the fluorescence intensity obtained after the complete PDA activation by heat as 100% (Figure 2.14B,C). This normalization enables the quantification of the fraction of PDA activated by melittin. For example, in ROI 5, melittin activated only 8.4% of PDA, while an additional 91.6% increase in the fluorescence was observed following heat activation (Figure 3C). These activation fractions by melittin were compared with the height of each PDA multilayer estimated by AFM (Figure 2.14D-F). The activation fraction by melittin was inversely correlated with the height of the PDA multilayer (Figure 2.14H). This implicates that thick PDA multilayers have some fraction of

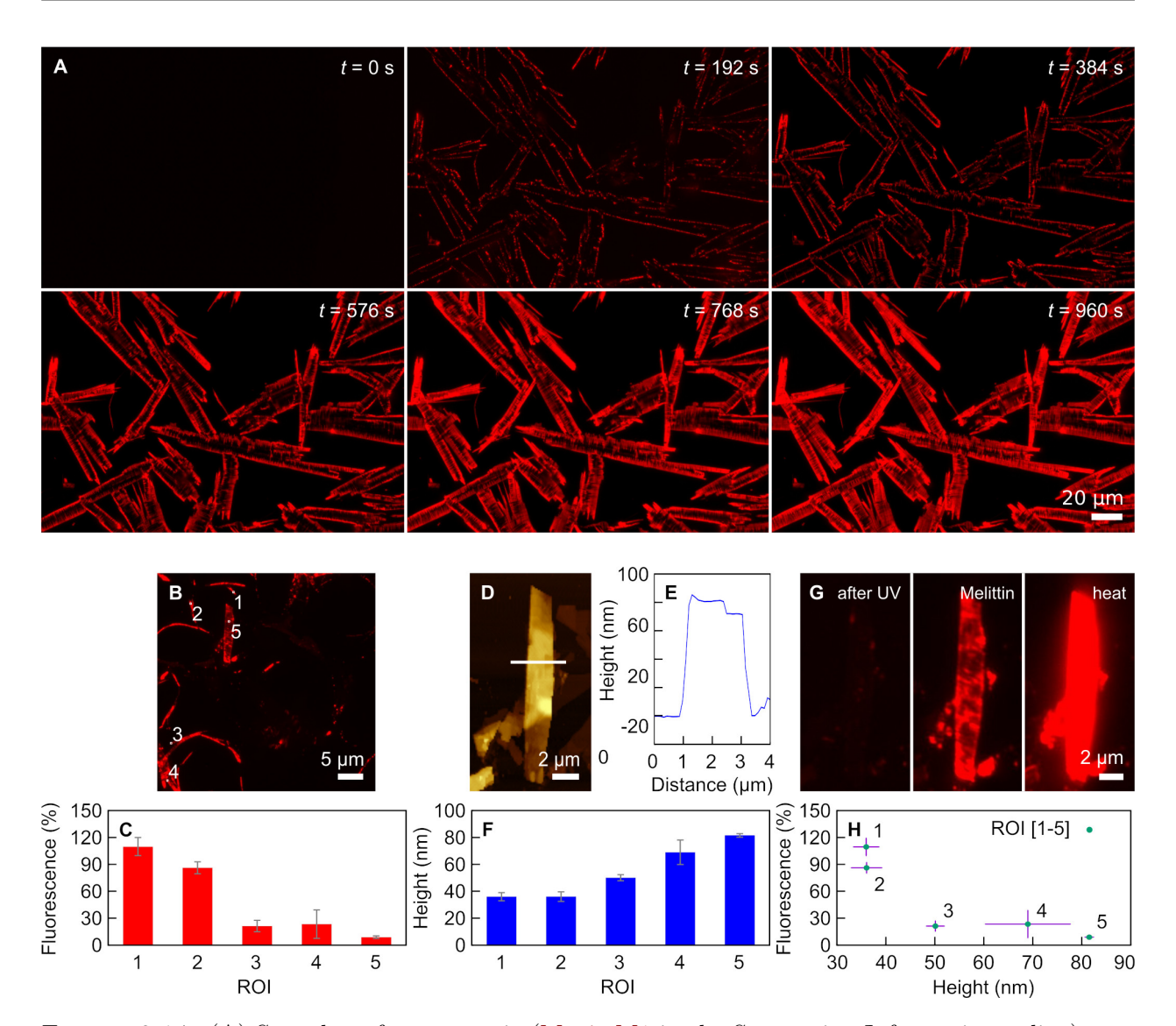


FIGURE 2.14: (A) Snapshots from a movie (Movie M1 in the Supporting Information online) during the incubation of the blue-state PDA with melittin at 30 µM imaged by fluorescence microscopy. Note that the time resolution is twice as high as the one in Figure 2.7 to clarify the migration of the fluorescence from the edge to the inner part of the PD crystal. (B) New set of PDA crystals exposed to melittin imaged by fluorescence microscopy. (C) Fluorescence increase at ROIs indicated in (B) when melittin is added, where the values are normalized by the amount of the fluorescence intensity after the heat activation as 100%. (D) Atomic force microscopy image of ROI 5 and (E) its cross section before adding melittin. (F) Height measured by AFM for the ROI indicated in (B). (G) PDA crystal in ROI 5 before and after adding melittin and after the heat treatment. (H) Fluorescence increase vs the height for 5 ROIs indicated in (B).

intact blue PDA inside their structures, where melittin failed to stimulate. This result is in agreement with our previous studies, where dynamic light scattering (DLS) and UV-Vis and fluorescence spectroscopy have been combined to show that the PDA activation by melittin takes a few hours until it reaches equilibrium in the PDA suspension with a large particle size due to the fact that melittin interacts with the outermost layer of PDAs and takes

2.3. Conclusion 61

time to penetrate the multilayer structure.¹⁴⁹ These results implicate that although both thermochromism and peptide-induced chromism stem from the melting of alkyl chains, the latter is influenced by the ability of peptides to penetrate the PDA crystals (Figure 2.14A), where the presence of leftover monomers may have an advantage by providing a less rigid matrix for melittin to migrate.

2.3 Conclusion

The data presented in this work supported our hypothesis: the peptide-induced color change originates from the peptide-induced lipid phase transition. However, whether anything that influences the lipid phase alters the color is still an open question. Unlike other mechanochromic polymers whose color is altered as a consequence of a change in their chemical structures ^{189–191} or quenching of incorporated dyes, ¹⁹² the chromism in PDA is rather close to that of mechanochromic fluorophores, ¹⁹³ where the increase in the amorphous domains is linked to the mechanism. The reported result provides an additional angle to look at the chromism in PDA, where among many different types of stimuli some may share a common mechanism like in the case of thermochromism and peptide-induced chromism.

2.4 New Experiments and Discussions

For a follow up study on the crystal behavior for a blue-to-red transition, fluorescence microscopy and TEM has been combined. A morphological change has been observed in areas where the crystal turned red after adding melittin. The crystal structure of the different states has been discussed in section 1.5. As visible in Figure 2.15 the fluorescence signal appears in areas in which the the crystal suffers cracks. These fractures arise from the density incremental from the blue - to the red state of the crystal. 40,153 As already presented in Figure 2.1 the blue-to-red transition starts preferably from the borders of the crystal and continues inwards along the backbone. Here, the density changes and therefore a further

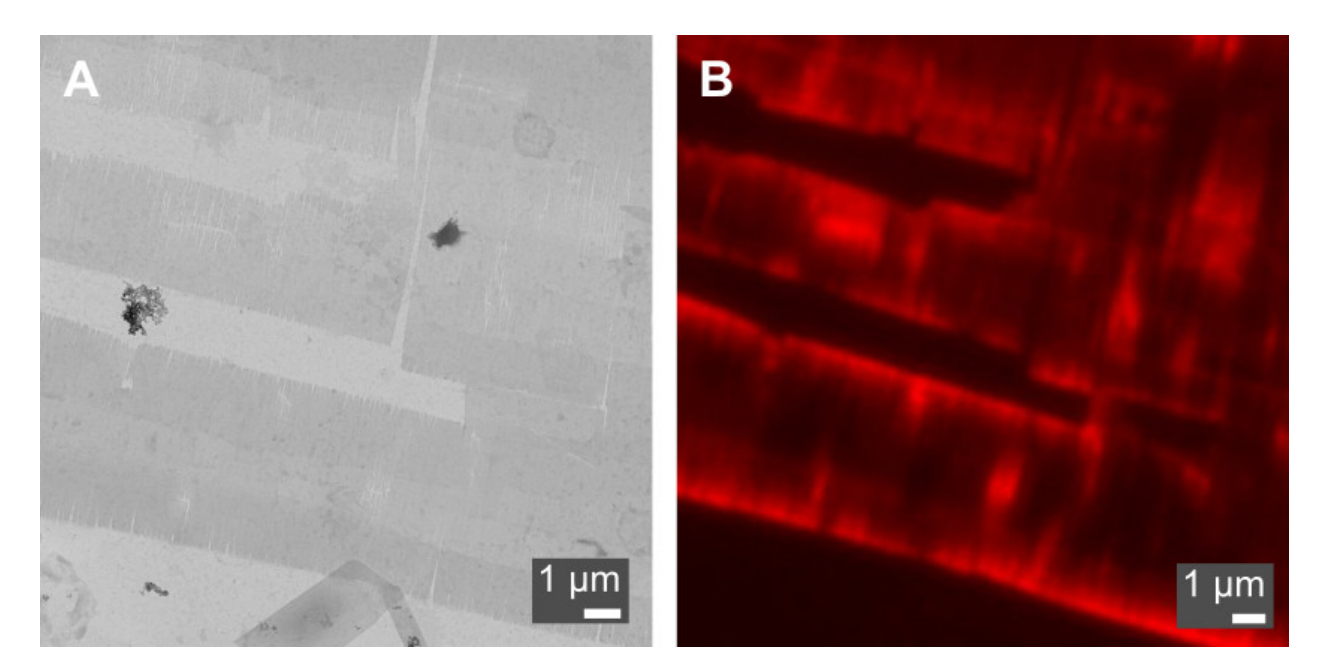


FIGURE 2.15: PDA crystal exposed to melittin observed by TEM (a)) and fluorescence microscopy (b)). Small cracks parallel to the direction of the PDAs backbone are visible in TEM. Unpublished data.

contraction of the crystal should help to provide more free space for melittin to penetrate deeper into the crystal.

Cracks could also arise during the drying process of the sample. As a control a DA crystal in buffer solution has been exposed to UV light continuously for several minutes to induce the blue-to-red transition. Under these conditions a possible contraction due to the desiccating is excluded. The process was monitored by optical microscopy. Fractures up to 200 nm appeared during the transition. The bright field (BF) - and fluorescence images were binarized by an adequate threshold grey value. Examples of frames at different time points (minute 2 and 38) are shown in Figure 2.16A,B for BF and C,D for the fluorescence images. The former pair is already binarized while for the latter pair the threshold mask is only laid over the original image (yellow). This demonstrates the workflow of the data post processing. In a further step this frame was binarized as well. The analyzed data is presented in E. The area of the crystal is calculated from the BF images (black squares). Within the first minutes the transparent monomer starts to polymerize and the contrast enhances. This explains the areas increase until minute ~ 3 where a plateau is reached (blue state). After around 10 minutes the blue-to-red transition takes place. The fluorescence increases (red dots) while

the area decreases. This experiment demonstrates the density change and therefore the

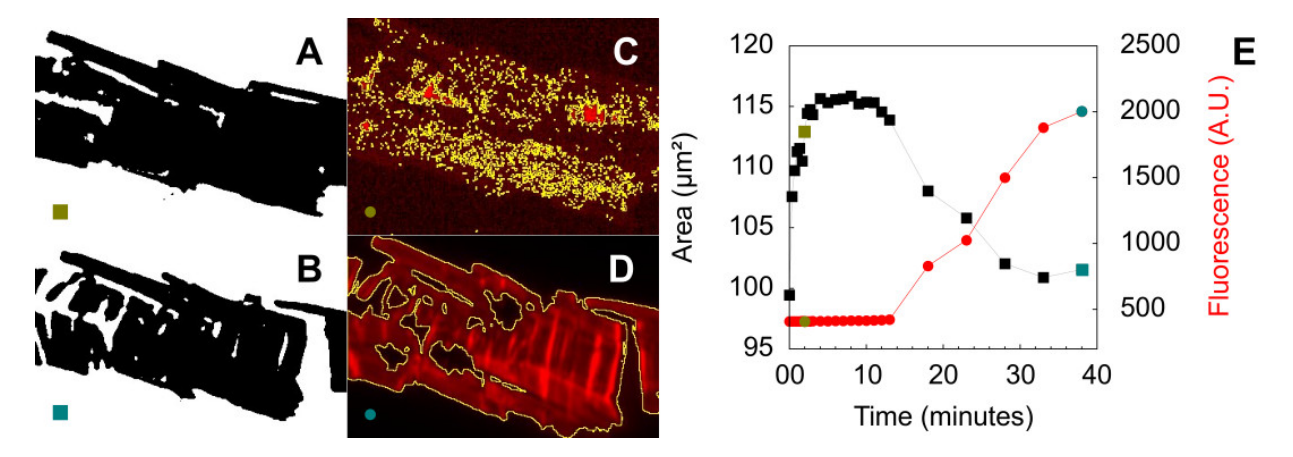
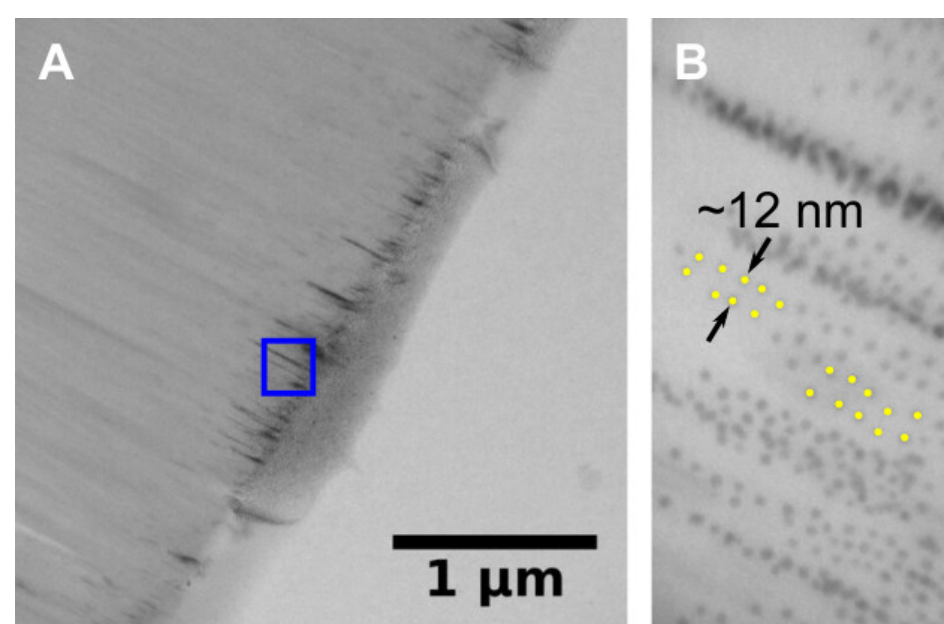


FIGURE 2.16: Induced blue-to-red transition by UV light. The binarized bright field (A,B) and binarized mask (yellow) laid over the fluorescence images (C,D) for time points at minute 2 and 38. E) reports the area of the PDA (black) and fluorescence (red) over time of irradiation. The olive and teal colored points refer to their corresponding frame A-D. Unpublished data.

formation of cracks within the PDA matrix. The area of the selected PDA crystal shrinks by $\alpha=13.6\%$. As the contraction takes place exclusively along the direction orthogonal to the backbone, the shrink factor α is the same for the area and along this direction. Our value is in the same order of magnitude as previously published data $(20\%^{153}, 15\%-32\%^{40})$. It is worth mentioning that the published data were obtained on compressed LB mono-/trilayer films. These films are quite mobile at the air-water interface unlike our multilayer crystals grown on the bottom of glass coverslip.

In order to gain further insight into these cracks, melittin was tagged with 5 nm gold particles. After a PDA crystal was incubated with the peptide-labeled solution, the sample was desiccated and analyzed via TEM. In Figure 2.17A the alternating contrast pattern indicates the crystal structure.¹⁷⁵ Moreover, the gold particles agglomerated at the crystal's border. At higher magnification (B) the individual gold particles can be identified. It appears that the cracks are filled with the particles. Interestingly, some are spaced equidistant around $d \sim 12$ nm. For a better visualization several gold particles are highlighted in yellow. This distance does not indicate the spacing between each polymer chain (~ 0.4 nm¹⁵³) but rather an area of stable aligned chains. The distance corresponds to around 15 chains. These results show that even on a nanoscopic scale a PDA crystal does not behave homogeneously. A schematic representation is shown in Figure 2.18



64

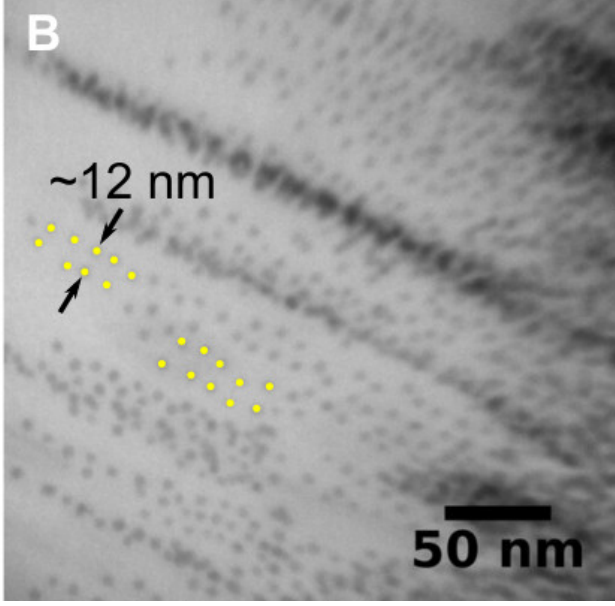


FIGURE 2.17: Gold-labeled melittin inducing a blue-to-red transition of PDA imaged by TEM. The blue square in (A) indicates the magnified area shown in (B). Unpublished data.

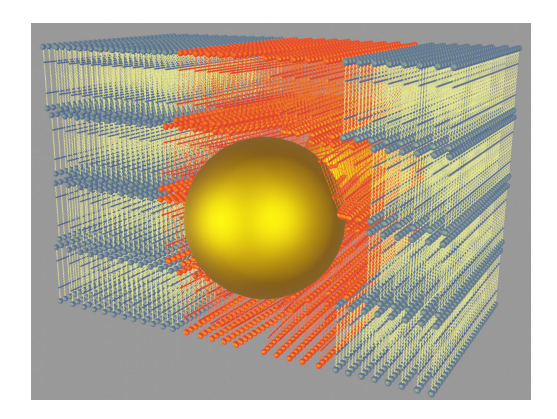


FIGURE 2.18: Schematic representation of a gold particle penetrating a PDA crystal. In this region PDA is stimulated and converted into its red state. Melittin attached to the gold particle has been omitted. Unpublished data.

The cracking between the aligned polymer chains is probably highly influenced by the ratio of monomer to polymer inside a DA/PDA crystal. When adding an external stimulus to the PDA crystals, the blue-to-red transition is not always uniform (compare Figure 2.19). The two crystals A/B and C/D, grown from the same DA solution on the same sample within and appeared at close proximity ($\sim 50 \, \mu m$). Nevertheless, they react quite differently to the added melittin. The first one demonstrates the typical blue-to-red transition: The conversion starts from the border direction inwards of the crystal (B). At the same time, monomeric TRCDA from the P/DA matrix is transported to the crystals outside similar to

Figure 2.7D. In addition, the conversion speed along the PDA backbone is different within this crystal. The second crystal almost does not respond to melittin: neither a great amount of monomer is leaking out (C) nor the fluorescence signal is increasing much (D). We suspect that a varying P/DA matrix is responsible for this behavior.

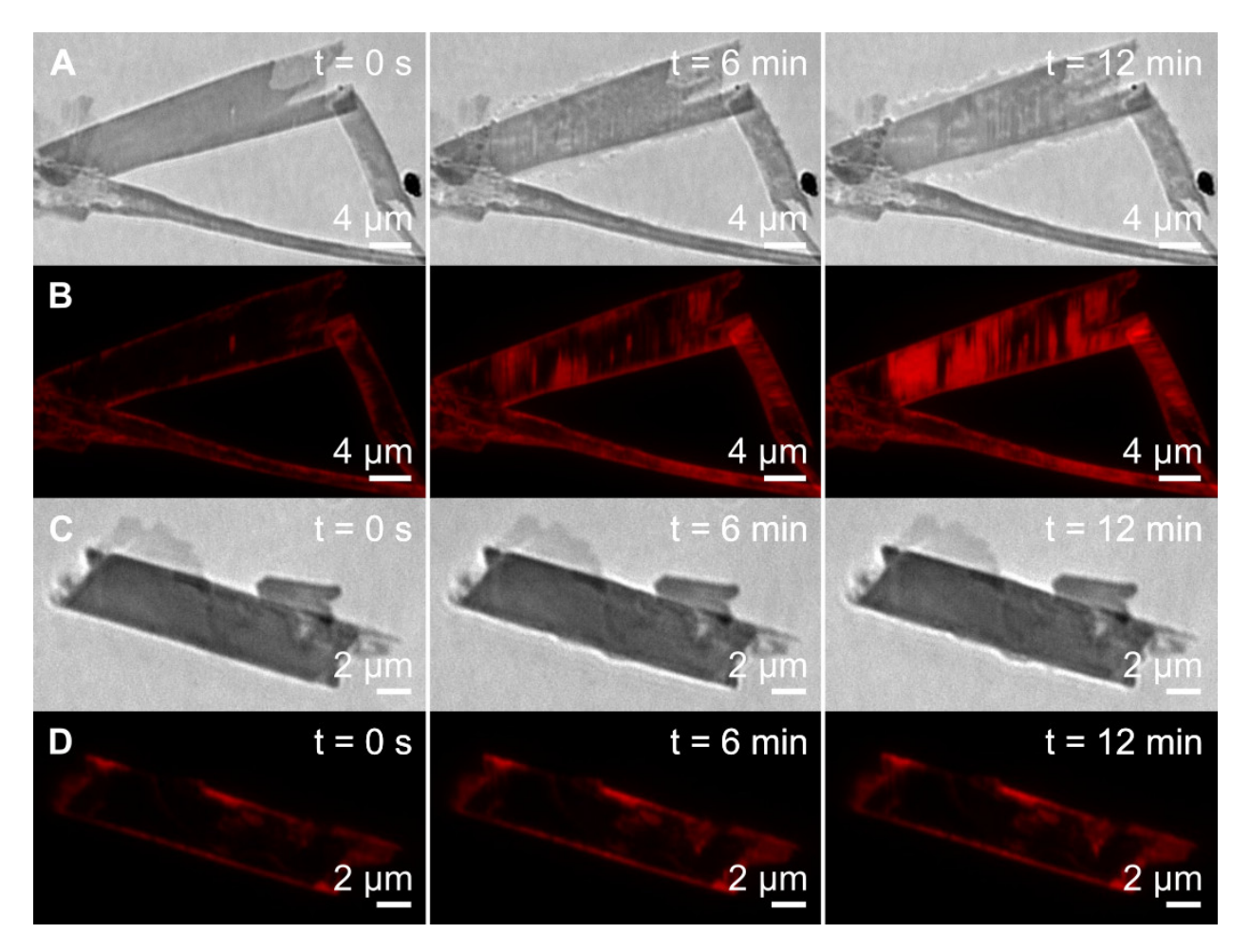
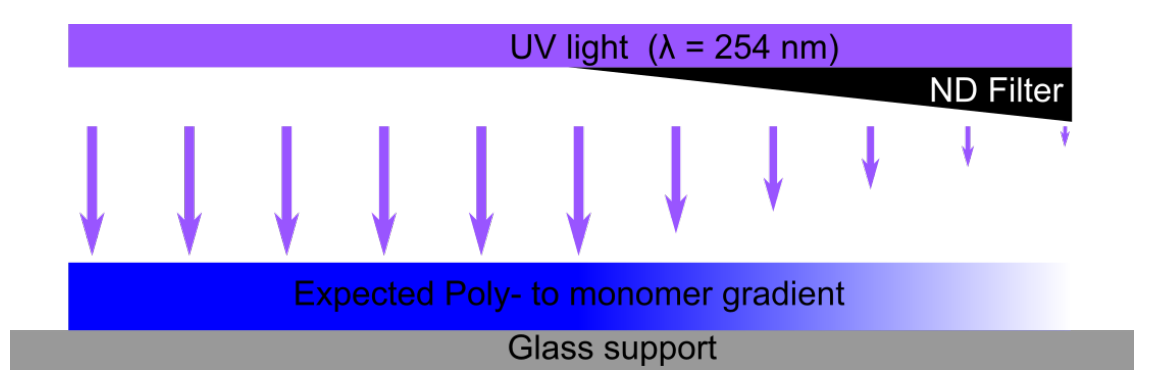


FIGURE 2.19: Snapshots of polymerized TRCDA crystals exposed to melittin imaged by bright field (A,C) and fluorescence microscopy (B,D) at different time points. These crystals were on the same sample in close proximity ($\sim 50~\mu m$ apart). Nevertheless they behave quite differently to melittin. Unpublished data.

In order to investigate our hypothesis, the following experiment was designed: instead of an uniform UV irradiation, an intensity gradient of UV light was applied to the monomeric TRCDA crystals. These crystals were fabricated via Langmuir-Blodgett method and transferred to a glass coverslip. A scheme is shown in Scheme 2.2, the UV blocker was achieved by a continuously variable reflective neutral density filter. Due to the varying intensity profile a polymer-to-monomer gradient was expected. The complete preparation is described in

section 3.10.



SCHEME 2.2: Experimental setup to expose monomeric TRCDA crystals to a continuously variable UV intensity profile. A continuously variable reflective neutral density filter with an operation range between 240 nm and 1200 nm was used as a ND filter.

Although the unpolymerized TRCDA on the far right (barely visible) was observed as expected (compare Figure 2.20A), the anticipated profile was surprisingly not obtained. It looks like that the structure inside the crystals has a higher influence on the polymerization efficiency than the intensity of the UV light (or irradiation time).

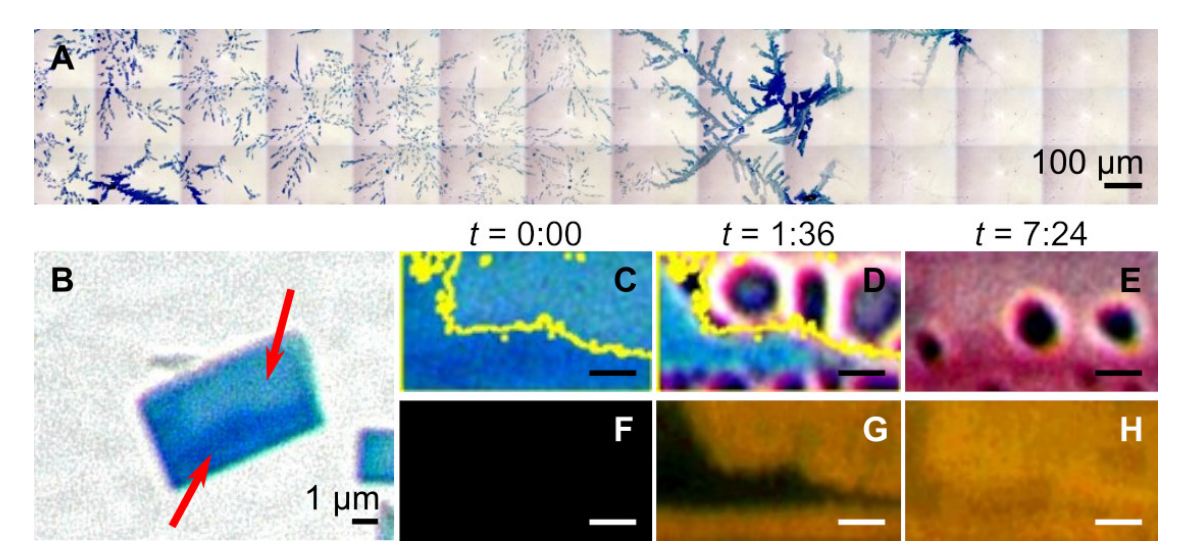


FIGURE 2.20: A) Monomeric TRCDA crystals exposed to a continuously variable reflective neutral density filter with an operation range between 240 nm and 1200 nm (NDL-10C-4, Thorlabs). The crystals on the right side are still in its monomeric form. The rectangular pattern arises from an uneven illumination of the individual images taken by BF microscopy and further stitching together. (B) selected crystal from the sample for further investigation. Time evolution of PDA crystals exposed to melittin imaged by BF (C-D) and fluorescence microscopy (F-H). The scale bar indicates 1 μm. Unpublished data.

2.5. Outlook 67

AFM measurements from similar crystals excluded great variation in the topology (data not shown). One crystal of the sample was selected (B) and further investigated. This crystal holds a 2D intensity profile with two dominant regions (marked by the two arrows). These two regions react at different blue-to-red transition rates when exposed to melittin. This is visible in C-E (true color bright field images) and in F-H (fluorescence images). It is even possible to predict the reaction towards the blue-to-red stimulus of different regions by analyzing the intensity of the blue color in the true color bright field images. The yellow mask added on top of the image in C and D separates the crystal into a region with a higher and a lower polymer content. The more transparent region, containing a higher percentage of monomeric TRCDA reacts faster than the region containing a higher content of polymer.

Taken together these results demonstrate how the monomer/polymer matrix of the crystal influences the sensitivity and blue-to-red transition. The observed variation for the polymerization efficiency and reaction to external stimuli quantified by UV-Vis spectroscopy can be explained with the nanoscopic picture: each polymer-chain inside a PDA crystal reacts differently to a certain extent. Analyzing the whole PDA solutions averages these characteristics.

2.5 Outlook

For further studies, a prediction model could be explored. The total absorbance A is the sum of individual absorbance centers δA :

$$A = n_{\text{poly}} \cdot \delta A$$

Only the polymerized diacetylene fraction (n_{poly}) contributes to the absorbance in the visible region. This fraction can be extracted from the true color bright field images. These images are recorded within a 24-bit color space (RGB), 8 bit (= $2^8 = 256$) for each channel (Red, green and yellow). Each pixel's color in an image is described by the 3 grey values (R,G,B) between 0-255. For a more realistic image, an additional channel, the so called α channel, is would be necessary. This leads to a 32-bit color space (RGBA). A microscope

68

camera works only in the RGB color space, transparency is interpreted as white. On a white background both images appear exactly the same, the information of α is lost (compare Figure 2.21 B). As the transparency of a certain P/DA crystal contains the information of the polymer/monomer fraction n_{poly} , this α is critical for the prediction model. The white background in the image should be transparent (compare A). The alpha channel can be calculated from a RGB image, the principle is shown in (C). The area indicated in (A) is polymerized by $\approx 30\%$. Mathematically, an alpha channel is added to the 24-bit image to create the full 32-bit image. The correct grey value (0-255) for the α channel arises from the color white by comparing the desired pixel with the background.

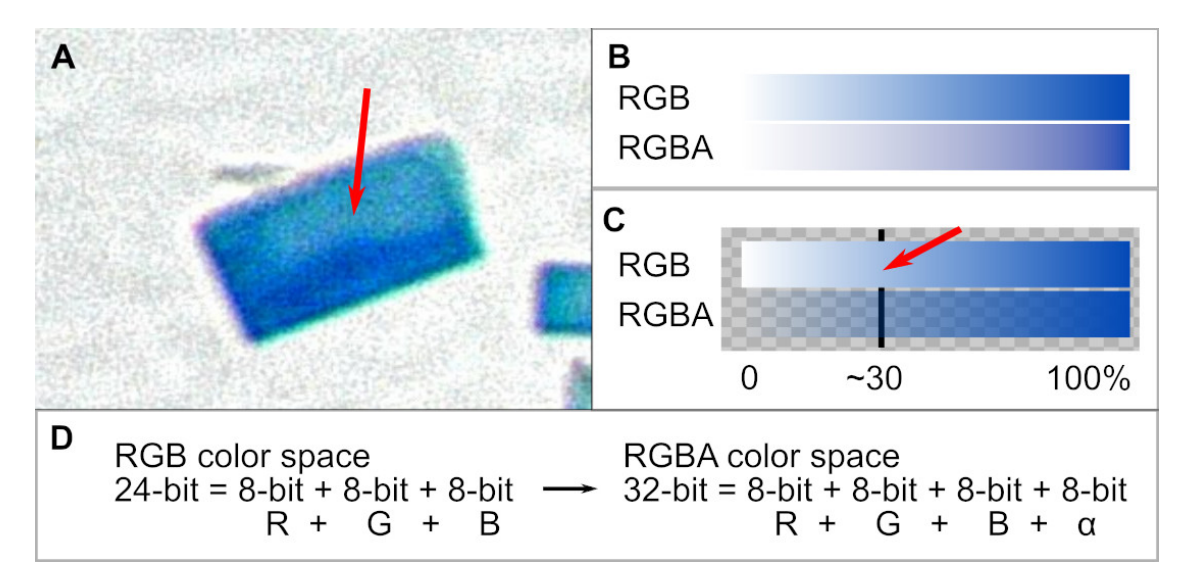


FIGURE 2.21: A) polymerized TRCDA crystal imaged by the 24-bit camera of the optical microscope. B and C compares a 24 (w/o α) and 32-bit (w/ α) image on a white (B) and (C) structured background. The red arrow indicates the corresponding color of the indicated pixel in A. The TRCDA crystal is polymerized by $\approx 30\%$ in this region. D shows the numerical composition of an image (for each pixel). Unpublished data.

To understand this behavior in detail, it is important to separate the influence of the crystal structure and the monomer-to-polymer ratio within the DA/PDA matrix. To improve the homogeneity of the crystal structure, the sample preparation has to be revised: even so the crystals in Figure 2.20 were prepared by the Langmuir-Blottget technique, the morphology of lipid domains still differs. This could not only be optimized by altering the sample preparation parameter (compression rate, temperature etc.) but also by exchanging the diacetylene derivative. For example 10,12-pentacosadiynoic acid (PCDA), slightly longer

2.5. Outlook 69

than TRCDA, is able to form very homogeneous islands ($\approx 9.0 \pm 0.9$ nm). From our own experience, these applies generally to DA derivatives with longer side groups: stronger interaction between the hydrocarbon chains improves the overall order within the crystal in the self-assembling process. In order to better control the monomer-to-polymer ratio, instead of polymerizing the monomer by an intensity gradient of UV light, a equidistant grid-like pattern with a narrow spacing, could overcome the problem. The spacing should still be resolvable by eg. fluorescence microscopy. Due to the grid pattern, a better signal could be extracted when data is post processed by Fast Fourier Transformation. Here, each region of a maxima and minima is expected to react similar to the blue-to-red transition respectively. This statistical supported analysis could minimize the morphology variation of the crystal structure. The suggested approach could provide insights of the non rigid monomer's role inside the PDA/DA matrix and lead finally to a better understanding of the blue-to-red transition of the polymer.

Chapter 3

Materials and Methods

3.1 HEPES Buffer Solution

The experiments were performed in physiological buffer solution prepared with 10 mM 4-(2-hydroxyethyl)piperazine-1-ethanesulfonic acid (HEPES, CAS RN: 7365-45-9, Fluka, Switzerland) and 150 mM sodium chloride (CAS RN: 7647-14-5, Roth, Germany) in ultra-pure water filtered through Milli-Q Gradient A10 filters (Millipore AG, Switzerland) having 18.2 M Ω -cm at 25 °C. The pH was adjusted to 7.4 using 6 M NaOH (CAS RN: 1310-73-2, Sigma-Aldrich Chemie GmbH, Switzerland).

3.2 TRCDA / DOPC Suspension Preparation

TRCDA / DOPC suspension preparation 10,12-Tricosadiynoic acid (TRCDA, CAS RN: 66990-30-5, Sigma-Aldrich, USA and Alfa Aesar, USA) was stored as follows. First, the powder was dissolved in chloroform, aliquoted, dried by a stream of nitrogen, and then resuspended in cyclohexane containing 4% ethanol. The resuspended TRCDA was cooled down with dry ice for 1 hour and lyophilized for 72 hours to remove cyclohexane/ethanol. This procedure minimizes unwanted crosslinking during the storage. The vials were filled with nitrogen (Nitrogen 4.5, PanGas, Lot. 756 311-00179757, CH) and stored in a freezer until use (T = -26 °C). Prior to use the powder was resuspended with chloroform. Once TRCDA was dissolved in chloroform, the aliquot was used within 4 months. 1,2-dioleoyl-sn-glycero-3-phosphocholine (DOPC, CAS RN: 4235-95-4, Avanti Polar Lipids, USA) and

1,2-dioleoyl-sn-glycero-3-phosphoethanolamine-N-(7-nitro-2-1,3-benzoxadiazol-4-yl) (ammonium salt) (NDB-PE, CAS RN: 384823-46-5, Avanti Polar Lipids, USA) stored in chloroform were used as received. Depending on the experiment, different molar ratios of TRCDA, DOPC and NDB-PE were mixed in a glass vial. The molar ratio for the samples presented in the section of "TRCDA/DOPC sample preparation" was 50:50:1 and 1:1:0 for the samples used in Figure 2.7B,D-G and Figure 2.14. After the evaporation of chloroform under a nitrogen stream, the vial was kept under vacuum at 400 mbar for at least 14 hours to completely remove the solvent residuals, followed by rehydration with HEPES buffer solution at a total lipid concentration of 1 mM, vortex for t = 30 s, and high-power probe sonication (Omni Sonic Ruptor 400 Ultrasonic Homogenizer, Omni International, USA) for 30 min in a water bath at T=65 °C. In order to remove titanium particles introduced by the probe sonication process, the TRCDA suspension was either sterile filtrated through a 0.22 µm filter or centrifuged by the Sorvall Legend X1R (Thermo Fisher scientific, USA) in a conical falcon tube for 5 minutes at 1000 rpm. The segregated titanium particles were visible at the bottom. Only the supernatant was used for the rest of the experiments. The second method was applied for ITC and UV-Vis measurements, whereas the first was used for the rest of the experiments. The suspension was then stored at T=2 °C for at least 12 hours in order to give enough time for the diacetylene to self-assemble (see also "TRCDA/DOPC sample preparation").

3.3 Polymerization

TRCDA monomer was polymerized either by a UV box (CL-1000 crosslinker, UVP, USA) or a UV hand light (NU-4 KL, Konrad Benda, Germany) with a UV dose of 0.1 J/cm² for supported crystals and 0.2 J/cm² for suspensions.

3.4 Peptide Preparation

Melittin from honey bee venom (CAS RN: 20449-79-0, GenScript, USA), polymyxin B (CAS RN: 1405-20-5, Sigma-Aldrich, USA), polymyxin E (CAS RN: 1264-72-8, Sigma-Aldrich, USA) and magainin 2 (CAS RN: 108433-95-0, Biobyt Ltd, UK) were aliquoted in HEPES buffer solution at different concentrations and stored in a freezer (T = -26 °C) until use. Once the stock solutions were thawed, they were kept in a fridge (T = 2 °C) and used within a couple of days.

3.5 UV-Vis Spectroscopy

The measurements for the experiments in Figure 2.8 were carried out with a UV-Visible Spectrophotometer (CARY 50 Scan, Varian/Agilent USA) using a 1 cm path length cell (High Precicion Cell, Hellma Analytics, Germany). The melittin solution was added to the vial containing the polymerized TRCDA/DOPC suspension with a plastic pipette and then gently agitated to mix the suspension. The peptide-to-lipid ratio was 0.03. The incubation time was 30 minutes. The scan rate, data interval, averaging time were 300 nm/min, 0.5 nm, and 0.1 s respectively. The measurements for the experiments in Figure 2.7A and Figure 2.12A were carried out with a microplate reader (Synergy H1, BioTek, USA) in the range of 300-800 nm and 1 nm spacing. The TRCDA suspension was prepared as described above, distributed into a 96 well-plate and polymerized by the CL-1000 crosslinker at 0.2 J/cm². The peptide solution was added and the plate was shaken for 15 minutes with an orbital shaker (Orbi-ShakerTM JR., Benchmark Scientific, USA) at 200 rpm. The total incubation time was 1 hour. Besides the subtraction of the baseline (HEPES buffer solution), Rayleigh scattering was either removed by fitting the data points with the function $f(x, a, b) = log \frac{1}{1 - 1 \cdot 10^{a + x^{-4}}} + b$ by freeing a and b over the range of 210 – 1100 nm while skipping the region 400 - 900 nm, where PDA signals present (S1) or a manual subtraction via fityk was performed. Data post processing was done by LibreOffice Calc v6.3.5.2 30, gnuplot v5.2 and fityk 1.3.1.

3.6 Calculation of Colorimetric Response

The calculation is discussed in the subsection 1.6.4.

3.7 TRCDA/DOPC Sample Preparation for Figure 2.7B,D-G and Figure 2.14

Glass coverslips were treated with an oxygen plasma cleaner (100 Plasma System, PVA TePla, Germany) and incubated with a hot ($T=65\,^{\circ}\text{C}$) suspension (preparation described in section 3.2) for 15 min on the bench, during which the samples cooled down to room temperature ($T\approx23\,^{\circ}\text{C}$). These samples rested further in a fridge ($T=2\,^{\circ}\text{C}$) at least for 12 hours and then were rinsed with HEPES buffer solution. This resting time is important for the crystal domain formation. Round-shaped holes were punched into PDMS (Sylgard 184 silicone elastomer kit, Dow Corning, USA). These wells were used to confine the suspension on the glass coverslips. Polymerization was carried out by the UV box as described in section 3.3. After the formation of the polymer in Figure 2.7B,D-G and Figure Figure 2.14A,B, melittin was added directly to the solution with a concentration of 30 μ M.

3.8 TRCDA Sample Preparation for Figure 2.7H,I

A 1 µl droplet of TRCDA dissolved in chloroform (100 mM) was placed on a cleaned glass coverslip at room temperature. After the chloroform was evaporated, another 1 µl droplet of chloroform was added on top of the dried out TRCDA. This procedure was repeated till a homogeneous film formed. The coverslip was then placed into a liquid cell (BioCellTM, JPK Instruments, Germany) and filled with the buffer solution. This liquid cell allows temperature control (Figure 2.7I). For Figure 2.7H melittin was added to match a molar ratio (P/L) of 0.03.

3.9 Gold-labeled Melittin

For the gold-labeled melittin peptide solution, a NHS-activated gold nanoparticle conjugation kit (cytodiagnostics, Canada) was used. The preparation was followed according to the protocol:

- 1. Allow all reagents to warm to room temperature before use.
- 2. Using the supplied protein re-suspension buffer, dilute or dissolve your protein/anti-body to the final concentration suitable for the particular gold nanoparticle size to be conjugated (5 nm gold nanoparticle diameter → suggested protein concentration 5 mg/ml
- 3. In a microcentrifuge tube combine your diluted protein solution (48 μ l) with the reaction buffer (60 μ l)
- 4. Transfer 90 µl of your protein/reaction buffer mix prepared in step 3 to one of the vials containing lyophilized NHS-activated gold nanoparticles and immediately mix well by pipetting up and down.
 - Note: Do not resuspend the lyophilized NHS-activated gold nanoparticles in buffer prior to addition of protein. NHS rapidly hydrolyzes in aqueous solution and may result in loss of conjugation efficiency.
- 5. Incubate the vial at room temperature for at least 2 hours.
- 6. Add 10 µl of quencher solution to the vial to stop the reaction.
- 7. 100kDa MWC Spin Column (Due to no access to this instrument, a microcentrifuge was used instead)
- 8. Discard the supernatant containing unbound protein.
- 9. Add 100ul (1ml for Midi Kit) of gold conjugate storage buffer to the vial to re-suspend your conjugate.
- 10. Store your protein conjugate at 4°C until use.

3.10 TRCDA Sample Preparation for Figure 2.20

A Langmuir-Blottget trough (Kibron Microtrough XS, Kibron, Finland) was cleaned with acetone, ethanol and afterwards rinsed with ultra-pure water. The trough was filled with ultra-pure water. A glass coverslips, treated with an oxygen plasma cleaner (100 Plasma System, PVA TePla, Germany) for 15 minutes, was submerged into the water reservoir. The temperature was kept at T=25 °C. Test compression has been performed to guarantee no contamination at the air-water interface. 1.5 µl of TRCDA dissolved in chloroform with a concentration of 50 mM were spread on both sides of the centered glass coverslip. To allow chloroform evaporation, compression of the film with a rate of 5 $\frac{mm}{min}$ was initiated after 15 min. After reaching a surface pressure of $\pi=25~\frac{mN}{m}$, the glass coverslip was lifted with a speed of v=1 $\frac{\mathrm{mm}}{\mathrm{s}}$. The transferred TRCDA monomer crystals were polymerized by a UV box (CL-1000 crosslinker, UVP, USA) with a UV dose of $0.1~\mathrm{J/cm^2}$ through to a continuously variable reflective neutral density filter with an operation range between 240 nm and 1200 nm (NDL-10C-4, Thorlabs). Round-shaped holes were punched into PDMS (Sylgard 184 silicone elastomer kit, Dow Corning, USA) and placed on the glass coverslip. These wells were used to confine the added HEPES buffer solution. Afterwards 1 µl of melittin, dissolved in MiliQ with a concentration of 5m were added into the well to induce the blue-to-red transition.

3.11 Bright Field and Fluorescence Microscopy

Both bright field and fluorescent images were recorded by the Eclipse Ti (Nikon, JP) with an oil immersion objective (Objective Plan-Apochromat 60x/1.40 Oil DIC, Nikon, JP), equipped with either a monochrome digital camera (DS-Qi2, Nikon, JP) or a color camera (DS-Ri2, Nikon, JP) with a resolution of 16.25 megapixel. For the bright field microscopy, a white light LED (CoolLED pE-100, UK) was used as a light source. For the fluorescence microscopy, a solid-state white light excitation source (Sola SE 5, lumencor, USA) was coupled with filter cubes (TRITC: 543 nm/emission, FITC: 482 nm/emission, Semrock BrightLine,

USA). Images were post processed by Nikon NIS Elements v4.51.01 and ImageJ v1.52i. For the images recorded by the color camera, a plugin for Imagej was written to be able to analyze the data. For further information see section 3.17. The contrast and the brightness were adjusted and the fluorescent images were presented with false colors for the figures.

3.12 Transmission Electron Microscopy (TEM)

TEM images were recorded by the TECNAI G^2 Sphera (FEI, Hillsboro, USA) with a 200 kV LaB6 cathode. The attached camera has a resolution of $2000 \cdot 2000$ pixel. The samples were prepared similar to the protocol of 3.7. Before injecting the solution into the wells of PDMS, a silicon nitride (Si₃Si₄) TEM window grid (Plano GmbH, Germany) were placed on the bottom. The grid itself has a 200 µm by 200 µm well and a thickness of 50 nm. The samples were stored for several hours at T=2 °C that the DA molecules can self-assemble on the grid. A fast check of a successful crystal grow can be archived by an optical microscope. Afterwards the grids were rinsed with ultra pure water in order to get rid of the HEPES buffer solution. Before placing the grid into the TEM, it was dried out for at least 8 hours in a desiccator at a pressure of $p=400\,\mathrm{mBar}$. The Images were post processed by ImageJ v1.52i.

3.13 Atomic Force Microscopy (AFM)

AFM imaging were performed by the NanoWizard 3 (JPK Instruments, Germany) in either Qi mode (Figure 2.14D, Figure 2.9A), which collects force-distance curves for each pixel, or in tapping mode (Figure 2.7B). For both methods gold coated n-type silicon cantilevers were employed (HQ:NSC15/Cr-Au, Mikromasch, Bulgaria and MLCT type B, Bruker, USA). The AFM resides on an active vibration isolation platform (halcyonics_i4, Accurion, Germany) in an acoustic enclosure (JPK Instruments, Germany). The setpoint and the tip velocity were in the range of 250 pN and 8-15µm/s respectively. The samples were inserted into

a liquid cell BioCell (BioCellTM, JPK Instruments, Germany). Data post processing was done by Gwyddion 2.55.

3.14 Isothermal Titration Calorimetry

Isothermal titration calorimetry (ITC) measurements were carried out with the MicroCal iTC₂₀₀ (Malvern, UK). The TRCDA suspension was prepared as described above with a lipid concentration of 0.1 mM or 0.2 mM. The solution was stored for at least 12 hours at $T=2^{\circ}$ C. The TRCDA suspension was placed into the sample chamber with a volume of 200 µl, while the reference chamber was filled with MiliQ. The syringe was filled with 25 µl of different peptide solutions (melittin, polymyxin B, polymyxin E, magainin 2) at different concentrations. 11 injections were carried out with a volume of 2 µl each, a duration of 4 s and an interval of 300 s at T=25 °C. The reference power was set to 6 µcal/s and the syringe stirring to 1000 rpm. Data post processing was done by Origin 7 SR4 v7.0522, LibreOffice Calc v6.3.5.2 30 and gnuplot v5.2.

3.15 Dynamic Light Scattering

The DLS experiment was performed by Zetasizer Nano ZS (Malvern Panalytical, UK) in the 173° backscatter mode. A TRCDA/DOPC solution (1:1) was prepared as described and stored at T=2 °C. Every hour, a part of the stock solution was measured 3 times at T=25 °C to obtain an average value and the standard deviation. The same sample was then polymerized (0.2 J/cm²) and UV-Vis spectra were recorded to obtain corresponding absorption. The raw data was post processed by LibreOffice Calc v6.3.6.2 and gnuplot v5.2.

3.16 Differential Scanning Calorimetry

The DSC experiment in Figure 2.10 was performed by the DSC 1 (Mettler Toledo, USA). 20 μ l TRCDA dissolved in Chloroform at a concentration of c = 50 mM was injected into an aluminum crucible of 40 μ l volume and dried out in a desiccator for 1 day. HEPES buffer

solution either with or without melittin dissolved in it was added to the dried-out monomer and dried-out again. The final peptide lipid molar ratio was ~ 0.15 . A range from 25-100 °C with a ramp of 5 °C/min were cycled 3 times. The experiment was performed in nitrogen at a natural room pressure. The raw data was post processed by fityk 1.3.1, LibreOffice Calc v6.3.6.2 and gnuplot v5.2.

3.17 Plugin for ImageJ

The Nikon NIS-Elements software from the Eclipse Ti produces files with the proprietary "nd2" file format. As black and white images only possess one channel (Grey-value for black: 0-254), these files can directly imported into the open source program Imagej when the Nikon ND2 Reader plugin is installed. However, when images taken by the color cam "DS-Ri2" a nd2 file consists three channels: red (0-254), green (0-254) and blue (0-254). In order to get a true colored image, these channels have to be composed in the correct channel order (eg. channel 1 = red, 2 = green, blue = 3). As this is not the case, the result of a composed image will not look correctly. Therefore a plugin for Imagej was written to swap the channels to obtain the correct order. This simple task is complicated when the nd2 file contains a "video" with different optical configuration. For example, when the NIS-Element software is instructed to record every minute a picture with the bright field (BF) - and fluorescence (F) setup for one hour, this will produce a file with 60 frames. Each of these frames has 6 channels (3 for BF, 3 for F) resulting in total 60*6=360 single images. To archive the correct true color video, these 360 images have to be reordered accordingly.

```
//Coded by johann nuck, University of Geneva, Switzerland
//Autoconvert nd2/tif files recorded by the colour cam "DS-Ri2" with the
Nikon NIS-Elements software into a correct composite image.
//contact: johann.nuck@gmail.com
//multiimage?
multi=nSlices;
//Hyperstack?
```

```
8 hyp = Stack.isHyperstack
9 if (hyp==1 || multi >3) {
    Dialog.create("");
11
    Dialog.addCheckbox("Split Channels?", true);
12
    Dialog.show();
13
    splt = Dialog.getCheckbox();
14
15
    titleName = getTitle();
16
    run("Stack to Images");
17
    names=newArray(nImages);
18
    colours=newArray("Red", "Green", "Blue");
19
20
    for (i=0;i<nImages;i++){</pre>
21
      selectImage(i+1);
22
      run(colours[i%3]);
23
      names[i]=getTitle;
24
      selectWindow(names[i]);
25
      rename(-floor(-(i+1)/3)+""+colours[i%3]);
26
      print(getTitle);
      run("Enhance Contrast", "saturated=0.35");
28
    }
29
30
    allpics=nImages; //nImages changes while merging
31
    for (i=0;i<allpics/3;i++) {</pre>
      print(nImages);
      a=i+1;
34
      merge="c1="+a+""+colours[0]+" c2="+a+""+colours[1]+" c3="+a+""+colours
      [2]+" "+"create";
      print(merge);
36
      run("Merge Channels...", merge);
37
      run("Stack to RGB");
38
      selectWindow("Composite");
39
       close();
40
    }
41
```

```
42
    run("Images to Stack", "name=Stack title=[] use");
43
    print("split: ");
45
    print(splt);
    print("Hyperstack?: ");
    print(hyp);
    selectWindow("Stack");
    if (hyp == 1) {
51
      rename("TRITC");
52
      run("Duplicate...", "duplicate");
53
      run("Reduce...", "reduction=2");
54
      rename("BF");
      selectWindow("TRITC");
56
      run("Delete Slice");
57
      run("Reduce...", "reduction=2");
58
59
      if (splt ==1) {
60
61
      run("Concatenate...", " title=names[0] open image1=BF image2=TRITC");
62
      }
    }
64
    else{
     if(splt == 1){
        run("Stack to Images");
      }
     rename(titleName);
    }
71 }
72 else{
    run("Stack to Images");
74
75
    names=newArray(nImages);
```

```
colours=newArray("Red", "Green", "Blue");
    for (i=0;i<nImages;i++) {</pre>
78
      selectImage(i+1);
      run(colours[i]);
      names[i]=getTitle;
      selectWindow(names[i]);
      rename(colours[i]);
83
      run("Enhance Contrast", "saturated=0.35");
    }
    run("Merge Channels...", "c1=Blue c2=Green c3=Red create");
86
    run("Stack to RGB");
87
    selectWindow("Composite");
    close();
89
90
    names[0] = replace(names[0], "c:1/3 - ","");
91
    print (names[0]);
92
    //due to "()" in the name, these cannot removed by "replace"
93
    len1=lengthOf(names[0]);
94
    names[0] = substring(names[0],0,len1-15);
95
    rename(names[0]);
97 }
```

LISTING 3.1: Source code for the ImageJ plugin to correct the channel order for multidimensional RGB nd2 files.

General Conclusion

The presented work summarizes the characteristics of (poly) diacetylene, its red state activation and especially the interaction with the model antimicrobial peptide melittin.

To get a better understanding of the crystal formation process, we studied (P)DA crystal formation by optical and fluorescence microscopy. Analysis of the spectra of PDA crystals at different time points showed that the TRCDA domains grows anisotropic and that the growth speed depends not only on the temperature and concentration but most importantly on the molecular orientation. These results are in agreement with previous studies that reported the TRCDA crystals have a tree-like morphology.

Next, the role of the soft lipid DOPC in the assembling process was studied by bright field and fluorescence microscopy. The supporting DOPC bilayer is essential for the crystal formation. Furthermore, the topology of PDA crystals was studied by TEM. An alternating contrast pattern could be appreciated indicating the PDA backbone.

To further characterize the crystals, we performed atomic force microscopy (AFM) on the PDA samples. Our results showed that the TRCDA domains are multilayers with a height up to 100 nm which corresponds to 40 DA monolayers. AFM also demonstrated that polymerization affects the TRCDA structures by increasing their height by 5-33%, while narrowing the width by 8-13%, also supported by previous studies. Moreover, dynamic light scattering (DLS) measurements of the particle size of assembling monomers revealed an increase in the particle size over time corresponding with an increase in the absorption peak of the polymerized sample.

Taken together these results support the following model: The TRCDA monomer self-assembles in the aqueous solution over time forming larger structures. Once polymerized, the absorbance increases in a linear manner.

To study the peptide-lipid interaction, we selected melittin as a peptide model due to its ability to induce blue-to-red transition. First, we confirmed by UV-Vis spectrometry that addition of melittin to a PDA suspension induced a blue-to-red transition. This effect was further quantified by calculating the colorimetric response. Optical microscopy and AFM showed droplets forming where the blue-to-red transition occurs. These droplets and the chromism coincide spatiotemporally, indicating that these droplets are made up of monomers that are leftover unpolymerized TRCDA within the PDA crystals. From these results we conclude that melittin causes a solid-to-liquid phase transition of TRCDA, which could be further confirmed by differential scanning calorimetry.

Furthermore, to study the thermodynamics of this phenomenon, we performed titration of TRCDA with peptides and monitored this process by isothermal titration calorimetry (ITC). The result suggests that there is a critical peptide-to-lipid ratio $\alpha_{\rm melt}$ at which TRCDA interacts with melittin and melts. To further confirm this result, the TRCDA suspension was polymerized by UV light. Then it was similarly titrated with melittin and monitored by UV-Vis spectroscopy. The colorimetric response showed that there is a similar threshold peptide-to-lipid ratio $\alpha_{\rm B2R}$ at which peptides induce the blue-to-red transition in PDA, coinciding with the previous ITC results: $\alpha_{\rm melt} \sim \alpha_{\rm B2R}$.

Moreover, to study whether this is a general phenomenon in antimicrobial peptides, these experiments were repeated with polymyxin B, polymyxin E, and magainin B. Bright field microscopy and ITC revealed that polymyxin B and polymyxin E have a similar behaviour to melittin. Magainin 2 did not induce the blue-to-red transition and consistently did not melted the monomer either.

Finally, to study the penetration of melittin inside PDA crystals, we correlated the height and the fraction of PDA that was activated by melittin by combining AFM and fluorescence microscopy. The results showed that PDA multilayers have some fraction of intact blue PDA inside where melittin failed to induce a transition.

In conclusion, these results implicate that although both thermochromism and peptideinduced chromism stem from the crystal structure melting, the latter is influenced by the ability of peptides to penetrate the PDA matrix, where the presence of leftover monomers may have an advantage by providing a less rigid structure for melittin to migrate.

As a follow-up study, the crystal behavior was studied during blue-to-red transition by fluorescence microscopy and TEM. A series of fractures in the crystal could be observed. These fractures arise from the density incremental from the blue - to the red state of the crystal. This experiment demonstrates the density change and therefore the formation of cracks within the PDA matrix.

In order to gain further insights of these cracks, melittin was tagged with 5 nm gold particles. TEM images revealed the cracks filled with the gold particles were spaced equidistant around 5 to 7 nm. This distance corresponds to around 15 PDA chains. Interestingly, two crystals from the same sample behaved differently upon addition of melittin. One displayed the typical blue-to-red transition: the conversion starts from the border direction inwards of the crystal; whereas the other is not affected by the addition of melittin. We suspect that a varying P/DA matrix is responsible for this behavior.

To test this hypothesis the following experiment was designed: an intensity gradient of UV light was applied to the monomeric TRCDA and the blue-to-red transition after adding melittin was followed by bright field and fluorescence microscopy. Surprisingly, the expected pattern, a profile polymer-to-monomer gradient, was not obtained. Even within a single crystal the polymer/monomer ratio seems different. The speed of the blue-to-red transition could be predicted by this ratio. This result indicates that the structure inside the crystals has a higher influence of the polymerization efficiency than the intensity of the UV light (or irradiation time).

Our own results were obtained with the diacetylene derivative 10,12-Tricosadiynoic acid. In order to answer the question if these results can be generalized, we already started working with other lipid-like DA derivatives. A longer one like 10,12-Pentacosadiynoic acid (PCDA) has a higher blue-to-red transitions temperature ($T_{\rm B2R,PCDA} = 65$ °C vs $T_{\rm B2R,TRCDA} = 60$ °C) in its polymeric form⁶ and also a higher melting point ($T_{\rm melt} = 62$ °C). This derivative has the same number of hydrocarbon units between the head and the DA unit and only differs in its tail length (compared to TRCDA: + 2). Therefore, a higher blue-to-red transition temperature for the polymer and a higher melting point for the monomer can be assumed for

increasing chain length after the DA unit. Note that the blue-to-red transition temperature of TRCDA is slightly higher than the temperature reported in the literature ($T_{\rm B2R,TRCDA} = 56~{\rm ^{\circ}C}$). Determining this temperature is not trivial as it depends also on the sample history (e.g annealing the monomer and polymerizing afterwards resulted in a divergent behavior regarding external stimuli). Therefore, the presented blue-to-red transition temperatures were all taken under equal conditions. Less clear appears the situation when various characteristics change at the same time. 5,7-Docosadiynoic acid (DCDA, Scheme D.3) for example has a shorter number of hydrocarbon units between the head and the DA unit (-5) while the tail is longer (+4). Here, the polymer has a lower blue-to-red transition temperature ($T_{\rm B2R} = 50~{\rm ^{\circ}C}$) but a higher melting point ($T_{\rm melt} = 68~{\rm ^{\circ}C}$). Hence, the synthesis of a variety of DA derivatives in a systematic manner and their investigation would be desirable to get insights on this behavior.

The following can be conclude from publications around lipid-like DA/PDA derivatives. The properties of a certain PDA can be summarized as follows: the main polymer chain defines the color depending on its torsion. ¹⁹⁴ The side chains, which influence the molecular structure, are responsible for the reversibility ⁹⁹ and its sensitivity ⁹⁸.

Appendix A

Appendix

A.1 Polymerizability Improvement by Soft Lipids

The soft lipid DOPC is supporting the growing mechanism of TRCDA crystals in the solution (compare Figure A.1) The total lipid concentration is kept constant (c = 1 mM). Without any influence of DOPC, a linear increase of the absorbance would be expected. The results clearly show an improving of the polymerizability in the presence of DOPC.

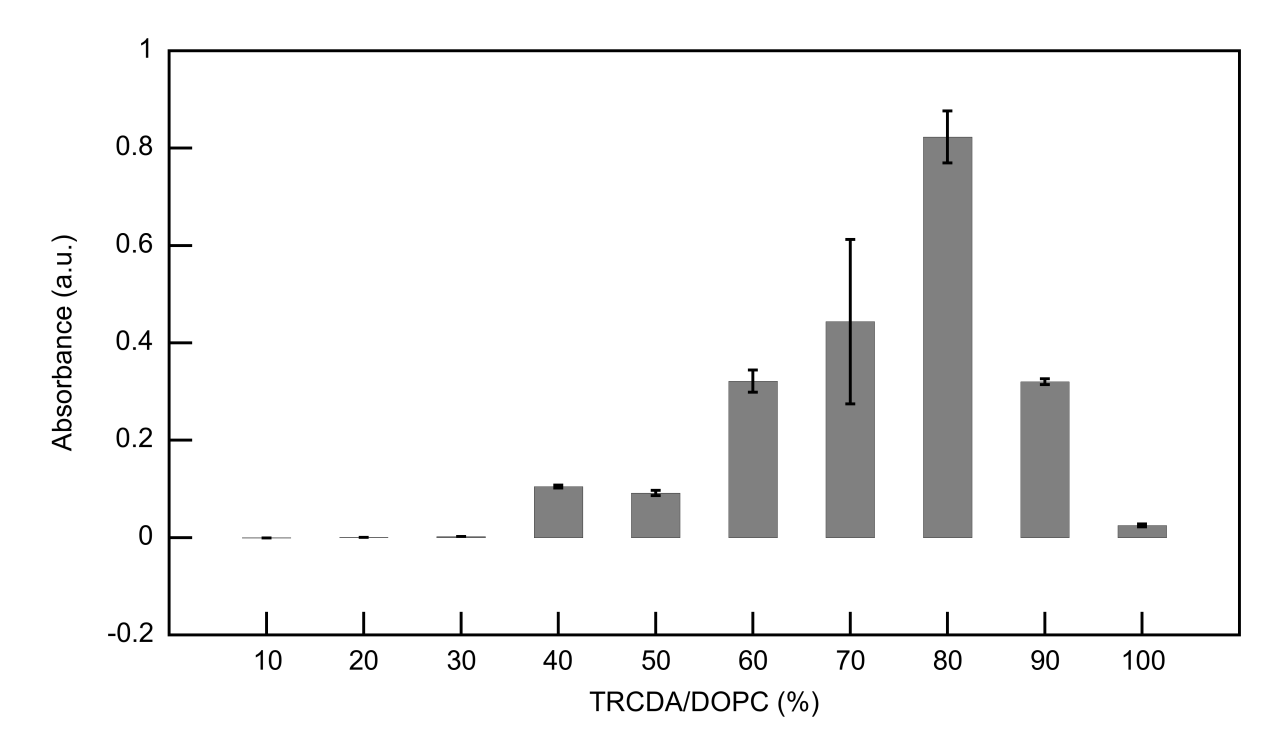


FIGURE A.1: Absorbance of DOPC/TRCDA suspension after polymerization. A maximum around 80% indicates a supporting function of the soft lipid DOPC regarding the diacetylenes crystal growing and polymerizability.

It has to be pointed out that these results were reproducible with TRCDA bought from Sigma Aldrich. After switching to the company Alfa Aesar, the polymerizability of pure (100%) TRCDA improved drastically (not shown). Due to these fluctuations it is extreme important to keep as many parameters constant when performing a series of experiments.

Appendix B

List of Publications

 Nuck, J. & Sugihara, K. Mechanism of Polydiacetylene Blue-to-Red Transformation Induced by Antimicrobial Peptides. *Macromolecules* 53, 6469–6475. ISSN: 15205835 (2020)

Appendix C

List of Talks, Posters and Awards

C.1 Talks

- Polydiacetylene-Peptide Interaction Mechanism in Mixed Lipid Systems
 Geneva Chemistry & Biochemistry Days 2021 (14th 15th of January 2021, Live Streaming Virtual Event)
- Developing a fluorescence force probe: peptides interacting with polydiacetylene 26th Swiss Soft Days (6th of March **2020**, University of Basel, Basel, Switzerland)
- How to visualise forces: Peptides interacting with a mechanosensitive polymer
 25th Swiss Soft Days (27th of August 2019, Nestlé Research Center, Lausanne, Switzerland)
- The mechanism of polydiacetylene activation by peptides

 Louis-Jeantet/LS² Satellite Meeting (10th October **2018**, Geneva, Switzerland)
- Polydiacetylene-peptide interaction mechanism in mixed lipid systems
 2018 International Symposium on Chemical Biology / Satellite event (10th-12th January
 2018, Geneva, Switzerland)

C.2 Posters

- How to visualise forces: Peptides interacting with a mechanosensitive polymer
 "2020 International Symposium on Chemical Biology" organized by the NCCR (22th-24th January 2020, Geneva, Switzerland)
- How peptides trigger the blue to red transition of Polydiacetylene
 Annual Retreat of Swiss National Centre of Competence in Research (NCCR) Chemical
 Biology (12th-14th June 2019, Villars-sur-Ollon, Switzerland)
- How peptides trigger the blue to red transition of Polydiacetylene
 14th International Symposium on Macrocyclic and Supramolecular Chemistry (ISMSC)
 (2nd 6th June 2019, Lecce, Italy)
- The mechanism of polydiacetylene activation by peptides

 Gordon Research Conference (17th-22nd June **2018**, Lucca (Barga), Italy)
- The mechanism of polydiacetylene activation by peptides
 Annual Retreat of Swiss National Centre of Competence in Research (NCCR) Chemical
 Biology (14th June 2018, Villars-sur-Ollon, Switzerland
- Polydiacetylene-peptide interaction mechanism in mixed lipid systems
 2018 International Symposium on Chemical Biology (10th-12th January 2018, Geneva, Switzerland)
- Polydiacetylene-peptide interaction mechanism in mixed lipid systems
 Swiss Soft Days XXI (8th September 2017, Lausanne, Switzerland)
- Polydiacetylene-peptide mixed systems: interaction mechanism at raft boundaries
 Joint FEBS EMBO Advanced Lecture Course (June 12th- 21st 2017, Cargèse, France)
- Decode polydiacetylene-peptide interaction mechanism at raft boundaries
 20th Swiss Soft Days (February 10th 2017, Geneva, Switzerland)

C.3. Awards

C.3 Awards

• Boehring Ingelheim travel grant, Joint FEBS – EMBO Advanced Lecture Course (June 12th- 21st **2017**, Cargèse, France)

Appendix D

List of Chemical Formulas

SCHEME D.1: 2,4-hexadiin-1,6-diol-bis-phenylurethane

$$R_i^*$$

Scheme D.2: Diacetylene (DA)

Scheme D.3: 5,7-Docosadiynoic acid (DCDA)

SCHEME D.4: 10,12-Tricosadiynoic acid (TRCDA)

SCHEME D.5: Polydiacetylene (PDA)

Scheme D.6: N-[2-(2-Hydroxyethoxy)ethyl]pentacosa- 10,12-diynamide (HEEPCDA)

SCHEME D.7: 10,12-Pentacosadiynoic acid (PCDA)

SCHEME D.8: 3-(pentacosa-10,12-diynamido)benzoic acid (PCDA-mBzA)

SCHEME D.9: 6-(pentacosa-10,12-diynamido)-2-naphthoic acid (PCDA-NPA)

SCHEME D.10: 4-(pentacosa-10,12-diynoyloxy)benzoic acid (PCDA-HBA)

Scheme D.11: 4-pentacosa-10,12-diynamidobenzoic acid (2) (PCDA-ABA)

$$N^+$$

SCHEME D.12: Cetyltrimethylammonium bromide (CTAB)

SCHEME D.13: Sodium dodecyl sulfate (SDS)

Scheme D.14: p-(1,1,3,3-tetramethylbutyl) phenoxypolyoxyethyleneglycol (Triton X-100)

SCHEME D.15: Cetyltrimethylammonium chloride (CTAC)

SCHEME D.16: Cetyltrimethylammonium chloride (DTAB)

SCHEME D.17: 1,2-dimyristoyl-sn-glycero-3-phosphatidylcholine (DMPC)

SCHEME D.18: polyvinylpyrrolidone (PVP10)

SCHEME D.19: N,N'-ethylenebispentacosa-10,12-diynamide (EBPCDA-2DA)

SCHEME D.20: Butanol

$$\bigcirc$$

SCHEME D.21: Tetrahydrofuran (THF)

SCHEME D.22: poly (5,7-dodecadiyne-1,12-diol-bis phenylurethane) (TCDU) monomeric form

Scheme D.23: Polydiacetylene-bis (toluene-sulphonat) (PTS) monomeric form

SCHEME D.24: 1,2-dioleoyl-sn-glycero-3-phosphocholine (DOPC)

Appendix E

List of Symbols and Abbreviations

h Planck constant $m^2 \cdot kg \cdot s^{-1}$

 k_B Boltzmann constant $J \cdot K^{-1}$

p Pressure $kg \cdot (m \cdot s)^{-2}$

 \vec{r} position vector

T Temperature K

 λ wavelength nm

 ν frequency cm⁻¹

AA Amino acid

ABA 4-aminobenzoic acid

AMP Antimicrobial peptides

CD Circular dichroism

BF Bright field

CR Colorimetric response

CTAB Cetyltrimethylammonium bromide

CTAC Cetyltrimethylammonium chlorid

DA Diacetylene

DLS Dynamic light scattering

DOPC 1,2-dioleoyl-sn-glycero-3-phosphocholine

DMPC 1,2-dimyristoyl-sn-glycero-3-phosphatidylcholine

DSC Differential scanning calorimetry

DTAB Dodecyltrimethylammonium bromide

EBPCDA-2DA N,N'-ethylenebispentacosa-10,12-diyamide

ECL effective conjugation length

FRAP Fluorescence recovery after photobleaching

FTIR 10,12-Fouriertransform infrared

HBA 4-hydroxybenzoic acid

HEEPCDA N-[2-(2-Hydroxyethoxy)ethyl]pentacosa- 10,12-diynamide

LB Langmuir-Blodgett

LCAO Linar combination of atomic orbitals

LPS Lipopolysaccharide

PCDA 10,12-Pentacosadiynoic acid

PCDA-ABA 4-pentacosa-10,12-diynamidobenzoic acid

PCDA-HBA 4-(pentacosa-10,12-diynoyloxy)benzoic acid

PCDA-mBzA 3-(pentacosa-10,12-diynamido)benzoic acid

PCDA-NPA 6-(pentacosa-10,12-diynamido)-2-naphthoic acid

PDA Polydiacetylene

(P)DA Polydiacetylene and diacetylene

PPPP Pariser-Parr-Pople-Peierls

PVP10 polyvinylpyrrolidone (n=10)

SDS Sodium dodecyl sulfate

TEM Transmission electron microscopy

TDDFT Time-dependent density functional theory

THF Tetrahydrofuran

TRCDA 10,12-Tricosadiynoic acid

Triton X-100 p-(1,1,3,3-tetramethylbutyl)phenoxypolyoxyethyleneglycol

WF Wave function

XRD X-ray powder diffraction

- 1. Lee, D. C., Sahoo, S. K., Cholli, A. L. & Sandman, D. J. Structural aspects of the thermochromic transition in urethane-substituted polydiacetylenes. *Macromolecules* **35**, 4347–4355. ISSN: 00249297 (2002).
- 2. Dolai, S. et al. Colorimetric polydiacetylene-aerogel detector for volatile organic compounds (VOCs). ACS Appl. Mater. Interfaces 9, 2891–2898. ISSN: 19448252 (2017).
- 3. Ma, Z. et al. Colorimetric detection of Escherichia coli by polydiacetylene vesicles functionalized with glycolipid [7]. J. Am. Chem. Soc. 120, 12678–12679. ISSN: 00027863 (1998).
- 4. Kolusheva, S., Boyer, L. & Jelinek, R. A colorimetric assay for rapid screening of antimicrobial peptides. *Nat. Biotechnol.* **18**, 225–227. ISSN: 10870156 (2000).
- 5. Tomioka, Y., Tanaka, N. & Imazeki, S. Surface-pressure-induced reversible color change of a polydiacetylene monolayer at a gas-water interface. *J. Chem. Phys.* **91**, 5694–5700. ISSN: 00219606 (1989).
- 6. Juhasz, L., Ortuso, R. D. & Sugihara, K. Quantitative and Anisotropic Mechanochromism of Polydiacetylene at Nanoscale. *Nano Lett.* ISSN: 15306992 (2020).
- 7. Pontes, B., Monzo, P. & Gauthier, N. C. Membrane tension: A challenging but universal physical parameter in cell biology. *Semin. Cell Dev. Biol.* **71**, 30–41. ISSN: 10963634. http://dx.doi.org/10.1016/j.semcdb.2017.08.030 (2017).
- 8. Jelinek, R. & Kolusheva, S. Biomolecular sensing with colorimetric vesicles. *Top. Curr. Chem.* **277**, 155–180. ISSN: 03401022 (2007).
- 9. Jung, Y. K., Park, H. G. & Kim, J. M. Polydiacetylene (PDA)-based colorimetric detection of biotin-streptavidin interactions. *Biosens. Bioelectron.* **21**, 1536–1544. ISSN: 09565663 (2006).
- 10. Reppy, M. A. & Pindzola, B. A. Biosensing with polydiacetylene materials: structures, optical properties and applications. *Chem. Commun.*, 4317–4338. ISSN: 1359-7345 (2007).
- 11. Park, D. H. et al. Smartphone-based VOC sensor using colorimetric polydiacetylenes. ACS Appl. Mater. Interfaces 10, 5014–5021. ISSN: 19448252 (2018).
- 12. Kew, S. J. & Hall, E. A. H. pH response of carboxy-terminated colorimetric polydiacetylene vesicles. *Anal. Chem.* **78**, 2231–2238. ISSN: 00032700 (2006).
- 13. Rossi, G., Chance, R. R. & Silbey, R. Conformational disorder in conjugated polymers. J. Chem. Phys. 90, 7594–7601. ISSN: 00219606 (1989).
- 14. Bigot, J. Y., Pham, T. A. & Barisien, T. Femtosecond time resolved molecular dynamics of a polydiacetylene backbone. *Chem. Phys. Lett.* **259**, 469–474. ISSN: 00092614 (1996).

15. Schott, M. The colors of polydiacetylenes: A commentary. *J. Phys. Chem. B* **110**, 15864–15868. ISSN: 15206106 (2006).

- 16. Yamagata, H. & Spano, F. C. Vibronic coupling in quantum wires: Applications to polydiacetylene. J. Chem. Phys. 135. ISSN: 00219606 (2011).
- 17. Grebíková, L., Whittington, S. G. & Vancso, J. G. Angle-Dependent Atomic Force Microscopy Single-Chain Pulling of Adsorbed Macromolecules from Planar Surfaces Unveils the Signature of an Adsorption-Desorption Transition. *J. Am. Chem. Soc.* **140**, 6408–6415. ISSN: 15205126 (2018).
- 18. Lee, L. M. & Liu, A. P. The application of micropipette aspiration in molecular mechanics of single cells. *J. Nanotechnol. Eng. Med.* **5**, 1–6. ISSN: 19492952 (2015).
- 19. Fin, A., Vargas Jentzsch, A., Sakai, N. & Matile, S. Oligothiophene amphiphiles as planarizable and polarizable fluorescent membrane probes. *Angew. Chemie Int. Ed.* **51**, 12736–12739. ISSN: 14337851 (2012).
- 20. Goujon, A. et al. Mechanosensitive Fluorescent Probes to Image Membrane Tension in Mitochondria, Endoplasmic Reticulum, and Lysosomes. J. Am. Chem. Soc. 141, 3380–3384. ISSN: 15205126 (2019).
- 21. Berezin, M. Y. & Achilefu, S. Fluorescence lifetime measurements and biological imaging. *Chem. Rev.* **110**, 2641–2684. ISSN: 00092665 (2010).
- 22. Wei, M. et al. A polydiacetylene-based fluorescence assay for the measurement of lipid membrane affinity. RSC Adv. 5, 66420–66425. ISSN: 20462069 (2015).
- 23. Kolusheva, S., Shahal, T. & Jelinek, R. Peptide-membrane interactions studied by a new phospholipid/polydiacetylene colorimetric vesicle assay. *Biochemistry* **39**, 15851–15859. ISSN: 00062960 (2000).
- 24. Jelinek, R, Okada, S, Norvez, S & Charych, D. Interfacial catalysis by phospholipases at conjugated lipid vesicles: colorimetric detection and NMR spectroscopy. *Chem. Biol.* 5, 619–629. ISSN: 10745521 (1998).
- 25. Van Den Bogaart, G., Guzmán, J. V., Mika, J. T. & Poolman, B. On the mechanism of pore formation by melittin. J. Biol. Chem. 283, 33854–33857. ISSN: 00219258 (2008).
- 26. Lee, M. T., Sun, T. L., Hung, W. C. & Huang, H. W. Process of inducing pores in membranes by melittin. *Proc. Natl. Acad. Sci. U. S. A.* **110**, 14243–14248. ISSN: 00278424 (2013).
- 27. Ortuso, R. D., Ricardi, N., Bürgi, T., Wesolowski, T. A. & Sugihara, K. The deconvolution analysis of ATR-FTIR spectra of diacetylene during UV exposure. Spectrochim. Acta Part A Mol. Biomol. Spectrosc. 219, 23–32. ISSN: 13861425. https://doi.org/10.1016/j.saa.2019.04.030 (2019).
- 28. Hébert, A. Sur un nouvel acide gras, non saturé, l'acide isanique. *Bull. la Société Chim. Paris* **3,** 941–945. ISSN: 15205126 (1896).
- 29. Steger, A. & van Loon., J. Das fette Oel der Samen von Onguekoa Gore Engler. Fette und Seifen, 243–246 (1937).
- 30. Wegner, G. Polymerisation von Derivaten des 2.4-Hexadiin-1.6-diols im kristallinen Zustand. Z. Naturforschg. 24b 24b, 824-832. https://doi.org/10.1515/znb-1969-0708 (1969).

31. Nallicheri, R. A. & Rubner, M. F. Investigations of the Mechanochromic Behavior of Poly(urethane-diacetylene) Segmented Copolymers. *Macromolecules* **24**, 517–525. ISSN: 15205835 (1991).

- 32. Hirshfeld, F. L. & Schmidt, G. M. J. Topochemical control of solid-state polymerization. J. Polym. Sci. A Gen. Pap. 2, 2181–2190. ISSN: 04492951 (1964).
- 33. Guo, C. et al. Two-dimensional self-assembly of diacetylenic acid derivatives and their light-induced polymerization on HOPG surfaces. Phys. Chem. Chem. Phys. 19, 16213–16218. ISSN: 14639076 (2017).
- 34. Enkelmann, V. Structural aspects of the topochemical polymerization of diacetylenes 91–136. ISBN: 978-3-540-13414-5 (Springer, Berlin, Heidelberg, 1984).
- 35. Menzel, H., Mowery, M. D., Cai, M. & Evans, C. E. Fabrication of noncovalent and covalent internal scaffolding in monolayer assemblies using diacetylenes. *Macromolecules* **32**, 4343–4350. ISSN: 00249297 (1999).
- 36. Tashiro, K. et al. Structure Analysis and Derivation of Deformed Electron Density Distribution of Polydiacetylene Giant Single Crystal by the Combination of X-ray and Neutron Diffraction Data. *Macromolecules* **51**, 3911–3922. ISSN: 15205835 (2018).
- 37. Tieke, B., Lieser, G. & Wegner, G. Polymerization of Diacetylenes in Multilayers. *J Polym Sci Polym Chem Ed* **17**, 1631–1644. ISSN: 0449296X (1979).
- 38. Enkelmann, V. & Wegner, G. Kristallographische Analyse einer topochemischen Polymerisation. *Angew. Chemie* **89**, 432–432. ISSN: 00448249 (1977).
- 39. Using, F.-p. et al. Preparation and Single Crystal Structure, 1–10 (2019).
- 40. Sasaki, D. Y., Carpick, R. W. & Burns, A. R. High Molecular Orientation in Monoand Trilayer Polydiacetylene Films Imaged by Atomic Force Microscopy. *J. Colloid* Interface Sci. 229, 490–496. ISSN: 00219797. http://linkinghub.elsevier.com/ retrieve/pii/S0021979700970437 (2000).
- 41. Day, D. & Ringsdorf, H. Polymerization of Diacetylene Carbonic Acid Monolayers At the Gas-Water Interface. *J Polym Sci Polym Lett Ed* **16**, 205–210. ISSN: 03606384 (1978).
- 42. Wegner, G. Topochemical reactions of monomers with conjugated triple bonds. III. Solid-state reactivity of derivatives of diphenyldiacetylene. J. Polym. Sci. Part B Polym. Lett. 9, 133–144 (1971).
- 43. Bloor, D., R. C. Polydiacetylenes: Synthesis, Structure and Electronic Properties 187–209. ISBN: 9789048182947 (1985).
- 44. Morrison, J. D. & Robertson, J. M. The crystal and molecular structure of certain dicarboxylic acids. Part VI. Sebacic acid. *J. Chem. Soc.*, 993–1001. ISSN: 03681769 (1949).
- 45. Enkelmann, V. The crystal structure of the low-temperature phase of poly[1,2-bis(p-tolylsulphonyloxymethylene)-1-buten-3-ynylene]. *Acta Crystallogr. Sect. B Struct. Crystallogr. Cryst. Chem.* **33**, 2842–2846. ISSN: 0567-7408 (1977).
- 46. Nuck, J. & Sugihara, K. Mechanism of Polydiacetylene Blue-to-Red Transformation Induced by Antimicrobial Peptides. *Macromolecules* **53**, 6469–6475. ISSN: 15205835 (2020).

47. Fouassier, J. P., Tieke, B. & Wegner, G. The Photochemistry of the Polymerization of Diacetylenes in Multilayers. *Isr. J. Chem.* **18**, 227–232. ISSN: 18695868 (1979).

- 48. Okada, S., Peng, S., Spevak, W. & Charych, D. Color and Chromism of Polydiacetylene Vesicles. Acc. Chem. Res. 31, 229–239. ISSN: 00014842 (1998).
- 49. Patel, G. N., Witt, J. D. & Khanna, Y. P. Thermochromism in Polydiacetylene Solutions. J. Polym. Sci. Part A-2, Polym. Phys. 18, 1383–1391. ISSN: 04492978 (1980).
- 50. Chance, R. R., Patel, G. N. & Witt, J. D. Thermal effects on the optical properties of single crystals and solution-cast films of urethane substituted polydiacetylenes. *J. Chem. Phys.* **71**, 206–211. ISSN: 00219606 (1979).
- 51. Deckert, A. A. et al. Kinetics of the Reversible Thermochromism in Langmuir-Blodgett Films of Cd2+ Salts of Polydiacetylenes Studied Using UV-Vis Spectroscopy. Langmuir 10, 1948–1954. ISSN: 15205827 (1994).
- 52. Mueller, A. & O'Brien, D. F. Supramolecular materials via polymerization of mesophases of hydrated amphiphiles. *Chem. Rev.* **102**, 727–757. ISSN: 00092665 (2002).
- 53. Race, A., Barford, W. & Bursill, R. J. Density matrix renormalization calculations of the relaxed energies and solitonic structures of polydiacetylene. *Phys. Rev. B Condens. Matter Mater. Phys.* **67**, 1–9. ISSN: 1550235X (2003).
- 54. Supramolecular Photosensitive and Electroative Materials (ed Nalwa, H.) 371–380. ISBN: 0125139047 (2001).
- 55. Brédas, J. L., Cornil, J., Beljonne, D., Dos Santos, D. A. & Shuai, Z. Excited-state electronic structure of conjugated oligomers and polymers: A quantum-chemical approach to optical phenomena. *Acc. Chem. Res.* **32**, 267–276. ISSN: 00014842 (1999).
- 56. Race, A., Barford, W. & Bursill, R. J. Low-lying excitations of polydiacetylene. *Phys. Rev. B Condens. Matter Mater. Phys.* **64**, 1–9. ISSN: 1550235X (2001).
- 57. Shuai, Z., Bredas, J.-L., Pati, S. K. & Ramasesha, S. Quantum confinement effects on the ordering of the lowest-lying excited states in conjugated polymers. *Opt. Probes Conjug. Polym.* **3145**, 293. ISSN: 0277-786X (1997).
- 58. Pandya, Raj and Alvertis, Antonios M. and Gu, Qifei and Sung, Jooyoung and Legrand, Laurent and Kreher, David and Barisien, Thierry and Chin, Alex W. and Schnedermann, Christoph and Rao, A. How Does the Symmetry of S1 Influence Exciton Transport in Conjugated Polymers? *HAL*. https://hal.sorbonne-universite.fr/hal-03083861 (2020).
- 59. Kobayashi, T., Ikuta, M. & Yuasa, Y. Sub 5 fs spectroscopy of polydiacetylene. Femtochemistry VII, 87–95 (2006).
- 60. Kobayashi, T., Furuta, A., Shimada, S. & Matsuda, H. Third-harmonic generation (THG) spectrum of polydiacetylenes measured by a novel multiplex method in CLEO/-Pacific Rim 1999 Pacific Rim Conf. Lasers Electro-Optics 4 (1999), 1324–1325. ISBN: 0780356616.
- 61. Kingdom, U. & Introduction, I. 11Bu--21Ag+ crossover in conjugated polymers: The phase diagram of the molecular-orbital model. *Phys. Rev. B* **59**, 48–55 (1999).
- 62. Chance, R. R., Baughman, R. H., Müller, H. & Eckhardt, C. J. Thermochromism in a polydiacetylene crystal. *J. Chem. Phys.* **67**, 3616–3618. ISSN: 00219606 (1977).

63. Müller, H. & Eckhard, C. OPTICAL AND ELECTRICAL PROPERTIES OF A POLYDIACETYLENE CRYSTAL: POLY(5,7-DODECADIYNE-I, I2-DIOL-BIS PHENY-LURETHANE. Chem. Phys. Lett. **50**, 225–235 (1977).

- 64. Reimer, B., Baessler, H., Hesse, J. & Weiser, G. Optical Properties of a Polydiacetylene Single Crystal Evidence for van Hove Singularities. *Phys. Status Solidi* **73**, 709–716. ISSN: 15213951 (1976).
- 65. Iqbal, Z., Chance, R. R. & Baughman, R. H. Electronic structure change at a phase transition in a polydiacetylene crystal. *J. Chem. Phys.* **66**, 5520–5525. ISSN: 00219606 (1977).
- 66. Sandman, D. J., Tripathy, S. K., Elman, B. S. & Samuelson, L. A. Polydiacetylenes and analogies to inorganic semiconductors and graphite. *Synth. Met.* **15**, 229–235. ISSN: 03796779 (1986).
- 67. Karpfen, A. Ab initio studies on polymers. IV. Polydiacetylenes. J. Phys. C Solid State Phys. 13, 5673. http://stacks.iop.org/0022-3719/13/i=31/a=009 (1980).
- 68. Tanaka, H., Gomez, M. A., Tonelli, A. E. & Thakur, M. Thermochromic Phase Transition of a Polydiacetylene, Poly(ETCD), Studied by High-Resolution Solid-State13C NMR. *Macromolecules* **22**, 1208–1215. ISSN: 15205835 (1989).
- 69. Kollmar, C. & Sixl, H. Theory of π -electron states in polydiacetylene molecules. *J. Chem. Phys.* **88**, 1343–1358. ISSN: 00219606 (1988).
- 70. Kuhn, H. The Electron Gas Theory of the Color of Natural and Artificial Dyes: Problems and Principles. Fortschr. Chem. Org. Naturstoffe 16 (1958).
- 71. Wenz, G., Müller, M. A., Schmidt, M. & Wegner, G. Structure of Poly(Diacetylenes) in Solution. *Macromolecules* 17, 837–850. ISSN: 15205835 (1984).
- 72. Porod, G. Zusammenhang zwischen mittlerem Endpunktsabstand und Kettenlänge bei Fadenmolekülen. *Monatshefte für Chemie* **80**, 251–255. ISSN: 00269247 (1949).
- 73. Kratky, O. & Porod, G. Röntgenuntersuchung gelöster Fadenmoleküle. *Recl. des Trav. Chim. des Pays-Bas* **68**, 1106–1122. ISSN: 01650513 (1949).
- 74. Huo, Q., Russell, K. C., Leblanc, R. M., Box, P. O. & Gables, C. Chromatic Studies of a Polymerizable Diacetylene Hydrogen Bonding Self-Assembly: A "Self-Folding" Process To Explain the Chromatic Changes of Polydiacetylenes, 3972–3980 (1999).
- 75. Rughooputh, S. D., Phillips, D., Bloor, D. & Ando, D. J. Spectroscopic studies of polydiacetylene solutions and glasses. Glasses of a hydrogen-bonding polymer. *Chem. Phys. Lett.* **114**, 365–370. ISSN: 00092614 (1985).
- 76. Koshihara, S. Y., Tokura, Y., Takeda, K., Koda, T. & Kobayashi, A. Reversible and irreversible thermochromic phase transitions in single crystals of polydiacetylenes substituted with alkyl-urethanes. *J. Chem. Phys.* **92**, 7581–7588. ISSN: 00219606 (1990).
- 77. Nagasawa, J., Kudo, M., Hayashi, S. & Tamaoki, N. Organogelation of diacetylene cholesteryl esters having two urethane linkages and their photopolymerization in the gel state. *Langmuir* **20**, 7907–7916. ISSN: 07437463 (2004).
- 78. Exarhos, G. J., Risen, W. M. & Baughmantb, R. H. Resonance Raman Study of the Thermochromic Phase Transition of a Polydiacetylene (1974).

79. Meier, H., Stalmach, U. & Kolshorn, H. Effective conjugation length and UV/vis spectra of oligomers. *Acta Polym.* **48**, 379–384. ISSN: 03237648 (1997).

- 80. Baughman, R. H. & Chance, R. R. Comments on the Optical Properties of Fully Conjugated Polymers: Analogy Between Polyenes and Polydiacetylenes. *J Polym Sci Polym Phys Ed* 14, 2037–2045 (1976).
- 81. Dobrosavljević, V. & Stratt, R. M. Role of conformational disorder in the electronic structure of conjugated polymers: Substituted polydiacetylenes. *Phys. Rev. B* **35**, 2781–2794. https://link.aps.org/doi/10.1103/PhysRevB.35.2781 (1987).
- 82. Campbell, A. J., Davies, C. K. & Batchelder, D. N. Raman shifts due to variations in backbone planarity in a group of polydiacetylenes. *Macromol. Chem. Phys.* **199**, 109–112. ISSN: 10221352 (1998).
- 83. Weiser, G. Stark effect of one-dimensional Wannier excitons in polydiacetylene single crystals. *Phys. Rev. B* **45**, 14076–14085. ISSN: 01631829 (1992).
- 84. Bloor, D., Ando, D. J., Preston, F. H. & Stevens, G. C. Fundamental and defect properties of a crystalline conjugated polymer. *Chem. Phys. Lett.* **24**, 407–411. ISSN: 00092614 (1974).
- 85. Díaz-Ponce, J. A., Morales-Saavedra, O. G., Beristaín-Manterola, M. F., Hernández-Alcántara, J. M. & Ogawa, T. Effect of metal salts in the optical properties of polydiacetylenes. *J. Lumin.* **128**, 1431–1441. ISSN: 00222313 (2008).
- 86. Barisien, T. et al. Exciton spectroscopy of red polydiacetylene chains in single crystals. Chem. Phys. Lett. 444, 309–313 (2007).
- 87. Dubin, F. *et al.* Macroscopic coherence of a single exciton state in an organic quantum wire. *Nat. Phys.* **2**, 32–35. ISSN: 17452481 (2006).
- 88. Sariciftci, N. S., Weiser, G. & Horváth, A. in *Prim. Photoexcitations Conjug. Polym. Mol. Excit. Versus Semicond. Band Model* 318–362 (1998).
- 89. Rawiso, M. et al. Solutions of Polydiacetylenes in Good and Poor Solvents: a Light and Neutron Scattering Study. J. Phys. Paris 49, 861–880. ISSN: 03020738 (1988).
- 90. Schott, M. Optical Properties of Single Conjugated Polymer Chains (Polydiacetylenes) 49–151. ISBN: 9783527404568 (2006).
- 91. Guo, C., Zhou, L. & Lv, J. Effects of expandable graphite and modified ammonium polyphosphate on the flame-retardant and mechanical properties of wood flour-polypropylene composites. *Polym. Polym. Compos.* **21**, 449–456. ISSN: 09673911. arXiv: 1206.4529 (2013).
- 92. Charych, D. H., Nagy, J. O., Spevak, W. & Bednarski, M. D. Direct colorimetric detection of a receptor-ligand interaction by a polymerized bilayer assembly. *Science* (80-.). **261**, 585–588. ISSN: 00368075 (1993).
- 93. Salje, E. K. Crystallography and structural phase transitions, an introduction. *Acta Crystallogr. Sect. A* **47**, 453–469. ISSN: 16005724 (1991).
- 94. Takeuchi, M., Imai, H. & Oaki, Y. Effects of the intercalation rate on the layered crystal structures and stimuli-responsive color-change properties of polydiacetylene. J. Mater. Chem. C 5, 8250–8255. ISSN: 20507526 (2017).

95. Carpick, R. W., Sasaki, D. Y. & Burns, A. R. First Observation of Mechanochromism at the Nanometer Scale. *Langmuir* **16**, 1270–1278. ISSN: 07437463 (2000).

- 96. Shin, M. J. & Kim, J. D. Reversible Chromatic Response of Polydiacetylene Derivative Vesicles in D2O Solvent. *Langmuir* **32**, 882–888. ISSN: 15205827 (2016).
- 97. Guo, H. *et al.* Ultrafast and reversible thermochromism of a conjugated polymer material based on the assembly of peptide amphiphiles. *Chem. Sci.* **5**, 4189–4195. ISSN: 20416539 (2014).
- 98. Khanantong, C., Charoenthai, N., Kielar, F., Traiphol, N. & Traiphol, R. Influences of bulky aromatic head group on morphology, structure and color-transition behaviors of polydiacetylene assemblies upon exposure to thermal and chemical stimuli. *Colloids Surfaces A Physicochem. Eng. Asp.* **561**, 226–235. ISSN: 18734359. https://doi.org/10.1016/j.colsurfa.2018.10.076 (2019).
- 99. Ahn, D. J. et al. Colorimetric reversibility of polydiacetylene supramolecules having enhanced hydrogen-bonding under thermal and pH stimuli. J. Am. Chem. Soc. 125, 8976–8977. ISSN: 00027863 (2003).
- 100. KATZ, J. J. CHEMICAL AND BIOLOGICAL STUDIES WITH DEUTERIUM. Am. Sci. 48, 544-580. ISSN: 15204995. http://www.jstor.org/stable/27827650 (1960).
- 101. Clark, T., Heske, J. & Kühne, T. D. Opposing Electronic and Nuclear Quantum Effects on Hydrogen Bonds in H2O and D2O. *ChemPhysChem* **20**, 2461–2465. ISSN: 14397641 (2019).
- 102. Lee, G. S., Kim, T. Y. & Ahn, D. J. Modulation of chromatic reversibility of polydiacetylene Langmuir Schafer (LS) films by cadmium ion Ad/desorption. *J. Ind. Eng. Chem.* 67, 312–315. ISSN: 22345957. https://doi.org/10.1016/j.jiec.2018.07.002 (2018).
- 103. Boal, A. K. *et al.* Self-assembly of nanoparticles into structured spherical and network aggregates Multi-scale ordering of materials is central for the application of molecular systems. *Nature* **404**, 746–748 (2000).
- 104. Gu, Y., Cao, W., Zhu, L., Chen, D. & Jiang, M. Polymer mortar assisted self-assembly of nanocrystalline polydiacetylene bricks showing reversible thermochromism. *Macromolecules* 41, 2299–2303. ISSN: 00249297 (2008).
- 105. Kamphan, A., Khanantong, C., Traiphol, N. & Traiphol, R. Structural-thermochromic relationship of polydiacetylene (PDA)/polyvinylpyrrolidone (PVP) nanocomposites: Effects of PDA side chain length and PVP molecular weight. *J. Ind. Eng. Chem.* 46, 130–138. ISSN: 22345957. http://dx.doi.org/10.1016/j.jiec.2016.10.023 (2017).
- Diamond, G., Beckloff, N., Weinberg, A. & Kisich, K. O. The roles of antimicrobial peptides in innate Host Defense. *Curr. Pharm. Des.* **15**, 2377–92. ISSN: 1873-4286. http://www.pubmedcentral.nih.gov/articlerender.fcgi?artid=2750833{\&}tool=pmcentrez{\&}rendertype=abstract (2009).
- 107. Sun, E., Belanger, C. R., Haney, E. F. & Hancock, R. E. *Host defense (antimicrobial)* peptides 253–285. ISBN: 9780081007426. http://dx.doi.org/10.1016/B978-0-08-100736-5.00010-7 (Elsevier Ltd, 2018).

108. Blobel, G. Protein targeting (Nobel lecture). Angew. Chemie (International Ed. English) 39, 87–102. ISSN: 05700833 (2000).

- 109. Torgersen, H., Lassen, J., Jelsoe, E., Rusanen, T. & Nielsen, T. H. antimicrobial resistance: the example of SA. J. Biolaw Bus. 3, 53–59. ISSN: 10955127 (2000).
- 110. Terwilliger, T. C. & Eisenberg, D. The structure of melittin. *J. Biol. Chem.* **257**, 6016-6022. http://onlinelibrary.wiley.com/doi/10.1111/j.1432-1033.1988.tb13977.x/full (1982).
- 111. Kleinschmidt, J. H., Mahaney, J. E., Thomas, D. D. & Marsh, D. Interaction of bee venom melittin with zwitterionic and negatively charged phospholipid bilayers: a spin-label electron spin resonance study. *Biophys. J.* 72, 767–78. ISSN: 0006-3495. http://www.pubmedcentral.nih.gov/articlerender.fcgi?artid=1185600{\&}tool=pmcentrez{\&}rendertype=abstract (1997).
- 112. Serra, M. D., National, I. & Lazarovici, P. Pore-forming Peptides and Protein Toxins October, 348. ISBN: 0415298520, 9780415298520 (2003).
- 113. Dawson, C. R., Drake, A. F., Helliwell, J. & Hider, R. C. The interaction of bee melittin with lipid bilayer membranes. *BBA Biomembr.* **510**, 75–86. ISSN: 00052736 (1978).
- 114. Haydon, D. A. & Taylor, J. The stability and properties of bimolecular lipid leaflets in aqueous solutions. *J. Theor. Biol.* 4, 281–296. ISSN: 10958541 (1963).
- 115. Ramalingam, K., Aimoto, S. & Bello, J. Conformational studies of anionic melittin analogues: Effect of peptide concentration, pH, ionic strength, and temperature models for protein folding and halophilic proteins. *Biopolymers* **32**, 981–992. ISSN: 10970282 (1992).
- 116. Pan, J. & Khadka, N. K. Kinetic Defects Induced by Melittin in Model Lipid Membranes: A Solution Atomic Force Microscopy Study. *J. Phys. Chem. B* **120**, 4625–4634. ISSN: 15205207 (2016).
- 117. Terwilliger, T. C., Weissman, L. & Eisenberg, D. The structure of melittin in the form I crystals and its implication for melittin's lytic and surface activities. *Biophys. J.* **37**, 353–361. ISSN: 00063495 (1982).
- 118. Vogel, H & Jähnig, F. The structure of melittin in membranes. *Biophys. J.* **50**, 573–582. ISSN: 0006-3495 (1986).
- 119. Perez-Paya, E., Houghten, R. A. & Blondelle, S. E. Determination of the secondary structure of selected melittin analogues with different haemolytic activities. *Biochem. J.* **299**, 587–591. ISSN: 02646021 (1994).
- 120. Wu, J., Zawistowski, A., Ehrmann, M., Yi, T. & Schmuck, C. Peptide functionalized polydiacetylene liposomes Act as a fluorescent turn-on sensor for bacterial lipopolysaccharide. J. Am. Chem. Soc. 133, 9720–9723. ISSN: 00027863 (2011).
- 121. Park, J. et al. Label-free bacterial detection using polydiacetylene liposomes. Chem. Commun. 52, 10346–10349. ISSN: 1364548X (2016).
- 122. Bouffioux, O. *et al.* Molecular organization of surfactin-phospholipid monolayers: Effect of phospholipid chain length and polar head. *Biochim. Biophys. Acta Biomembr.* **1768**, 1758–1768. ISSN: 00052736 (2007).

123. Carpick, R. W., Mayer, T. M., Sasaki, D. Y. & Burns, A. R. Spectroscopic ellipsometry and fluorescence study of thermochromism in an ultrathin poly(diacetylene) film: reversibility and transition kinetics. *Langmuir* 16, 4639–4647. ISSN: 07437463 (2000).

- 124. Patel, G. N. & Walsh, E. K. Polydiacetylenes: Solution conformation characteristics. J. Polym. Sci. Polym. Lett. Ed. 17, 203–208. ISSN: 03606384 (1979).
- 125. Yuan, Z., Lee, C. W. & Lee, S. H. Reversible thermochromism in hydrogen-bonded polymers containing polydiacetylenes. *Angew. Chemie Int. Ed.* **43**, 4197–4200. ISSN: 14337851 (2004).
- 126. Khanantong, C. *et al.* Influences of solvent media on chain organization and thermochromic behaviors of polydiacetylene assemblies prepared from monomer with symmetric alkyl tails. *J. Ind. Eng. Chem.* **58**, 258–265. ISSN: 22345957. https://doi.org/10.1016/j.jiec.2017.09.035 (2018).
- 127. Kamphan, A., Charoenthai, N. & Traiphol, R. Fine tuning the colorimetric response to thermal and chemical stimuli of polydiacetylene vesicles by using various alcohols as additives. *Colloids Surfaces A Physicochem. Eng. Asp.* **489**, 103–112. ISSN: 18734359. http://dx.doi.org/10.1016/j.colsurfa.2015.10.035 (2016).
- 128. Herglotz, H. Topics in surface chemistry. J. Colloid Interface Sci. 77. ISSN: 00219797 (1980).
- 129. Su, Y. L., Li, J. R. & Jiang, L. Effect of amphiphilic molecules upon chromatic transitions of polydiacetylene vesicles in aqueous solutions. *Colloids Surf B Biointerfaces* **39**, 113–118. ISSN: 09277765 (2004).
- 130. Lee, K. M. *et al.* Diverse colorimetric changes of polydiacetylenes with cationic surfactants and their mechanistic studies. *J. Mater. Chem.* **21**, 17160–17166. ISSN: 09599428 (2011).
- 131. Oliveira, C. P. D., Soares, N. D. F. F., Fontes, E. A. F., Oliveira, T. V. D. & Filho, A. M. M. Behaviour of polydiacetylene vesicles under different conditions of temperature, pH and chemical components of milk. *Food Chem.* **135**, 1052–1056. ISSN: 03088146 (2012).
- 132. Song, J., Cheng, Q., Kopta, S. & Stevens, R. C. Modulating artificial membrane morphology: pH-induced chromatic transition and nanostructural transformation of a bolaamphiphilic conjugated polymer from blue helical ribbons to red nanofibers. *J. Am. Chem. Soc.* **123**, 3205–3213. ISSN: 00027863 (2001).
- 133. Boullanger, P. *et al.* The use of glycolipids inserted in color-changeable polydiacetylene vesicles, as targets for biological recognition. *Comptes Rendus Chim.* **11**, 43–60. ISSN: 16310748 (2008).
- 134. Traiphol, N., Chanakul, A., Kamphan, A. & Traiphol, R. Role of Zn2 + ion on the formation of reversible thermochromic polydiacetylene/zinc oxide nanocomposites. *Thin Solid Films* **622**, 122–129. ISSN: 00406090. http://dx.doi.org/10.1016/j.tsf. 2016.12.037 (2017).
- 135. Pattanatornchai, T., Rueangsuwan, J., Phonchai, N., Traiphol, N. & Traiphol, R. Reversible thermochromic polydiacetylene/Zn(II) ion assemblies prepared via co-assembling in aqueous phase: The essential role of pH. *Colloids Surfaces A Physicochem. Eng. Asp.*

- **594**, 124649. ISSN: 18734359. https://doi.org/10.1016/j.colsurfa.2020.124649 (2020).
- 136. Weston, M., Kuchel, R. P., Ciftci, M., Boyer, C. & Chandrawati, R. A polydiacetylene-based colorimetric sensor as an active use-by date indicator for milk. *J. Colloid Inter-face Sci.* **572**, 31–38. ISSN: 10957103. https://doi.org/10.1016/j.jcis.2020.03.040 (2020).
- 137. Lifshitz, Y. et al. Phase transition kinetics in Langmuir and spin-coated polydiacety-lene films. Phys. Chem. Chem. Phys. 12, 713–722. ISSN: 14639076 (2010).
- 138. Zhang, W., Xu, H., Chen, Y., Cheng, S. & Fan, L. J. Polydiacetylene-polymethylmethacrylate/graphe composites as one-shot, visually observable, and semiquantative electrical current sensing materials. *ACS Appl. Mater. Interfaces* 5, 4603–4606. ISSN: 19448244 (2013).
- 139. Pimsen, R., Khumsri, A., Wacharasindhu, S., Tumcharern, G. & Sukwattanasinitt, M. Colorimetric detection of dichlorvos using polydiacetylene vesicles with acetylcholinesterase and cationic surfactants. *Biosens. Bioelectron.* **62**, 8–12. ISSN: 18734235. http://dx.doi.org/10.1016/j.bios.2014.05.069 (2014).
- 140. Kamphan, A., Traiphol, N. & Traiphol, R. Versatile route to prepare reversible thermochromic polydiacetylene nanocomposite using low molecular weight poly(vinylpyrrolidone). Colloids Surfaces A Physicochem. Eng. Asp. 497, 370–377. ISSN: 18734359. http://dx.doi.org/10.1016/j.colsurfa.2016.03.041 (2016).
- 141. Park, D. H., Hong, J., Park, I. S., Lee, C. W. & Kim, J. M. A Colorimetric hydrocarbon sensor employing a swelling-induced mechanochromic polydiacetylene. *Adv. Funct. Mater.* 24, 5186–5193. ISSN: 16163028 (2014).
- 142. Patlolla, A., Zunino, J., Frenkel, A. I. & Iqbal, Z. Thermochromism in polydiacetylenemetal oxide nanocomposites. *J. Mater. Chem.* **22**, 7028–7035. ISSN: 09599428 (2012).
- 143. Guo, J. et al. Reversible thermochromism via hydrogen-bonded cocrystals of polydiacetylene and melamine. Polymer (Guildf). 105, 440–448. ISSN: 00323861 (2016).
- 144. Girard-Reydet, C., Ortuso, R. D., Tsemperouli, M. & Sugihara, K. Combined Electrical and Optical Characterization of Polydiacetylene. *J. Phys. Chem. B* **120**, 3511–3515. ISSN: 15205207 (2016).
- 145. Xu, Q. et al. Polydiacetylene-based colorimetric and fluorescent chemosensor for the detection of carbon dioxide. J. Am. Chem. Soc. 135, 17751–17754. ISSN: 00027863 (2013).
- 146. Chen, X. et al. Photo-controlled molecular recognition of α -cyclodextrin with azobenzene containing polydiacetylene vesicles. Chem. Commun., 1356–1358. ISSN: 13597345 (2009).
- 147. Chen, X., Lee, J., Jou, M. J., Kim, J. M. & Yoon, J. Colorimetric and fluorometric detection of cationic surfactants based on conjugated polydiacetylene supramolecules. *Chem. Commun.*, 3434–3436. ISSN: 13597345 (2009).
- 148. Kim, J. M. *et al.* A polydiacetylene-based fluorescent sensor chip. *J. Am. Chem. Soc.* **127**, 17580–17581. ISSN: 00027863 (2005).

149. Ortuso, R. D., Cataldi, U. & Sugihara, K. Mechanosensitivity of polydiacetylene with a phosphocholine headgroup. *Soft Matter* 13, 1728–1736. ISSN: 1744-683X. http://xlink.rsc.org/?DOI=C6SM02579J (2017).

- 150. Lee, J., Jun, H. & Kim, J. Polydiacetylene-liposome microarrays for selective and sensitive mercury(II) detection. *Adv. Mater.* **21**, 3674–3677. ISSN: 09359648 (2009).
- 151. Park, E. Y., Kim, J. W., Ahn, D. J. & Kim, J. M. A polydiacetylene supramolecular system that emits red, green, and blue fluorescence. *Macromol. Rapid Commun.* 28, 171–175. ISSN: 10221336 (2007).
- 152. Yoo, H. O., Chae, S. K., Kim, J. M. & Ahn, D. J. Conjugated polymer-embedded thermochromic strip sensors with a tunable colorimetric response. *Macromol. Res.* **15**, 478–481. ISSN: 15985032 (2007).
- 153. Lifshitz, Y., Golan, Y., Konovalov, O. & Berman, A. Structural transitions in polydiacetylene langmuir films. *Langmuir* **25**, 4469–4477. ISSN: 07437463 (2009).
- 154. Tanaka, H., Gomez, M. A., Tonelli, A. E. & Thakur, M. Thermochromic Phase Transition of a Polydiacetylene, Poly(ETCD), Studied by High-Resolution Solid-State13C NMR. *Macromolecules* 22, 1208–1215. ISSN: 15205835 (1989).
- 155. Sixl, H., Neumann, W., Huber, R., Denner, V. & Sigmund, E. Electron-spin-resonance experiments and theory of the butatriene-to- acetylene transition in short-chain polydiacetylene molecules. *Phys. Rev. B* **31**, 142–148. ISSN: 01631829 (1985).
- 156. Chance, R. R. & Patel, G. N. SOLID-STATE POLYMERIZATION OF A DIACETY-LENE CRYSTAL: THERMAL, ULTRAVIOLET, AND gamma -RAY POLYMER-IZATION OF 2,4-HEXADIYNE-1,6-DIOL BIS-(p-TOLUENE SULFONATE). *J Polym Sci Polym Phys Ed* 16, 859–881 (1978).
- 157. Schoen, P. E. & Yager, P. Spectroscopic Studies of Polymerized Surfactants: 1,2-Bis(10,12-Tricosadiynoyl)-Sn-Glycero-3-Phosphocholine. *J. Polym. Sci. Part A-2, Polym. Phys.* **23**, 2203–2216. ISSN: 04492978 (1985).
- 158. Okawa, Y. & Aono, M. Linear chain polymerization initiated by a scanning tunneling microscope tip at designated positions. *J. Chem. Phys.* **115**, 2317–2323. ISSN: 00219606 (2001).
- 159. Burns, A. R., Carpick, R. W., Sasaki, D. Y., Shelnutt, J. A. & Haddad, R. Shear-induced mechanochromism in polydiacetylene monolayers. *Tribol. Lett.* **10**, 89–96. ISSN: 10238883 (2001).
- 160. Okawa, Y & Aono, M. Materials science Nanoscale control of chain polymerization. *Nature* **409**, 683–684 (2001).
- 161. Dobrosavljević, V. & Stratt, R. M. Role of conformational disorder in the electronic structure of conjugated polymers: Substituted polydiacetylenes. *Phys. Rev. B* **35**, 2781–2794 (1987).
- 162. Park, I. S. *et al.* Low Temperature Thermochromic Polydiacetylenes: Design, Colorimetric Properties, and Nanofiber Formation. *Macromolecules* **49**, 1270–1278. ISSN: 15205835 (2016).
- 163. Hammond, P. T. & Rubner, M. F. Thermochromism in liquid crystalline polydiacetylenes. *Macromolecules* **30**, 5773–5782. ISSN: 00249297 (1997).

164. Mino, N., Tamura, H. & Ogawa, K. Analysis of Color Transitions and Changes on Langmuir-Blodgett Films of a Polydiacetylene Derivative. *Langmuir* 7, 2336–2341. ISSN: 15205827 (1991).

- 165. Rubner, M. F. Synthesis and Characterization of Polyurethane-Diacetylene Segmented Copolymers. *Macromolecules* **19**, 2114–2128. ISSN: 15205835 (1986).
- 166. Khanantong, C. *et al.* Phase transition, structure and color-transition behaviors of monocarboxylic diacetylene and polydiacetylene assemblies: The opposite effects of alkyl chain length. *Colloids Surfaces A Physicochem. Eng. Asp.* **553**, 337–348. ISSN: 18734359. https://doi.org/10.1016/j.colsurfa.2018.05.081 (2018).
- 167. Mapazi, O., Matabola, K. P., Moutloali, R. M. & Ngila, C. J. High temperature thermochromic polydiacetylene supported on polyacrylonitrile nanofibers. *Polymer (Guildf)*. **149**, 106–116. ISSN: 00323861. https://doi.org/10.1016/j.polymer. 2018.06.028 (2018).
- 168. Hankin, S. H. W., Downey, M. J. & Sandman, D. J. On the structural origins of solid-state urethane polydiacetylene thermochromism: thermal and structural properties of IPUDO monomer and polymer. *Polymer (Guildf)*. **33**, 5098–5101 (1992).
- 169. Ohki, K. A region-matched hydrophobic interaction between melittin and dimyristoylphosphatidylcholine in a ternary mixture of phosphatidylcholines. *Biochem Biophys Res Commun* **164**, 850–856 (1989).
- 170. Prenner, E. J., Lewis, R. N. A. H., Kondejewski, L. H., Hodges, R. S. & McElhaney, R. N. Differential scanning calorimetric study of the effect of the antimicrobial peptide gramicidin S on the thermotropic phase behavior of phosphatidylcholine, phosphatidylethanolamine and phosphatidylglycerol lipid bilayer membranes. *Biochim. Biophys. Acta Biomembr.* 1417, 211–223. ISSN: 00052736 (1999).
- 171. Arouri, A., Dathe, M. & Blume, A. Peptide induced demixing in PG/PE lipid mixtures: A mechanism for the specificity of antimicrobial peptides towards bacterial membranes? *Biochim. Biophys. Acta Biomembr.* 1788, 650–659. ISSN: 00052736. http://dx.doi.org/10.1016/j.bbamem.2008.11.022 (2009).
- 172. Joanne, P. et al. Lipid reorganization induced by membrane-active peptides probed using differential scanning calorimetry. Biochim. Biophys. Acta Biomembr. 1788, 1772–1781. ISSN: 00052736. http://dx.doi.org/10.1016/j.bbamem.2009.05.001 (2009).
- 173. Kolusheva, S., Shahal, T. & Jelinek, R. Cation-selective color sensors composed of ionophore-phospholipid- polydiacetylene mixed vesicles. *J. Am. Chem. Soc.* **122**, 776–780. ISSN: 00027863 (2000).
- 174. Volinsky, R, Gaboriaud, F, Berman, A & Jelinek, R. Morphology and organization of phospholipid/diacetylene Langmuir films studied by brewster angle microscopy and fluorescence microscopy. *J. Phys. Chem. B* **106**, 9231–9236. ISSN: 10895647 (2002).
- 175. Zhou, W. & Greer, H. F. What Can Electron Microscopy Tell Us beyond Crystal Structures? Eur. J. Inorg. Chem. 2016, 941–950. ISSN: 10990682 (2016).
- 176. Pakhomov, S., Hammer, R. P., Mishra, B. K. & Thomas, B. N. Chiral tubule self-assembly from an achiral diynoic lipid. *Proc. Natl. Acad. Sci. U. S. A.* **100**, 3040–3042. ISSN: 00278424 (2003).

177. Volinsky, R., Kolusheva, S., Berman, A. & Jelinek, R. Investigations of antimicrobial peptides in planar film systems. *Biochim. Biophys. Acta - Biomembr.* **1758**, 1393–1407. ISSN: 00052736 (2006).

- 178. Kuriyama, K., Kikuchi, H. & Kajiyama, T. Molecular Packings-Photopolymerization Behavior Relationship of Diacetylene Langmuir-Blodgett Films. *Langmuir* **12**, 6468–6472. ISSN: 0743-7463 (1996).
- 179. Saito, A., Urai, Y. & Itoh, K. Infrared and Resonance Raman Spectroscopic Study on the Photopolymerization Process of the Langmuir-Blodgett Films of a Diacetylene Monocarboxylic Acid, 10,12-Pentacosadiynoic Acid. *Langmuir* 12, 3938–3944. ISSN: 0743-7463. http://pubs.acs.org/doi/abs/10.1021/la951503z (1996).
- 180. Terwilliger, T. C. & Eisenberg, D. The structure of melittin. II. Interpretation of the structure. J. Biol. Chem. 257, 6016–6022. ISSN: 00219258 (1982).
- 181. Lazarev, V. N. *et al.* Induced expression of melittin, an antimicrobial peptide, inhibits infection by Chlamydia trachomatis and Mycoplasma hominis in a HeLa cell line. *Int. J. Antimicrob. Agents* **19**, 133–137. ISSN: 09248579 (2002).
- 182. Sugihara, K., Vörös, J. & Zambelli, T. A gigaseal obtained with a self-assembled long-lifetime lipid bilayer on a single polyelectrolyte multilayer-filled nanopore. *ACS Nano* 4, 5047–5054. ISSN: 19360851 (2010).
- 183. Sugihara, K. et al. Simultaneous OWLS and EIS monitoring of supported lipid bilayers with the pore forming peptide melittin. Sensors Actuators, B Chem. 161, 600-606. ISSN: 09254005. http://dx.doi.org/10.1016/j.snb.2011.11.007 (2012).
- 184. Tosteson, M. T. & Tosteson, D. C. The sting. Melittin forms channels in lipid bilayers. *Biophys. J.* **36**, 109–116. ISSN: 00063495. http://dx.doi.org/10.1016/S0006-3495(81)84719-4 (1981).
- 185. Batchelder, D. N. in *Polydiacetylenes* 187–212 (1985).
- 186. Jeon, S., Yoon, B. & Kim, J. M. Polymerization temperature-dependent thermochromism of polydiacetylene. *Bull. Korean Chem. Soc.* **36**, 1949–1950. ISSN: 12295949 (2015).
- 187. Raahauge, C. Isothermal Titration Calorimetry and Differential Scanning Calorimetry of DPPC membranes and ethanol. *Methods Mol. Biol.* **572**, 101–133. ISSN: 19406029 (2009).
- 188. Wieprecht, T. & Seelig, J. Isothermal titration calorimetry for studying interactions between peptides and lipid membranes. *Curr. Top. Membr.* **52**, 31–56. ISSN: 10635823 (2002).
- 189. Yang, Q. Z. *et al.* A molecular force probe. *Nat. Nanotechnol.* **4**, 302–306. ISSN: 17483395 (2009).
- 190. Lin, Y., Hansen, H. R., Brittain, W. J. & Craig, S. L. Strain-Dependent Kinetics in the Cis-to-Trans Isomerization of Azobenzene in Bulk Elastomers. *J. Phys. Chem. B* 123, 8492–8498. ISSN: 15205207 (2019).
- 191. Berkowski, K. L., Potisek, S. L., Hickenboth, C. R. & Moore, J. S. Ultrasound-induced site-specific cleavage of azo-functionalized poly(ethylene glycol). *Macromolecules* **38**, 8975–8978. ISSN: 00249297 (2005).

192. Sagara, Y. et al. Rotaxanes as mechanochromic fluorescent force transducers in polymers. J. Am. Chem. Soc. 140, 1584–1587. ISSN: 15205126 (2018).

- 193. Seki, T. et al. Luminescent Mechanochromic 9-Anthryl Gold(I) Isocyanide Complex with an Emission Maximum at 900 nm after Mechanical Stimulation. J. Am. Chem. Soc. 139, 6514–6517. ISSN: 15205126 (2017).
- 194. Filhol, J. S. et al. Polymorphs and colors of polydiacetylenes: A first principles study. J. Am. Chem. Soc. 131, 6976–6988. ISSN: 00027863 (2009).